# Development and Application of Microenvironment for Regulation of Stem Cell Behaviors

SATOSHI FUJITA

2008

# CONTENTS

# ABBREVIATIONS

| | |
|---|---|
| 5-FU | 5-fluorouracil |
| ANOVA | analysis of variance |
| APC | allophycocyanin |
| BSE | bovine spongiform encephalopathy |
| CAFC | cobblestone area-forming cell |
| cDNA | complementary deoxyribonucleic acid |
| CFC | colony-forming cell |
| CFU | colony-forming units |
| CFU-GEMM | colony-forming units granulocytes/ erythroid cells/ macrophages/ megakaryocytes |
| CFU-GM | colony-forming units granulocytes/ macrophages |
| CM | conditioned medium |
| DMEM | Dulbecco's modified essential medium |
| DNA | deoxyribonucleic acid |
| DPBS | Dulbecco's phosphate-buffered saline |
| DTT | dithiothreitol |
| EDTA | ethylenediaminetetraacetic acid |
| FBS | fetal bovine serum |
| FCM | flow cytometry |
| FITC | fluorescein isothiocyanate |
| FL | fms-related tyrosine kinase 3 ligand |

| | |
|---|---|
| FRPC | 5-fluorouracil resistant progenitor cells |
| FSC | forward scattering |
| GAPDH | glyceraldehyde-3-phosphate dehydrogenase |
| GM-CSF | granulocyte macrophage colony-stimulating factor |
| HBSS | Hanks' balanced salt solution |
| hMSC | human mesenchymal stem cell |
| HPC | hematopoietic progenitor cell |
| HPP-CFC | high-proliferative potential colony-forming cell |
| HSC | hematopoietic stem cell |
| HSD | honestly significant difference |
| hTERT | human telomerase reverse transcriptase |
| IgG | immunoglobulin G |
| LTC-IC | long-term culture-initiating cell |
| MEM | minimal essential medium |
| MSC | mesenchymal stem cell |
| MuLV | murine leukemia virus |
| NG | nanogrooved |
| NT | non-treated |
| PC | polycarbonate |
| PCR | polymerase chain reaction |
| PE | phycoerythrin |
| PERV | porcine endogenous retrovirus |
| RNA | ribonucleic acid |

| | |
|---|---|
| RT-PCR | reverse transcriptase-polymerase chain reaction |
| RUNX2 | runt-related transcription factor 2 |
| SCF | stem cell factor |
| SEM | scanning electron microscope |
| SPM | scanning probe microscope |
| SSC | side scattering |
| Tg | glass transition temperature |
| TPO | thrombopoietin |
| UCB | umbilical cord blood |
| XPS | X-ray photoelectron spectroscopy |

# GENERAL INTRODUCTION

A stem cell is defined as the cell that has both self-renewal potency and mutipotency [1]. Since bone marrow has proved experimentally to be a reservoir of hematopoietic stem cells (HSC) in the early 1960s [2], recent studies revealed their surface markers, differentiation pathways, and their localization *in vivo* precisely [3]. Besides hematopoietic stem cells, several groups provided the direct evidence of stem cells of other tissues, such as intestine [4] and hair follicle [5] of mouse. In human tissues, neural stem cells [6], mesenchymal stem cells [7] and so on were also identified. It is now appreciated that somatic stem cells exist in various tissues and organs widely and they play an important role for their repair [8]. Meanwhile, in 1981, embryonic stem cells (ES cells) were established from mouse embryos as pluripotent stem cells that can form an individual mouse [9]. By contrast, it has been difficult to establish human ES cells for a long time, whereas Thomson et al. succeeded at last in 1998 [10]. In addition, a surprising report was published in 2006 that somatic cells derived from murine skin were reprogrammed into pluripotent cells, which resembled ES cells [11]. This type of cell was named as an induced pluripotent stem cell (iPS cell) and has been brought to public attention as a new approach to obtain stem cells. In the following 2007, iPS cells were established from human somatic cells [12]. Thus, researches on stem cells have been in rapid progress these days, accompanied by the novel therapies for intractable diseases, severe injuries, congenital abnormalities and orthopedic

procedure, which exploit various types of stem cell [13].

Here, let us describe the definition of the term ‘stem cell’ and ‘progenitor cell’ to avoid confusion. The both of ‘stem cell’ and ‘progenitor cell’ are immature cells [14], but they can be conceptually discriminated by self-renewal potency. A stem cell produces at least a same cell as itself in a cell division, whereas a progenitor cell produces two of more mature cells. However, it is difficult to distinguish them experimentally. The term ‘stem cells’ usually refers to heterogeneous stem cell population including progenitor cells. This terminology is used in this thesis.

It is known that the microenvironments around stem cells commonly affect the proliferation and differentiation *in vivo* [15,16]. For example, HSC in bone marrow are know to be localized at and in direct contact with endosteal microenvironments composed of osteoblasts [17,18]. These microenvironments are called as hematopoietic niches. A stem cell that detaches from a niche is thought to divide and differentiate into progenitors or lineage commitment cells. The similar maintaining mechanism was also proposed in other organs, such as follicle stem cells and spermatogonial stem cells [15,16]. Thus, the appropriate microenvironments around stem cells would regulate their proliferation and differentiation, and achieve the quality control of cells for therapy.

This thesis aimed at developing culture system that is available for the regulation of stem cell proliferation and differentiation, and applicable for prospective clinical applications. The thesis consists of two parts. Part I described the co-culture system of hematopoietic stem cells that mimics hematopoietic niche. Part II described the behavior of human mesenchymal stem cells on finely-structured culture substrate.

In Part I, HSCs derived from human umbilical cord blood was focused as a target. The transplantation of HSC has been already accepted as the standard therapy for intractable blood disease (e.g., leukemia, aplastic anemia) [19]. Bone marrow, peripheral blood and umbilical cord blood are known as the source of HSC. Especially, umbilical cord blood has been noted because it can be collected noninvasively, compared with other sources. Since the successive case in 1988 [20], cord blood transplantation has come into wide use rapidly, because it can be applicable for not only patients with mismatched HLA, but also those who needed emergent transplantation [21]. In Japan, more than 700 cases of cord blood transplantations were performed to patients in 2007, and more than 4000 were performed totally since 1997 [22]. However, cord blood transplantation has a limitation that the total number of cells obtained from a donor is limited. According to the current guideline of HSC transplantation in Japan, only cord blood unit which has more than $6 \times 10^8$ nucleated cells is used for transplantation [23], because the success of HSC transplantation primarily depends on the number of infused cells [19]. Therefore, if effective expansion of cord blood HSC would be available, the cord blood units to be discarded under the current guideline would be provided for patients waiting for cell transplantation.

Many studies have been made on the expansion of HSC by miscellaneous approaches [24,25]. For example, various combinations of cytokines, such as stem cell factor (SCF), interleukin-6 (IL-6), and thrombopoietin (TPO), were examined in suspension culture [26-29], but adequate expansion has not yet been achieved. Direct injection of transcription factors into cells has been also tried. This approach is expected to be safer strategy than gene transfection for clinical use, but has been still in

progress [30]. Since it has been showed that co-culture with stromal cells was effective for the expansion of hematopoietic progenitors in 1970s [31-33], a considerable number of studies have been conducted on co-culture with stromal cells [24,25]. Especially, murine stromal cell line HESS-5 serves to achieve a successive expansion as feeder cells in the presence of a combination of several growth factors [34,35]. However, the problem to be considered was co-culture with xenogenic mouse cells, which might cause the contamination of cells derived from mouse. Transplantation of xenogenic cells might contribute to the onset of unknown diseases or acute rejection [36-38]. Therefore, Ministry of Health, Labour and Welfare of Japan has prohibited murine cells as feeder cells for the expansion of hematopoietic stem cells for transplantation [39].

To avoid the risks emerging from xenogenic cells, human-derived feeder cells have been investigated avidly. Recently, it was found that mesenchymal stem cells (MSCs) derived from human bone marrow had hematopoiesis-supporting activity as well as murine stromal cells [40-43]. However, handling of primary MSCs is inconvenient for the expansion of HSCs because it takes more than a few weeks to isolate human MSCs [7]. Moreover, the proliferative activity of primary MSC is limited and over-passaged cells would change their characteristics [44].

In Chapter 1, the availability of human bone marrow MSCs that was immortalized with human telomerase reverse transcriptase (hTERT) and human papiroma virus-derived E6/E7 genes [45] was investigated for the expansion of human cord blood-derived HSC. Immortalization of human MSC would improve laborious efforts of maintenance and cryopreservation as well as normal cell line. When genes were transduced into primary MSC, many clones were obtained from a parental MSC

population. These clones have showed the distinctive differentiation potency [45]. The author postulated that the hematopoiesis-supporting activity also differs among each clone. To examine this hypothesis, hematopoiesis-supporting activity of provided 16 clones was evaluated by co-culture of human cord blood-derived $CD34^+$ cells. As a result, 6 clones could support the proliferation of early hematopoietic progenitors, $CD34^+CD38^-$ cells. Moreover, these clones expressed membrane protein Jagged-1 and showed high osteogenic potency. Jagged-1 is known as one of components of Notch pathway, which plays an important role for the determination of stem cell fate [46]. Jagged-$1^+$ osteoblasts have been also revealed to contact with HSCs in bone marrow [17]. The result of this chapter was consistent with such previous findings. Thus, the hematopoiesis-supporting activity of MSC was elucidated in a clonal level and selected clones that were appropriate for HSC expansion.

Chapter 2 described the expansion culture system using culture supernatant of hematopoiesis supportive MSC clone, which was found in Chapter 1. Culture supernatant contains growth factors and cytokines secreted from MSC, but it is avoided to be contaminated by MSC itself. Therefore, HSC expansion by using MSC culture supernatant would be safer culture for clinical applications. Indeed, culture supernatants of hematopoiesis-supportive MSC clones facilitated significantly effective expansion in comparison to the suspension culture in the absence of feeder cells, but the effect was lower than conventional co-culture with feeder cells. This lower result was attributed to the destabilization of soluble factors in the supernatant during incubation, because secreted growth factors were usually stabilized by the interaction with extracellular matrix around cells [47]. Accordingly, to raise amounts

of effective growth factors in medium, constant supplying them was attempted by encapsulated MSC. MSC aggregates were formed, encapsulated in agarose gel that is permeable to soluble factors [48], and then co-cultured HSC. As a result, $CD34^{+}CD38^{-}$ cells were effectively expanded. The expanded HSCs can be easily separated from MSCs by filtration because the sizes of HSCs were quite different from those of encapsulated MSCs. This system would lead to a safer culture system for clinical application in the future.

Chapter 3 described the development of cell-based array chips for HSC assay. To enumerate HSC *in vitro*, flow cytometric surface antigen analysis [49] and colony assays [50-53] were conventionally performed, as used in the previous chapters. However, these assays have some limitations. Surface antigen analysis does not directly reflect stem cell function. It takes a few weeks to perform colony assay. A colony assay also requires experienced skill to identify colonies. The simple and convenient method to directly quantify the HSC function has been eagerly awaited. In this chapter, to demonstrate the efficacy of a cell-based array chip for HSC enumeration, HSCs were seeded with murine stromal cells in silicone microwells ($\phi$ 1 mm) stuck on a 2 cm × 2 cm substrate, and then two-step culture was performed. The first step was a purging phase of proliferating cells by cell cycle inhibitor, and the following step was a proliferating phase of surviving cells by cytokine stimulation. It has been known that primitive stem cells are in a quiescent or very slow cell cycle in common [54,55] and that they have high efflux activity of drugs [56,57]. Therefore, progenitors and lineage committed cells would be purged and only quiescent cells survive in the first step. Surviving quiescent primitive cells would be fallen into active cell cycles and proliferate in the following second step. According to this

strategy, the number of primitive HSCs in cord blood $CD34^+$ cell fraction was enumerated by the combination of fluorescent microscopic observation and statistic analysis. This approach is principally available for other stem cells, and thereby, efficacious as an assay tool for them. The merits of cell-based array are as follows. First, the doses of medium, additives and cells to be provided can be curtailed. Second, high-throughput parallel and time-lapse analysis is available because all of wells can be imaged simultaneously by CCD camera. Third, every cell shares the same medium because cells on a chip can be cultured in small amounts of medium [58], and thereby, this assay will bring about the minimization of the inhomogeneity in the culture conditions, such as medium components, secreting soluble factors, oxygen concentration, and temperature, compared with conventional 96- or 384-multiwell plates.

In Part II, MSC itself was focused. MSC is a heterogeneous cell population that can differentiate into various mesenchymal tissues, such as osteoblasts, adipocytes and chondrocytes. MSC can be procured from umbilical cord blood, placenta, amniotic fluid, adipose, a root of extracted tooth, and so on, besides bone marrow [7,59]. Clinical investigations of MSC have already been performed for the therapy of bone defects, cartilage defects, myocardial infarction, and so on [60-64]. In these therapeutic protocols, MSCs were directly infused into a vein in suspension or directly implanted with scaffolds at a target site without the cultivation of MSC beforehand, because it was difficult not only to culture in 3D but also to precisely regulate cell responses throughout long-term cell culture. MSCs are usually maintained in a cell culture dish with supplemented by fresh medium at appropriate intervals. However, the conditions of cultured cells can be affected readily by cell density or fluctuation of

medium components in a dish. It has been still difficult to control cell behaviors both spatially and temporally. To spatially regulate cell differentiation, considerable numbers of trials by surfaces modification with cytokines or growth factors have been reported [65,66]. Indeed, these methods might lead to novel implantable biomaterials or culture substrates, but more simple and convenient approaches are also desired because surface modification with proteins requires labors in sterilization and preservation.

In recent decades, it has been revealed that the physical properties, such as strain, topography and elasticity affect cell functions [67-72]. It is considered that cytoskeleton or intracellular tension affected the expression of transcription factors via Rho family proteins [73]. The comprehensive analysis of the effect on surface physical properties would lead to the cell regulation by material engineering, but it has not yet been performed to date. Part II described the researches aimed at controlling cell behavior directly by topographical effect.

Chapter 4 described the novel fabrication process appropriate for functional regulation of cells. Various processes (*e.g.*, imprint, etching) were exploited for surface fabrication [74-76]. But miscellaneous factors should be considered for cell culture besides the surface topology: for example, the residue of releasing reagents, the distortion by high temperature, and the alteration of surface chemistry in fabrication process. In addition, the target polymers of these processes were restricted, and thereby, it was difficult to apply for the surface fabrication of culture substrate and implants. In this chapter, polymer surfaces were plasticized by the impregnation of supercritical $CO_2$ and then pressed with fine-structured mold. As a result, the chemically uniform surface was fabricated under lower temperature without using

releasing agent. When cultured on the fabricated substrate, MSCs were limited to extend on microlens structure and they aligned along with deeper nano-grooved structures. Thus, the availability of this fabrication process was displayed for the regulation of cell behaviors.

Chapter 5 described the mechanism of cell alignment on nano-grooves that found in the previous chapter. To date, several reports tried to explain the mechanism of cell alignment. According to the explanation by some groups, filopodia probes the topographies of fine-structure when cells extends, whereas others explain that cell adhesiveness to substrates differs from the topography and it causes cell alignment [77-82]. Thus, the experimental results were interpreted on every occasion and a consistent explanation has not yet been established. In this chapter, to reveal the mechanism of cell alignment on nano-grooves, the cell behaviors on grooves, especially filopodial probing, were tracked successively by a time-lapse microscope. As a result, cell alignment was found to be independent of filopodial movements. Cells protrusions retracted more rapidly in the direction perpendicular to grooves than parallel to grooves, indicating that cell alignments on grooves was attributed to anisotropic adhesion.

In summary, this thesis focused on the microenvironments around stem cells and aimed at developing the functional materials. To date, the expansion of HSC has been performed by mainly biological approaches without using biomaterials, because HSC is a non-adherent cell. But in this thesis, as shown in Part I, the HSC niche mimicking-microenvironment was proved to be available in combination with feeder cells, which would lead to exploitation in research and clinical applications. Part II described the basic findings to regulate stem cell adhesion and extension by physical

properties, and showed the beacon that the cell adhesion should be focused to regulate cell alignment. However, the topographical effect on differentiation and proliferation could not been observed experimentally, although the cell alignment was regulated. This is an important issue to be addressed in the future. Moreover, the relationship between morphology, scale effects, cell types, and intercellular effects should be quantified to gain clearer insights into the topographical effects. Comprehensive understandings should make it possible to strictly regulate cell fates for the future clinical application.

Furthermore, it was pointed out that the self-renewal ability of stem cells is common to cancer cells [83]. Researches on stem cells were linked to the field of cancer cells, where cancer stem cells interact with cells in their surrounding 'niche' [84]. For example, the proliferation of leukemia cells was shown to be common to the mechanism of the niche-dependent self-renewal of hematopoietic stem cells [85,86]. And yet, the safety should be adequately considered in the cell therapy using stem cells. Especially, long-term cultivation has a potential risk of irreversible change of cell characteristics or oncogenesis [87,88]. Hopefully, the findings and developed devices proposed in this thesis would lead to not only the quality control of cells but also the success of clinical application in the near future.

# REFERENCES

1 Molofsky AV, Pardal R, Morrison SJ. Diverse mechanisms regulate stem cell self-renewal. *Curr. Opin. Cell Biol.*, 2004, **16**, 700-707.

2 Till JE, McCulloch EA. A direct measurement of the radiation sensitivity of normal mouse bone marrow cells. *Radiat. Res.*, 1961, **14**, 213-222.

3 Bryder D, Rossi DJ, Weissman IL. Hematopoietic stem cells: the paradigmatic tissue-specific stem cell. *Am. J. Pathol.*, 2006, **169**, 338-346.

4 Bjerknes M, Cheng H. Clonal analysis of mouse intestinal epithelial progenitors. *Gastroenterology*, 1999, **116**, 7-14.

5 Alonso L, Fuchs E. Stem cells of the skin epithelium. *Proc. Natl. Acad. Sci. U. S. A.*, 2003, **100** Suppl 1, 11830-11835.

6 Eriksson PS, Perfilieva E, Björk-Eriksson T, Alborn AM, Nordborg C, Peterson DA, Gage FH. Neurogenesis in the adult human hippocampus. *Nat. Med.*, 1998, **4**, 1313-1317.

7 Pittenger MF, Mackay AM, Beck SC, Jaiswal RK, Douglas R, Mosca JD, Moorman MA, Simonetti DW, Craig S, Marshak DR. Multilineage potential of adult human mesenchymal stem cells. *Science*, 1999, **284**, 143-147.

8 Wagers AJ, Weissman IL. Plasticity of adult stem cells. *Cell*, 2004, **116**, 639-648.

9 Evans MJ, Kaufman MH. Establishment in culture of pluripotential cells from mouse embryos. *Nature*, 1981, **292**, 154-156.

10 Thomson JA, Itskovitz-Eldor J, Shapiro SS, Waknitz MA, Swiergiel JJ, Marshall VS, Jones JM. Embryonic stem cell lines derived from human blastocysts. *Science*, 1998, **282**, 1145-1147.

11 Takahashi K, Yamanaka S. Induction of pluripotent stem cells from mouse embryonic and adult fibroblast cultures by defined factors. *Cell*, 2006, **126**, 663-676.

12 Takahashi K, Tanabe K, Ohnuki M, Narita M, Ichisaka T, Tomoda K, Yamanaka S. Induction of pluripotent stem cells from adult human fibroblasts by defined factors. *Cell*, 2007, **131**, 861-872.

13 Vats A, Bielby RC, Tolley NS, Nerem R, Polak JM. Stem cells. *Lancet*, 2005, **366**, 592-602.

14 Zipori D. The stem state: plasticity is essential, whereas self-renewal and hierarchy are optional. *Stem Cells*, 2005, **23**, 719-726.

15 Fuchs E, Tumbar T, Guasch G. Socializing with the neighbors: stem cells and their niche. *Cell*, 2004, **116**, 769-778.

16 Moore KA, Lemischka IR. Stem cells and their niches. *Science*, 2006, **311**, 1880-1885.

17 Calvi LM, Adams GB, Weibrecht KW, Weber JM, Olson DP, Knight MC, Martin RP, Schipani E, Divieti P, Bringhurst FR, Milner LA, Kronenberg HM, Scadden DT. Osteoblastic cells regulate the haematopoietic stem cell niche. *Nature*, 2003, **425**, 841-846.

18 Zhang J, Niu C, Ye L, Huang H, He X, Tong WG, Ross J, Haug J, Johnson T, Feng JQ, Harris S, Wiedemann LM, Mishina Y, Li L. Identification of the haematopoietic stem cell niche and control of the niche size. *Nature*, 2003, **425**, 836-841.

19 Copelan EA. Hematopoietic stem-cell transplantation. *N. Engl. J. Med.*, 2006, **354**, 1813-1826.

20 Rocha V, Gluckman E. Clinical use of umbilical cord blood hematopoietic stem cells. *Biol. Blood Marrow Transplant.*, 2006, **12**, 34-41.

21 Taniguchi S. The current status and future prospect of cord blood stem cell transplantation. *Clinic. All-round*, 2005, **54**, 1786-1790.

22 Monthly results of cord blood transplantation. Tokyo, Japan: Japanese Cord Blood Bank Network. Online. 2008, Available from URL: https://www.j-cord.gr.jp/ja/status/result.html

23 Takanashi M. The cord blood banks. *Igaku no Ayumi*, 2006, **218**, 669-679.

24 Robinson S, Niu T, de Lima M, Ng J, Yang H, McMannis J, Karandish S, Sadeghi T, Fu P, del Angel M, O'Connor S, Champlin R, Shpall E. *Ex vivo* expansion of umbilical cord blood. *Cytotherapy*, 2005, **7**, 243-250.

25 Sorrentino BP. Clinical strategies for expansion of haematopoietic stem cells. *Nat. Rev. Immunol*., 2004, **4**, 878-888.

26 Piacibello W, Sanavio F, Garetto L, Severino A, Bergandi D, Ferrario J, Fagioli F, Berger M, Aglietta M. Extensive amplification and self-renewal of human primitive hematopoietic stem cells from cord blood. *Blood*, 1997, **89**, 2644-2653.

27 Ueda T, Tsuji K, Yoshino H, Ebihara Y, Yagasaki H, Hisakawa H, Mitsui T, Manabe A, Tanaka R, Kobayashi K, Ito M, Yasukawa K, Nakahata T. Expansion of human NOD/SCID-repopulating cells by stem cell factor, Flk2/Flt3 ligand, thrombopoietin, IL-6, and soluble IL-6 receptor. *J. Clin. Invest*., 2000, **105**, 1013-1021.

28 Murray LJ, Young JC, Osborne LJ, Luens KM, Scollay R, Hill BL. Thrombopoietin, flt3, and kit ligands together suppress apoptosis of human mobilized CD34+ cells and recruit primitive CD34+ Thy-1+ cells into rapid division. *Exp. Hematol*., 1999, **27**, 1019-1028.

29 Levac K, Karanu F, Bhatia M. Identification of growth factor conditions that reduce *ex vivo* cord blood progenitor expansion but do not alter human repopulating cell

function in vivo. *Haematologica*, 2005, **90**, 166-172.

30 Antonchuk J, Sauvageau G, Humphries RK. HOXB4-induced expansion of adult hematopoietic stem cells ex vivo. *Cell*, 2002, **109**, 39-45.

31 Schofield R. The relationship between the spleen colony-forming cell and the haemopoietic stem cell. *Blood Cells*, 1978, **4**, 7-25.

32 Dexter TM, Allen TD, Lajtha LG. Conditions controlling the proliferation of haemopoietic stem cells in vitro. *J. Cell Physiol*., 1977, **91**, 335-344.

33 Verfaillie CM. Hematopoietic stem cells for transplantation. *Nat. Immunol*., 2002, **3**, 314-317.

34 Kawada H, Ando K, Tsuji T, Shimakura Y, Nakamura Y, Chargui J, Hagihara M, Itagaki H, Shimizu T, Inokuchi S, Kato S, Hotta T. Rapid ex vivo expansion of human umbilical cord hematopoietic progenitors using a novel culture system. *Exp. Hematol*., 1999, **27**, 904-915.

35 Nakamura Y, Ando K, Chargui J, Kawada H, Sato T, Tsuji T, Hotta T, Kato S. Ex vivo generation of CD34(+) cells from CD34(-) hematopoietic cells. *Blood*, 1999, **94**, 4053-4059.

36 Chapman LE, Folks TM, Salomon DR, Patterson AP, Eggerman TE, Noguchi PD. Xenotransplantation and xenogeneic infections. *N. Engl. J. Med*., 1995, **333**, 1498-1501.

37 Fishman JA, Patience C. Xenotransplantation: infectious risk revisited. *Am. J. Transplant*., 2004, **4**, 1383-1390.

38 Bucher P, Morel P, Bühler LH. Xenotransplantation: an update on recent progress and future perspectives. *Transpl. Int*., 2005, **18**, 894-901.

39 Director, Research and Development Division, Health Policy Bureau, Ministry of

Health, Labour and Welfare of Japan. Public Health Guidelines on Infectious Disease Issues in Xenotransplantation. *Iseikenhatsu*, No. 0709001, July 9, 2002.

40 Reese JS, Koc ON, Gerson SL. Human mesenchymal stem cells provide stromal support for efficient CD34+ transduction. *J. Hematother. Stem Cell Res*., 1999, **8**, 515-523.

41 Kawano Y, Kobune M, Yamaguchi M, Nakamura K, Ito Y, Sasaki K, Takahashi S, Nakamura T, Chiba H, Sato T, Matsunaga T, Azuma H, Ikebuchi K, Ikeda H, Kato J, Niitsu Y, Hamada H. Ex vivo expansion of human umbilical cord hematopoietic progenitor cells using a coculture system with human telomerase catalytic subunit (hTERT)-transfected human stromal cells. *Blood*, 2003, **101**, 532-540.

42 Kögler G, Radke TF, Lefort A, Sensken S, Fischer J, Sorg RV et al. Cytokine production and hematopoiesis supporting activity of cord blood-derived unrestricted somatic stem cells. *Exp. Hematol.*, 2005, **33**, 573-583.

43 Zhang Y, Chai C, Jiang XS, Teoh SH, Leong KW. Co-culture of umbilical cord blood CD34+ cells with human mesenchymal stem cells. *Tissue Eng*., 2006, **12**, 2161-2170.

44 Digirolamo CM, Stokes D, Colter D, Phinney DG, Class R, Prockop DJ. Propagation and senescence of human marrow stromal cells in culture: a simple colony-forming assay identifies samples with the greatest potential to propagate and differentiate. *Br. J. Haematol*., 1999, **107**, 275-281.

45 Okamoto T, Aoyama T, Nakayama T, Nakamata T, Hosaka T, Nishijo K, Nakamura T, Kiyono T, Toguchida J. Clonal heterogeneity in differentiation potential of immortalized human mesenchymal stem cells. *Biochem. Biophys. Res. Commun*., 2002, **295**, 354-361.

46 Androutsellis-Theotokis A, Leker RR, Soldner F, Hoeppner DJ, Ravin R, Poser SW,

Rueger MA, Bae SK, Kittappa R, McKay RDG. Notch signalling regulates stem cell numbers in vitro and in vivo. *Nature*, 2006, **442**, 823-826..

47 Taipale J, Keski-Oja J. Growth factors in the extracellular matrix. *FASEB J.*, 1997, **11**, 51-59.

48 Iwata H, Takagi T, Amemiya H, Shimizu H, Yamashita K, Kobayashi K, Akutsu T. Agarose for a bioartificial pancreas. *J. Biomed. Mater. Res*., 1992, **26**, 967-977.

49 Wognum AW, Eaves AC, Thomas TE. Identification and isolation of hematopoietic stem cells. *Arch. Med. Res*., 2003, **34**, 461-475.

50 Broxmeyer HE. Colony assays of hematopoietic progenitor cells and correlations to clinical situations. *Crit. Rev. Oncol. Hematol*., 1984, **1**, 227-257.

51 Sutherland HJ, Lansdorp PM, Henkelman DH, Eaves AC, Eaves CJ. Functional characterization of individual human hematopoietic stem cells cultured at limiting dilution on supportive marrow stromal layers. *Proc. Natl. Acad. Sci. U. S. A*., 1990, **87**, 3584-3588.

52 Breems DA, Blokland EA, Neben S, Ploemacher RE. Frequency analysis of human primitive haematopoietic stem cell subsets using a cobblestone area forming cell assay. *Leukemia*, 1994, **8**, 1095-1104.

53 Ploemacher RE, van der Sluijs JP, Voerman JS, Brons NH. An in vitro limiting-dilution assay of long-term repopulating hematopoietic stem cells in the mouse. *Blood*, 1989, **74**, 2755-2763.

54 Hao QL, Thiemann FT, Petersen D, Smogorzewska EM, Crooks GM. Extended long-term culture reveals a highly quiescent and primitive human hematopoietic progenitor population. *Blood*, 1996, **88**, 3306-3313.

55 Cheng T, Rodrigues N, Shen H, Yang Y, Dombkowski D, Sykes M, Scadden DT.

Hematopoietic stem cell quiescence maintained by p21cip1/waf1. *Science*, 2000, **287**, 1804-1808.

56 Zhou S, Schuetz JD, Bunting KD, Colapietro AM, Sampath J, Morris JJ, Lagutina I, Grosveld GC, Osawa M, Nakauchi H, Sorrentino BP. The ABC transporter Bcrp1/ABCG2 is expressed in a wide variety of stem cells and is a molecular determinant of the side-population phenotype. *Nat. Med*., 2001, 7, 1028-1034.

57 Scharenberg CW, Harkey MA, Torok-Storb B. The ABCG2 transporter is an efficient Hoechst 33342 efflux pump and is preferentially expressed by immature human hematopoietic progenitors. *Blood*, 2002, 99, 507-512.

58 El-Ali J, Sorger PK, Jensen KF. Cells on chips. *Nature*, 2006, **442**, 403-411.

59 Deans RJ, Moseley AB. Mesenchymal stem cells: biology and potential clinical uses. *Exp. Hematol*., 2000, **28**, 875-884.

60 Mauney JR, Volloch V, Kaplan DL. Role of adult mesenchymal stem cells in bone tissue engineering applications: current status and future prospects. *Tissue Eng*., 2005, **11**, 787-802.

61 Redman SN, Oldfield SF, Archer CW. Current strategies for articular cartilage repair. *Eur. Cell. Mater*., 2005, **9**, 23-32.

62 Dimmeler S, Zeiher AM, Schneider MD. Unchain my heart: the scientific foundations of cardiac repair. *J. Clin. Invest*., 2005, **115**, 572-583.

63 Tögel F, Hu Z, Weiss K, Isaac J, Lange C, Westenfelder C. Administered mesenchymal stem cells protect against ischemic acute renal failure through differentiation- independent mechanisms. *Am. J. Physiol. Renal. Physiol*., 2005, **289**, F31-F42.

64 Oreffo RO, Cooper C, Mason C, Clements M. Mesenchymal stem cells: lineage,

plasticity, and skeletal therapeutic potential. *Stem Cell Rev*., 2005, **1**, 169-178.

65 Kong HJ, Mooney DJ. Microenvironmental regulation of biomacromolecular therapies. *Nat. Rev. Drug Discov*., 2007, **6**, 455-463.

66 Dumont JE, Dremier S, Pirson I, Maenhaut C. Cross signaling, cell specificity, and physiology. *Am. J. Physiol. Cell Physiol*., 2002, **283**, C2-C28.

67 Chen CS, Mrksich M, Huang S, Whitesides GM, Ingber DE. Geometric control of cell life and death. *Science*, 1997, **276**, 1425-1428.

68 Park JS, Chu JSF, Cheng C, Chen F, Chen D, Li S. Differential effects of equiaxial and uniaxial strain on mesenchymal stem cells. *Biotechnol. Bioeng.,* 2004, **88**, 359-368.

69 Kurpinski K, Chu J, Hashi C, Li S. Anisotropic mechanosensing by mesenchymal stem cells. *Proc. Natl. Acad. Sci. U. S. A*., 2006, **103**, 16095-16100.

70 Zhu B, Lu Q, Yin J, Hu J, Wang Z. Alignment of osteoblast-like cells and cell-produced collagen matrix induced by nanogrooves. *Tissue Eng*., 2005, **11**, 825-834.

71 Dalby MJ, Gadegaard N, Tare R, Andar A, Riehle MO, Herzyk P, Wilkinson CD, Oreffo RO. The control of human mesenchymal cell differentiation using nanoscale symmetry and disorder. *Nat. Mater*., 2007, **6**, 997-1003.

72 Engler AJ, Sen S, Sweeney HL, Discher DE. Matrix elasticity directs stem cell lineage specification. *Cell*, 2006, **126**, 677-689.

73 McBeath R, Pirone DM, Nelson CM, Bhadriraju K, Chen CS. Cell shape, cytoskeletal tension, and RhoA regulate stem cell lineage commitment. *Dev. Cell*., 2004, **6**, 483-495.

74 Lee LJ, Polymer nanoengineering for biomedical applications, *Ann. Biomed. Eng*.,

2006, **34**, 75-88.

75 Giboz J, Copponnex T, Mélé P. Microinjection molding of thermoplastic polymers: A review. *J. Micromech. Microeng*., 2007, **17**, R96-R109.

76 Charest JL, Bryant LE, Garcia AJ, King WP. Hot embossing for micropatterned cell substrates. *Biomaterials*, 2004, **25**, 4767-4775.

77 Wójciak-Stothard B, Curtis A, Monaghan W, MacDonald K, Wilkinson C. Guidance and activation of murine macrophages by nanometric scale topography. *Exp. Cell. Res*., 1996, **223**, 426-435.

78 Clark P, Connolly P, Curtis ASG, Dow JAT, Wilkinson CDW. Topographical control of cell behaviour: II. multiple grooved substrata. *Development*, 1990, **108**, 635-644.

79 Curtis A, Wilkinson C. Topographical control of cells. *Biomaterials*, 1997, **18**, 1573-1583.

80 Flemming RG, Murphy CJ, Abrams GA, Goodman SL, Nealey PF. Effects of synthetic micro- and nano-structured surfaces on cell behavior. *Biomaterials*, 1999, **20**, 573-588.

81 Teixeira AI, McKie GA, Foley JD, Bertics PJ, Nealey PF, Murphy CJ. The effect of environmental factors on the response of human corneal epithelial cells to nanoscale substrate topography. *Biomaterials*, 2006, **27,** 3945-3954.

82 Lim JY, Donahue HJ. Cell sensing and response to micro- and nanostructured surfaces produced by chemical and topographic patterning. *Tissue Eng*., 2007, **13**, 1879-1891.

83 Miller SJ, Lavker RM, Sun TT. Interpreting epithelial cancer biology in the context of stem cells: tumor properties and therapeutic implications. *Biochim. Biophys. Acta*., 2005, **1756**, 25-52.

84 Sneddon JB, Werb Z. Location, location, location: the cancer stem cell niche. *Cell Stem Cell*, 2007, **1**, 607-611.

85 Jin L, Hope KJ, Zhai Q, Smadja-Joffe F, Dick JE. Targeting of CD44 eradicates human acute myeloid leukemic stem cells. *Nat. Med*., 2006, **12**, 1167-1174.

86 Krause DS, Lazarides K, von Andrian UH, Van Etten RA. Requirement for CD44 in homing and engraftment of BCR-ABL-expressing leukemic stem cells. *Nat. Med*., 2006, **12**, 1175-1180.

87 Weissman I. Stem cell research: paths to cancer therapies and regenerative medicine. *J. Am. Med. Assoc.*, 2005, **294**, 1359-1366.

88 Hentze H, Graichen R, Colman A. Cell therapy and the safety of embryonic stem cell-derived grafts. *Trends Biotechnol*., 2007, **25**, 24-32.

# PART I

# EXPANSION OF HEMATOPOIETIC STEM CELLS BY MIMICKING HEMATOPOIETIC NICHE

# CHAPTER 1

# Clonal analysis of hematopoiesis-supporting activity of human mesenchymal stem cells in association with Jagged1 expression and osteogenic potential

## INTRODUCTION

Hematopoietic stem cells (HSCs) exist in endosteal hematopoietic microenvironments created by osteoblasts [1,2], and receive hematopoiesis signals through direct contacts with various adherent molecules of cells in the microenvironment, such as N-cadherin / ß-catenin [1,3,4], angiopoietin-1 / Tie-2 [5] and Jagged1 / Notch [2]. In recent years, interest in the role of mesenchymal stem cells (MSCs) in hematopoietic microenvironments has grown. Human MSCs (hMSC) isolated from bone marrow can be used as effective feeder cells for *ex vivo* expansion of HSCs [6-8]. Noort and colleagues showed that the co-transplantation of umbilical cord blood HSCs and hMSCs into immunodeficient mice efficiently promoted engraftment of HSCs [9]. Furthermore, calcium-sensing receptors expressed on HSCs detected calcium ion concentration in their surroundings and thereby osteogenic progeny of hMSCs are expected to play an important role in the engraftment of HSCs

within an endosteal hematopoietic niche [10]. Taken together, these studies suggest that hMSC or their progeny committed to osteoblasts have the potential to form a hematopoietic niche. Therefore, an examination of the correlation between the hematopoiesis-supporting activity of hMSC and their potential to differentiate to osteogenic progeny would be valuable.

Primary hMSCs are heterogeneous within a cell population, and each hMSC has an individual potential toward different lineages [11-15]. This heterogeneity causes difficulty in understanding the experimental results of hMSC analysis. In this chapter, clonal cell lines of hMSCs immortalized by gene modification [12] were used, and their abilities to support hematopoiesis by *in vitro* coculture experiments was examined. The results were analyzed in conjunction with the osteogenic potential and expression of genes related to osteogenesis.

## EXPERIMENTAL

### *Collection of cord blood hematopoietic stem cells*

Studies were approved by the institutional review board. Umbilical cord blood was obtained from healthy donors, with their informed consent. The $CD34^+$ cell fraction that is rich in HSCs was isolated from fresh umbilical cord blood as previously reported [16]. In brief, mononuclear cells were collected by the density gradient centrifugation using Lymphoprep (AXIS-SHIELD PoC AS, Oslo, Norway). After washing twice with Dulbecco's phosphate-buffered saline $Ca^{2+}Mg^{2+}$ free (DPBS(-); Nissui Pharmaceutical Co. Ltd., Tokyo, Japan), $CD34^+$ cells were isolated using magnetic

beads (Direct CD34 Progenitor Cell Isolation Kit; Miltenyi Biotech GmbH, Bergisch Gladbach, Germany) in accordance with the manufacturer's instructions. Isolated $CD34^+$ cells were cryopreserved using a cryopreservation solution containing bovine serum (Cellbanker, Nippon Zenyaku Kogyo Co., Ltd., Fukushima, Japan) until use.

***Culture of mesenchymal stem cells***

Sixteen hMSC clones were established from human bone marrow MSCs immortalized by genetic modification using human telomerase reverse transcriptase (hTERT) gene and human papilloma virus E6 and E7 genes [12], kindly donated by Dr. T. Aoyama (Institute for Frontier Medical Sciences, Kyoto University). Each hMSC clone was maintained in Dulbecco's Modified Essential Medium (DMEM; Invitrogen Corp., CA, USA) supplemented with 10% fetal bovine serum (FBS; BIOWEST, France), 100 U/mL penicillin and 100 μg/mL streptomycin (Invitrogen) at 37 °C under 5% $CO_2$ in a humidified atmosphere, and subcultured at 5 - 8 × $10^3$ per $cm^2$ every three to four days.

***Coculture of hematopoietic stem cells with mesenchymal stem cells***

Hematopoiesis-supporting activity of each hMSC clone was evaluated by the increase of $CD34^+CD38^-$ cells after coculture of $CD34^+$ cells. Immortalized hMSCs were seeded at 2 × $10^5$ per well of a 12-well multiplate. After adhesion, they were irradiated by X-ray at a dose of 15 Gy to stop proliferation and then washed five times with Hanks' Balanced Salt Solution containing $Ca^{2+}$ and $Mg^{2+}$ (HBSS (+); Invitrogen). $CD34^+$ cells were obtained by thawing a frozen stock, suspended at 2.5 × $10^3$ cells/mL in serum-free medium for hematopoietic cell culture (StemPro-34 SFM; Invitrogen) supplemented with 2 mM L-alanyl-L-glutamine (GLUTAMAX I; Invitrogen), 50 ng/mL

Flt-3 ligand, 50 ng/mL stem cell factor and 50 ng/mL thrombopoietin (StemSpan CC110; Stemcell Technologies Inc., Vancouver, Canada), and inoculated into each well of irradiated hMSCs at $5 \times 10^3$ cells/well. After 7-day coculture at 37 °C under 5% $CO_2$ in a humidified atmosphere without exchanging culture medium, all cells were dissociated with 0.05% Trypsin-EDTA solution (Invitrogen) and collected for cell counting and characterization by flow cytometry (FCM).

***Flow cytometric analyses of CD34$^+$ cell progeny***

Immunophenotypic enumeration of the $CD34^+$ cell progeny was performed by FCM [16]. Collected cells ($1–10 \times 10^5$ cells) were suspended in 100 μL of DPBS with 0.1% FBS, with addition of 2 μL of the fluorescence dye-conjugated antibodies (1:50 dilution), and incubated at 4 °C for 30 min to label surface antigens. Thawed cells were additionally co-stained with propidium iodide to exclude dead cells in the following FCM analysis. Stained cells were washed twice with DPBS with 0.1% FBS, and subjected to FCM analysis by FACSCalibur (BD Biosciences). For quantification of cell number, a 50 μL aliquot of a polystyrene fluorescent microsphere suspension (Flow-Count; Beckman Coulter, Inc., CA, USA) (containing $5 \times 10^4$ particles) was added into the sample cell suspension prior to analysis. To reduce the noise of non-blood cells, the region of blood cells was determined by a FSC - SSC gating and a following $CD45^+$ gating. The $CD34^+$ and $CD38^+$ quadrants were determined by reference to isotypic controls. $CD45^{bright}CD34^+$ cells were excluded as being non-specifically stained cells.

Monoclonal antibodies used for cell surface markers were as follows: fluorescein isothiocyanate (FITC)–conjugated anti-human CD34 (clone 581) and

allophycocyanin (APC)-conjugated anti-human CD45 (clone HI30) were purchased from BD Pharmingen (CA, USA), and phycoerythrin (PE)-conjugated anti-human CD38 (clone HB7) was purchased from Becton, Dickinson and Co. (CA, USA).

***Gene expression analyses of mesenchymal stem cells***

The gene expression of hMSCs was analyzed by reverse transcriptase polymerase chain reaction (RT-PCR). Total RNA was extracted from approximately 3 × $10^6$ hMSCs using SV Total RNA Isolation System (Promega Corp., WI, USA), in which DNase processing is included. Complementary DNA (cDNA) was then synthesized from extracted total RNA using Ready-To-Go You-Prime First-Strand Beads (Amersham Biosciences Corp., NJ, USA) with oligo $d(T)_{12-18}$ primers (Promega). Specific cDNA was amplified by PCR under the following conditions: 1) a reaction mix (25 μL) was composed of 2 mM Tris-HCl (pH 8.0), 10 mM KCl, 0.01 mM EDTA, 0.1 mM DTT, 1 U DNA polymerase (*TaKaRa Ex Taq*; Takara Bio Inc., Shiga, Japan), 0.2 mM dNTP mixture, 0.5 μM of each primer and approximately 100 ng of cDNA

***Table 1-1.*** Primer sequences for RT-PCR

| Gene | Primer Ssequences (5' – 3') | GenBank Accession No. | Annealing Temp. | Number of Cycles | Size of Product | Ref. |
|---|---|---|---|---|---|---|
| RUNX2 | CAGTTCCCAAGCATTTCATCC<br>TCAATATGGTCGCCAAACAG | AF001450 | 55 | 35 | 443 | [17] |
| Osterix | TTGACTGCAGAGCAGGTTCCT<br>GCTGCAAGCTCTCCATAACCA | AF477981 | 62 | 35 | 97 | [18] |
| Jagged1 | AGTCACTGGCACGGTTGTAG<br>TCGCTGTATCTGTCCACCTG | U61276 | 62 | 35 | 227 | [19] |
| Delta-1 | AGACGGAGACCATGAACAAC<br>TCCTCGGATATGACGTACAC | AF003522 | 60 | 35 | 382 | [19] |
| N-cadherin | CAAGTGCCATTAGCCAAGG<br>TTAAGCCGAGTGATGGTCC | S42303 | 60 | 25 | 578 | [20] |
| Wnt-3 | TGAACAAGCACAACAACGAG<br>CAGTGGCATTTTTCCTTCC | AB067628 | 60 | 35 | 439 | [21] |
| Angiopoietin-1 | GGAAGTCTAGATTTCCAAAGAGGC<br>CTTTATCCCATTCAGTTTTCCATG | D13628 | 62 | 35 | 429 | [22] |
| GAPDH | AGCCGCATCTTCTTTTGCGTC<br>TCATATTTGGCAGGTTTTTCT | NM_002046 | 55 | 25 | 816 | [17] |

template; 2) temperature settings for each cycle were 95 °C for 30 sec for denaturing, 55 - 62 °C for 1 min for annealing, and 72 °C for 2 min for extension. The optimal PCR cycle conditions were adjusted by the brightness of the visualized band. All primer sequences are listed in Table 1-1. Amplified products (9 μL) were electrophoresed in 2% SeaKem GTG Agarose gel containing 0.5 μg/mL ethidium bromide at 100 V for 30 min, and the bands of PCR products were observed on an ultraviolet illuminator.

Real-time quantitative PCR was performed using ABI Prism StepOne System (Applied Biosystems, CA, USA) to quantify Jagged1 expression level. In brief, the PCR 2× master mix was based on AmpliTaq Gold DNA polymerase (Applied Biosystems). Samples (2 μl for a total volume of 20 μL per reaction) were analyzed for the gene expression of both Jagged1 and GAPDH (as a reference). All primers were the same as mentioned above. Expression levels of Jagged1 for each MSC were evaluated by normalizing the quantified mRNA amount to GAPDH. Each sample was assessed at least in duplicate.

***Osteogenic differentiation of mesenchymal stem cells***

The differentiation of MSC was performed following the method reported by Pittenger *et al* [11]. An immortalized MSC clone was seeded at $5 \times 10^5$ per well of a 6-well multiplate. Cells were cultured with DMEM supplemented with 100 nM dexamethasone (Sigma-Aldrich, MO, USA), 50 μM ascorbic acid 2-phosphate (Wako Pure Chemical Industries, Ltd., Osaka, Japan), 10 mM ß-glycerophosphate (Wako) and 10 % FBS. Culture media were changed freshly every 2 or 3 day. The presence of mineralized deposits after osteogenic differentiation was determined with von Kossa

staining. In brief, on day 14, triplets of cultured wells were rinsed twice with DPBS(-), then fixed with 10% formaldehyde for 30 min, and washed three times with distilled water. One mL of 5% (w/v) silver nitrate (Nacalai Tesque, Inc., Kyoto, Japan) was added per well, and the cultures were placed in the dark for 30 min. Cultures were then washed with water and were developed with 5% (w/v) sodium carbonate in 25% formaldehyde for 5 min. After development, cultures were washed and sodium thiosulfate (5%) was added to stop development. Cultures were washed again with water and air-dried. Amounts of calcium deposits were evaluated from image analyses using the software ImageJ ver.1.37.

***Adipogenic differentiation of mesenchymal stem cells***

A hMSC clone was seeded at $5 \times 10^5$ per well of a 6-well multiplate. The adipogenic differentiation was initiated by three cycles of induction / maintenance culture. Each cycle consists of 3 days of culture in the induction medium, [DMEM containing 1 μM dexamethasone (Sigma-Aldrich), 0.2 mM indomethacin (Wako), 10 μg/mL insulin (Sigma-Aldrich), 0.5 mM 3-isobutyl-l-methylxanthine (Sigma-Aldrich), and 10% FBS], followed by a 2-day culture in the maintenance medium (DMEM with 10% FBS and 10 μg/mL insulin). After adipogenic induction, cells were fixed in 4% paraformaldehyde and incubated with Oil Red-O (Wako) to stain lipid vacuoles.

***Coculture of hematopoietic stem cells with osteogenic progeny of hMSC***

Hematopoiesis-supporting activity of differentiated hMSC clone was also evaluated by coculturing $CD34^+$ cells. Immortalized hMSCs were seeded at confluent density ($2 \times 10^5$ per well of a 12-well multiplate). The hMSCs were cultured with an

osteogenic induction medium as mentioned above for 7 days. Culture media were changed freshly at day 3 and 6. $CD34^+$ cells were inoculated into each well of hMSC progeny and cocultured in a serum-free medium for hematopoietic cell culture as mentioned above. After 7-day coculture, all cells were dissociated and collected for flow cytometry.

***Statistical analyses***

Comparisons between two groups were performed by Student's t-test. $P < 0.05$ was considered statistically significant. All statistical calculations were performed using the software JMP ver.5.1.1.

## RESULTS

***Expansion of $CD34^+$ cells by coculture with hMSC***

Sixteen immortalized hMSC clones were examined to analyze their hematopoiesis-supporting activities at the clonal level. All of hMSC clones were derived from the identical parental hMSCs using the same procedures. The $CD34^+CD38^-$ cell population in progeny of $CD34^+$ cells, known to be rich in early HSCs [23,24], was determined by FCM after 7-day coculture of $CD34^+$ cells with hMSC clones. Representative FCM profiles of the progeny of $CD34^+$ cells for CD34 and CD38 before and after 7-day coculture were examined (Fig. 1-1). Interestingly, the proliferation of $CD34^+$ cells cocultured with hMSC differed among different hMSC clones. In Clone 18, a large number of $CD34^+CD38^-$ cells were observed, suggesting

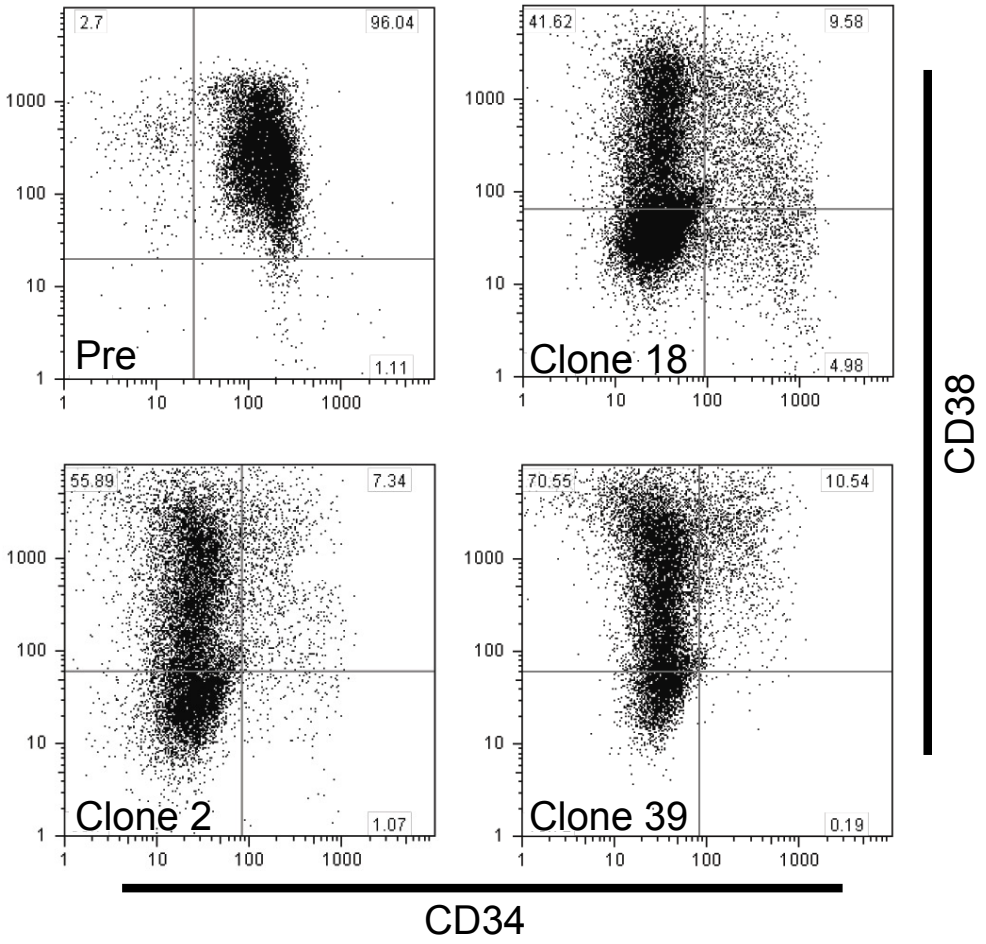


***Figure 1-1.*** FCM analyses of progeny of $CD34^+$ cells after 7 days coculture with hMSCs. Pre: typical cytogram of pre-culture $CD34^+$ cells; Clones 18, 2 and 39: typical cytograms of progeny of $CD34^+$ cells cocultured with each hMSC. In all cytograms, both $CD45^-$ cells (MSC) and $CD45^{bright}CD34^+$ cells (non-specifically stained) were excluded. The quadrant regions were determined by referring to isotypic controls.

that this clone has a high potential to expand the population of early HSCs. On the other hand, poor expansion of $CD34^+CD38^-$ cells was noted in cocultures with Clones 2 or 39 (Fig. 1-1, lower panels).

After 7-day coculture with hMSC clones, numbers of total nucleated cells, $CD34^+$ cells, and $CD34^+CD38^-$ cells were determined from FCM profiles (Fig. 1-2). Total nucleated cell numbers significantly increased more than 100-fold in all hMSC clones after coculture, as compared to inoculated $CD34^+$ cells, but among the hMSC clones, no clear differences in their potentials were evident (Fig. 1-2(A)). Thirteen of 16 clones effectively increased numbers of $CD34^+$ cells (Fig. 1-2(B)). In addition, Clones 18, 27, 17, 3, 35 and 44 efficiently increased numbers of $CD34^+CD38^-$ cells 658-, 534-, 511-, 862-, 515- and 576-fold with respect to their respective initial numbers of $CD34^+CD38^-$ cells in seeded cells (Fig. 1-2(C)). Although Clones 14, 2, 6 and 55 expanded $CD34^+$ cells significantly, the same trend was not apparent for $CD34^+CD38^-$ cells.

The formation of a colony that looks like cobblestones underneath feeder cells is accepted as a distinctive feature for expanding HSCs upon coculture [25,26]. Phase contrast microphotographs of $CD34^+$ progeny after 7-day coculture show numerous cobblestone colonies for Clones 18 and 27 (Fig. 1-3, upper panels). A smaller number of cobblestone colonies were found in the coculture with Clone 2, and only a few were observed for Clone 39 (Fig. 1-3, lower panels). The colony sizes in cocultures with Clones 2 and 39 were much smaller than those found in cocultures with Clones 18 and 27 (Fig. 1-3).

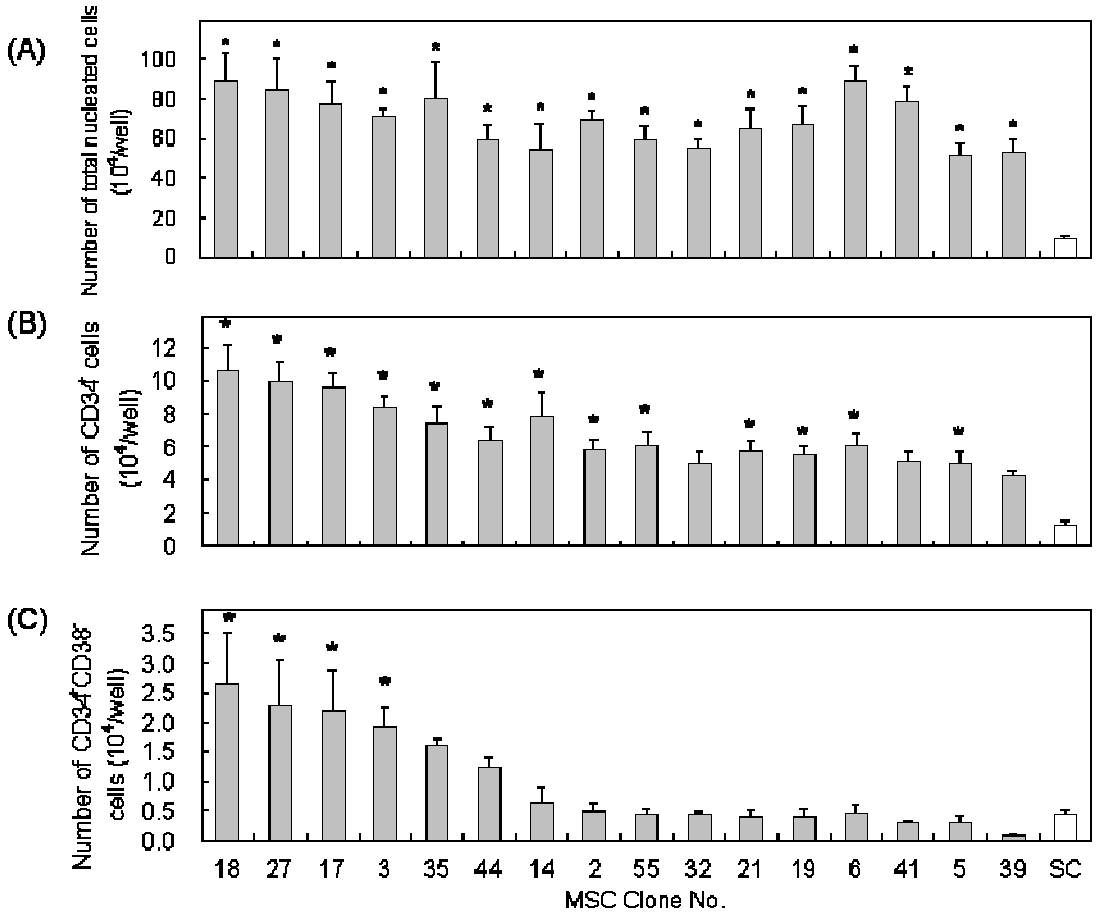


***Figure 1-2.*** Summary of cell number expansion by coculturing $CD34^+$ cells with hMSCs for 7 days. (A) Total nucleated cells; (B) $CD34^+$ cells; (C) $CD34^+CD38^-$ cells. Numbers on x-axis represent hMSC clone numbers, and SC means the suspension culture without hMSC feeder layer as a control. Cell numbers are expressed by means ± SEM [n = 16 (MSC-2 and 3), 13 (SC), 6 (MSC-5, 6 and 55), 3 (others)]. Asterisks indicate significantly larger cell numbers than those of SC ($p < 0.05$).

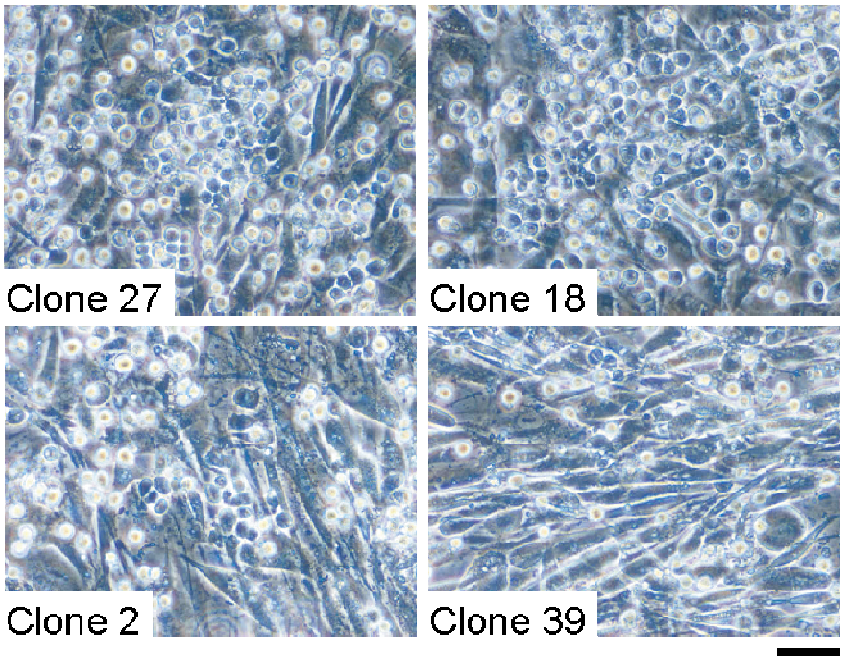


***Figure 1-3.*** Phase contrast microphotographs of cobblestone area-forming cells (CAFCs) observed after 7-day coculture with Clones 27, 18, 2 and 39. CAFCs are seen as round and black cells in pictures, whereas MSCs are elongated, fibroblastic cells. White round-shape cells are non-adherent blood cells and not CAFCs. Bar = 50 μm.

***mRNA expression profiles in undifferentiated MSC clones***

To investigate the proposal that the hematopoiesis-supporting activities of the hMSC clones are correlated with their osteogenic potentials, the mRNA expression levels of the osteogenic transcriptional factors, RUNX2 and Osterix in undifferentiated hMSC clones were examined. All of clones expressed RUNX2 clearly, but none of the clones expressed Osterix (Fig. 1-4). No clear differences were observed among hMSC clones in an osteogenic stage from the standpoint of mRNA expressions of RUNX2 and

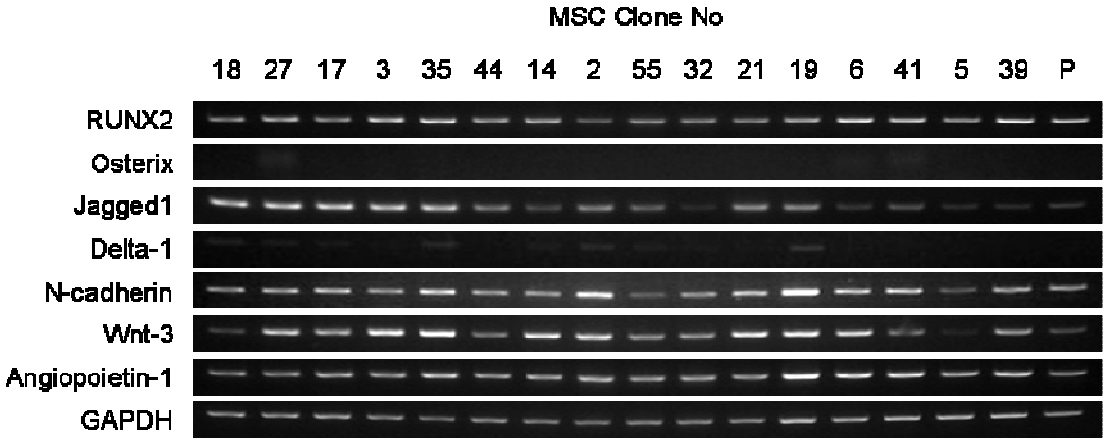


***Figure 1-4.*** Gene expression analysis of undifferentiated MSC clones by RT-PCR. Primers used are listed in Table 1-1. MSC clone numbers are shown above the figure. 'P' represents a primary bone marrow hMSC. GAPDH was used as a loading control.

Osterix. Gene expression of Wnt-3, N-cadherin and Angiopoietin-1 in MSC clones, which have been reported as key proteins included in hematopoiesis [1,3-5], was also examined, but no remarkable difference in their expression levels was found among clones as shown in Fig. 1-4. The expression of Notch ligands, Jagged1 and Delta-1, which serve as signal membrane molecules between stem cells and stromal cells [2,27], were also examined. Clones 3, 17, 18, 27 and 35 expressed Jagged1 at high levels. On the other hand, Delta-1 was poorly expressed in most of clones.

***Calcium deposition on hMSC cells after osteogenic differentiation***

Calcium-sensing receptors expressed on HSCs play an important role in the engraftment of HSCs in endosteal hematopoietic microenvironments [10]. Correlation between osteogenic potential and hematopoiesis-supporting activity was examined. Each hMSC clone was cultured in an osteogenic induction medium for 14 days, and then mineral deposits were visualized by von Kossa staining (Fig. 1-5). hMSCs were also characterized by potential to differentiate into adipogenic cells (Fig 1-6). The results are summarized in Table 1-2. Calcium deposits seen as a large number of black nodules were seen on progenies of Clones 18 and 27 after 14-day osteogenic induction. Taken together, the results presented in Figs. 1-1, 1-5, 1-6 and Table 1-2 showed that all of the hMSC clones that differentiated to osteogenic lineages effectively supported

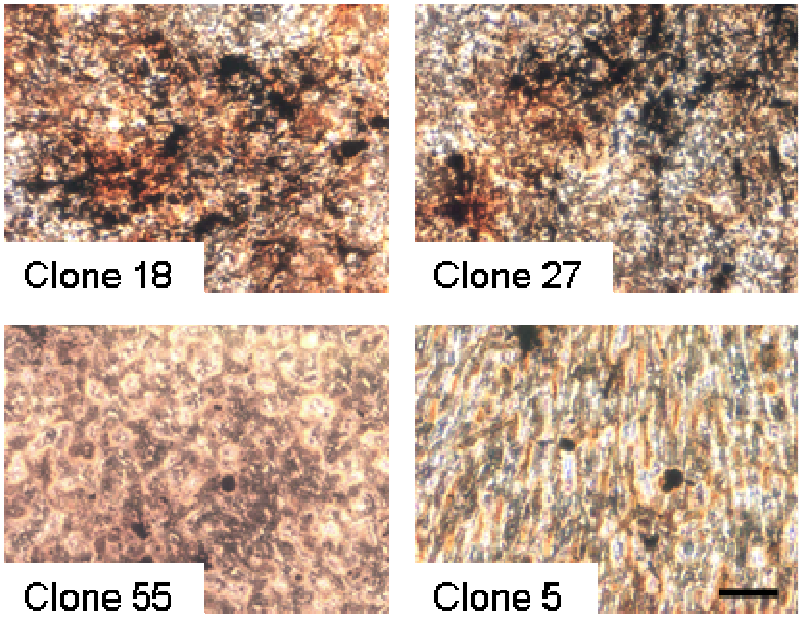


***Figure 1-5.*** Inverted phase contrast microscopic images of von Kossa-stained hMSCs after osteogenic induction at day 14. Calcium deposits were clearly seen on progenies of Clones 18 and 27. Bar = 50 μm

generation of $CD34^+CD38^-$ cells from $CD34^+$ cells after 7-day coculture. In contrast, neither negative nor positive correlation between adipogenic potential and hematopoiesis-supporting activity was found.

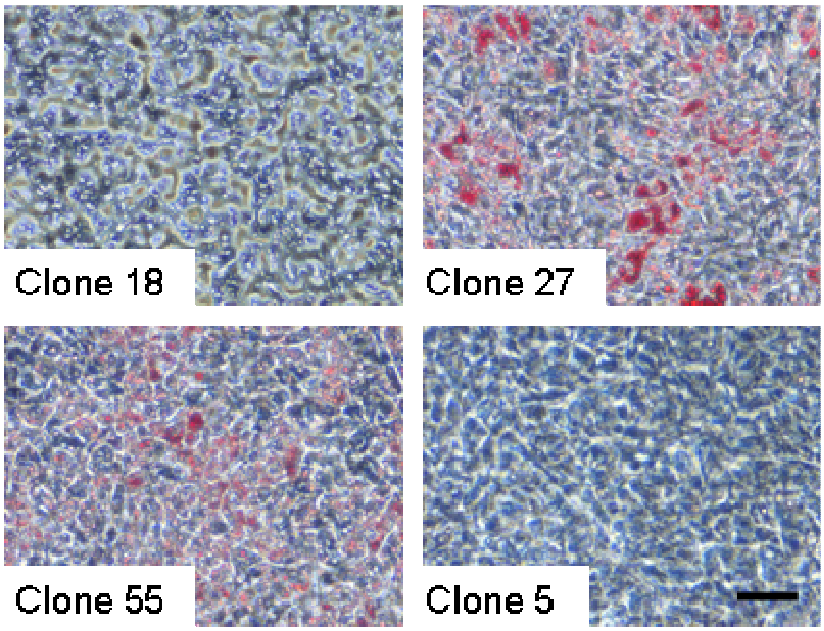


***Figure 1-6.*** Lipid vacuoles on progenies of hMSCs after adipogenic induction. hMSCs were culture in an adipogenic condition for 9 days and then cells were stained by Oil-Red-O. Lipid vacuoles stained with Oil-Red-O were clearly seen on progenies of Clones 27 and 55. Bar = 50 μm.

| Clone No | 18 | 27 | 17 | 3 | 35 | 44 | 14 | 2 | 55 | 32 | 21 | 19 | 6 | 41 | 5 | 39 |
|---|---|---|---|---|---|---|---|---|---|---|---|---|---|---|---|---|
| Osteogenic Potency | + | + | + | + | + | + | + | + | - | - | - | - | - | - | - | - |
| Adipogenic Potency | - | + | + | + | + | - | + | + | + | + | - | + | + | + | - | + |

***Table 1-2.*** The notations represent the osteogenic and adipogenic potential of each clone.

Calcium deposition of hMSCs which occurs after differentiation to osteogenic lineage seems to afford a favorable microenvironment for HSCs. $CD34^+$ cells were cocultured with progeny of hMSC which was prepared by culturing in an osteogenic induction medium for 7 days (Fig. 1-7). In contrast to the expectation, Clones 18 and 27which can effectively increase total cell and $CD34^+$ numbers and support generation of $CD34^+CD38^-$ cells lost their hematopoiesis-supporting activity after osteogenic induction.

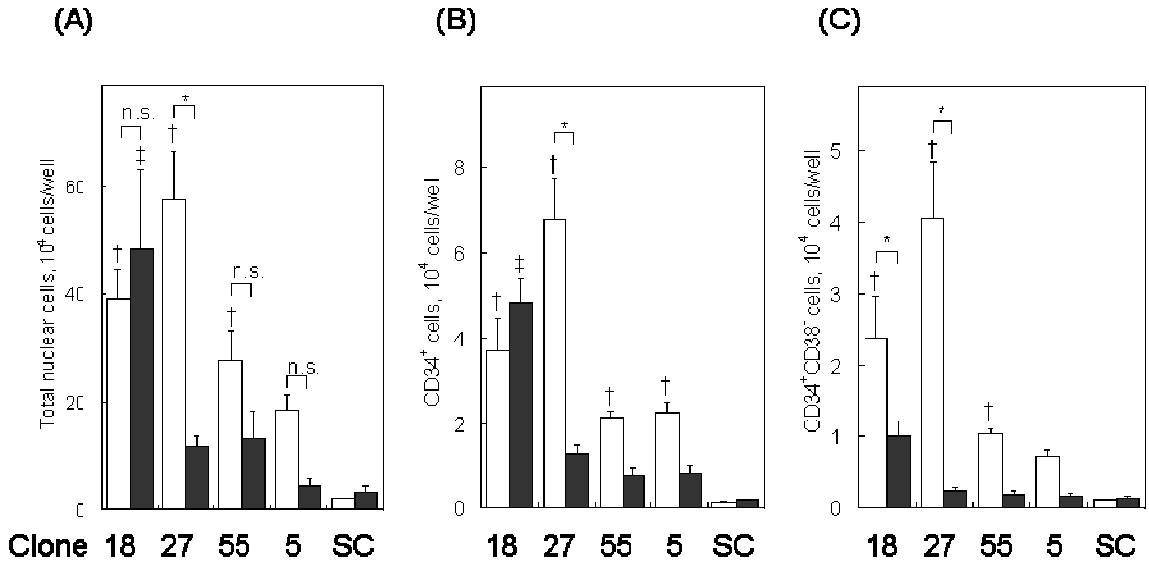


***Figure 1-7.*** Summary of cell number expansion by 7-days coculture of $CD34^+$ cells with progeny of hMSCs after 7-day osteogenic induction. (A): Total nucleated cells, (B): $CD34^+$ cells, (C): $CD34^+CD38^-$ cells. Numbers on x-axis represent hMSC clone numbers, and SC means the suspension culture without hMSC feeder layer as a control. Values represents means ± SEM (n = 3). White bars = coculture with undifferentiated hMSCs; black bars = coculture with progeny of hMSCs after 7-day osteogenic induction. *, significant difference between hMSCs pre- and post-osteogenesis; † and ‡, significant difference with SC ($p < 0.05$).

***Correlations of hematopoiesis-supporting activity with Jagged1 expression and calcium deposition***

The relationship between hematopoiesis-supporting activity of each hMSC clone with Jagged1 expression and with calcium deposition was quantitatively evaluated. The numbers of $CD34^{+}CD38^{-}$ cells after 7-day coculture were plotted against the amounts of calcium deposits after osteogenic differentiation (Fig. 1-8), and against

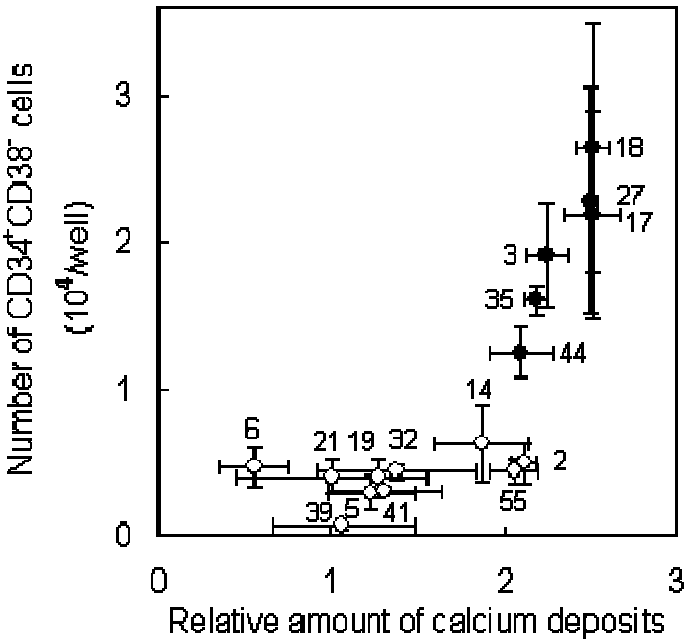


***Figure 1-8.*** Correlations of hematopoiesis-supporting activity of each hMSC clone with their amounts of calcium deposits on their progeny Closed circles represent higher hematopoiesis-supportive hMSC clones (Clones 18, 27, 17, 3, 35 and 44) and open circles represent other hMSC clones (Clone 14, 2, 55, 21, 19, 6, 41, 5 and 39). The values are represented by means ± SEM (of 3 independent pictures).

Jagged1 expression levels (Fig. 1-9). The most hematopoiesis-supportive clones showed both high osteogenic potential and high Jagged1 expression, indicating that hMSC clones which have differentiation potential to the osteoblast lineage can support expanding HSCs.

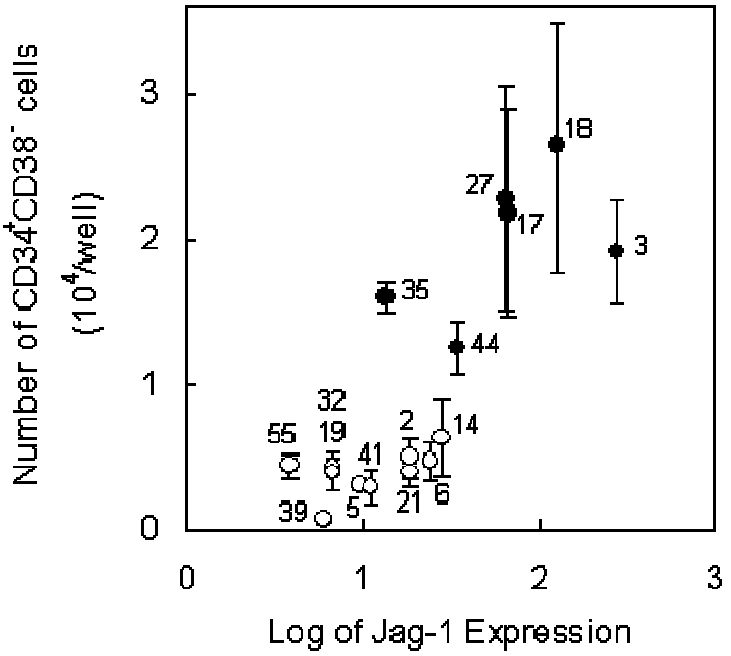


***Figure 1-9.*** Correlations of hematopoiesis-supporting activity of each hMSC clone with their Jagged1 expression levels. Closed circles represent higher hematopoiesis-supportive hMSC clones (Clones 18, 27, 17, 3, 35 and 44) and open circles represent other hMSC clones (Clone 14, 2, 55, 21, 19, 6, 41, 5 and 39). The values are represented by means ± SEM (of 3 independent pictures).

# DISCUSSION

The intention of this chapter was to examine hematopoiesis-supporting activity of hMSCs at a clonal level. However, cloning of primary hMSCs is difficult because phenotypic changes occasionally occur during clonal selection of primary hMSCs [28], making establishment of human cell lines more difficult than that of rodent cell lines [29]. Thus, several hMSC lines have been established by transduction of the hTERT gene and their hematopoiesis-supporting activities have been already examined [30]. However, hMSC lines immortalized by hTERT alone seem to be unstable to the examination of various properties over the long term. Therefore, hMSC lines established by hTERT and $p16^{INK4a}$/RB inactivation with E7 and telomerase activation with E6 [11] were used. The inhibition of the p16/RB pathway in addition to transduction of hTERT gene is necessary to avoid senescence [31,32].

Osteoblastic cells play an important role in the engraftment of HSCs to an endosteal hematopoietic niche [10]. The author supposed that the heterogeneous hematopoiesis-supporting activities of primary hMSCs are relevant to their osteogenic potential. Using calcium deposition as an index, the potential of immortalized hMSCs to differentiate toward osteogenic lineages following conventional osteogenic induction for 14 days was examined. Remarkable differences in calcium deposition between hMSC clones (Fig. 1-5 and Table 1-2), and as well as correlation of hematopoiesis-supporting activities of each MSC clone with calcium deposition on each MSC clone (Figs. 1-2, 1-5 and Table 1-2) were found. On the other hand, correlations of hematopoiesis-supporting activities with neither adipogenic potentials

(Fig. 1-6 and Table 1-2) nor chondrogenic potentials (private communication from Dr. Aoyama) were found. hMSCs with high osteogenic potential offer a highly adhesive environment to HSCs because of the tropism of hHSCs toward high concentration of calcium ions [10]. The gene expression level of RUNX2 and Osterix to evaluate the osteogenic stage of each hMSC clone was also examined. RUNX2 is known as one of the earliest transcriptional factors for the osteoblast lineage [33], and Osterix is also a transcriptional factor of osteogenesis and located downstream of RUNX2 [34]. No clear differences were observed between hMSC clones in expression level of either gene (Fig. 1-4). Interestingly, not all of clones with high osteogenic potential showed high hematopoiesis-supporting potential as illustrated by Clones 2 and 14. This exception implies that a hematopoiesis-supportive clone requires other characteristics in addition to osteogenic potential. Key proteins related to hematopoiesis-supporting activity, including N-cadherin, Wnt-3, Ang-1 and Jagged1 [1-5,35], were analyzed. In analyses of gene expression, no remarkable differences, except for Jagged1, among hMSC clones were found (Fig. 1-4). All of the highly hematopoiesis-supportive clones expressed Jagged1 in high levels. Genes of the Notch family are known to be expressed in various kinds of undifferentiated cells and their gene products regulate their own fates, *i.e.* differentiation, proliferation, and apoptosis. The interaction between Notch-1 expressing on HSC and Notch-1 ligands, such as Jagged1, expressed on stromal cells plays an important role in the self-renewal of HSC.

The higher hematopoiesis-supportive clones, such as Clones 27, 18, 17 and 3, demonstrated high potential to deposit large amounts of calcium after osteogenic induction, and they also showed high expression of the Jagged1 gene. This result is comparable to the observation by Calvi *et al*. that Jagged1$^{+}$ osteoblastic cells form a

HSC niche in murine bone marrow [2]. Although Clones 18 and 35 demonstrated both high osteogenic potential and high expression of Jagged1, there were notable differences in the expansion of $CD34^{+}CD38^{-}$ cell number, suggesting that other factors may stimulate self-renewal of HSCs. As shown in Fig. 1-7, Clone 18 and 27 lost hematopoiesis supporting activities after osteogenic differentiation. Minor amounts of secreted cytokines or other membrane proteins from immature hMSCs may affect self-renewal of HSCs and the differentiation of $CD34^{+}$ cells, resulting in changes in the $CD34^{+}CD38^{-}$ subpopulation. Comprehensive analysis by DNA microarray will be needed to reveal these unknown factors. Conversely, whether both of $Jagged1^{+}$ and osteoblastic cells are absolutely required as components of the hematopoietic niche is still unknown. To clarify this question, the establishment of a Jagged1-expressing hMSC clone remains as a matter of future investigation.

Umbilical cord blood collected from a newborn baby is accepted as one of the promising sources of HSCs for transplantation [36,37]. Numerous efforts have been made to expand HSCs *ex vivo* to improve engraftment time and to reduce the graft failure rate in the recipients, particularly in development of therapies for adult patients [36,38]. The co-culture of UCB cells with murine stromal cells, such as MS-5 [39] or HESS-5 [40], is the currently accepted method for expansion of HSCs. Use of the xenogeneic stromal cells to expand HSCs in the clinical setting, however, has encountered several obstacles. Therefore, murine stromal cells should be replaced by cells of human origin, and a co-culture system free from contamination of feeder cells or their debris has been under development [16]. The higher hematopoiesis-supportive clones identified here, such as Clones 27, 18, 17 and 3, are candidates for promising feeder cells in the expansion of HSCs.

# REFERENCES

1. Zhang J, Niu C, Ye L, Huang H, He X, Tong WG, Ross J, Haug J, Johnson T, Feng JQ, Harris S, Wiedemann LM, Mishina Y, Li L. Identification of the haematopoietic stem cell niche and control of the niche size. *Nature*, 2003, **425**, 836-841.
2. Calvi LM, Adams GB, Weibrecht KW, Weber JM, Olson DP, Knight MC, Martin RP, Schipani E, Divieti P, Bringhurst FR, Milner LA, Kronenberg HM, Scadden DT. Osteoblastic cells regulate the haematopoietic stem cell niche. *Nature*, 2003, **425**, 841-846.
3. Reya T, Duncan AW, Ailles L, Domen J, Scherer DC, Willert K, Hintz L, Nusse R, Weissman IL. A role for Wnt signalling in self-renewal of haematopoietic stem cells. *Nature*, 2003, **423**, 409-414.
4. Willert K, Brown JD, Danenberg E, Duncan AW, Weissman IL, Reya T, Yates JR 3rd, Nusse R. Wnt proteins are lipid-modified and can act as stem cell growth factors. *Nature*, 2003, **423**, 448-452.
5. Arai F, Hirao A, Ohmura M, Sato H, Matsuoka S, Takubo K, Ito K, Koh GY, Suda T. Tie2/angiopoietin-1 signaling regulates hematopoietic stem cell quiescence in the bone marrow niche. *Cell*, 2004, **118**, 149-161.
6. Majumdar MK, Thiede MA, Haynesworth SE, Bruder SP, Gerson SL. Human marrow-derived mesenchymal stem cells (MSCs) express hematopoietic cytokines and support long-term hematopoiesis when differentiated toward stromal and osteogenic lineages. *J. Hematother. Stem Cell Res*., 2000, **9**, 841-848.
7. Kadereit S, Deeds LS, Haynesworth SE, Koc ON, Kozik MM, Szekely E, Daum-Woods K, Goetchius GW, Fu P, Welniak LA, Murphy WJ, Laughlin MJ.

Expansion of LTC-ICs and maintenance of p21 and BCL-2 expression in cord blood CD34(+)/CD38(-) early progenitors cultured over human MSCs as a feeder layer. *Stem Cells*, 2002, **20**, 573-582.

8. Zhang Y, Li C, Jiang X, Zhang S, Wu Y, Liu B, Tang P, Mao N. Human placenta-derived mesenchymal progenitor cells support culture expansion of long-term culture-initiating cells from cord blood $CD34^+$ cells. *Exp. Hematol*., 2004, **32**, 657-664.
9. Noort WA, Kruisselbrink AB, in't Anker PS, Kruger M, van Bezooijen RL, de Paus RA, Heemskerk MH, Löwik CW, Falkenburg JH, Willemze R, Fibbe WE. Mesenchymal stem cells promote engraftment of human umbilical cord blood-derived CD34(+) cells in NOD/SCID mice. *Exp. Hematol*., 2002, **30**, 870-878.
10. Adams GB, Chabner KT, Alley IR, Olson DP, Szczepiorkowski ZM, Poznansky MC, Kos CH, Pollak MR, Brown EM, Scadden DT. Stem cell engraftment at the endosteal niche is specified by the calcium-sensing receptor. *Nature*, 2006, **439**, 599-603.
11. Pittenger MF, Mackay AM, Beck SC, Jaiswal RK, Douglas R, Mosca JD, Moorman MA, Simonetti DW, Craig S, Marshak DR. Multilineage potential of adult human mesenchymal stem cells. *Science*, 1999, **284**, 143-147.
12. Okamoto T, Aoyama T, Nakayama T, Nakamata T, Hosaka T, Nishijo K, Nakamura T, Kiyono T, Toguchida J. Clonal heterogeneity in differentiation potential of immortalized human mesenchymal stem cells. *Biochem. Biophys. Res. Commun*., 2002, **295**, 354-361.
13. in 't Anker PS, Noort WA, Scherjon SA, Kleijburg-van der Keur C, Kruisselbrink AB, van Bezooijen RL, Beekhuizen W, Willemze R, Kanhai HH, Fibbe WE. Mesenchymal stem cells in human second-trimester bone marrow, liver, lung, and

spleen exhibit a similar immunophenotype but a heterogeneous multilineage differentiation potential. *Haematologica*, 2003, **88**, 845-852.

14. Kucia M, Ratajczak J, Ratajczak MZ. Are bone marrow stem cells plastic or heterogenous--that is the question. *Exp. Hematol*., 2005, **33**, 613-623.
15. Nandoe Tewarie RD, Hurtado A, Levi AD, Grotenhuis JA, Oudega M. Bone marrow stromal cells for repair of the spinal cord: Towards clinical application. *Cell Transplant*., 2006, **15**, 563-577.
16. Fujimoto N, Fujita S, Tsuji T, Toguchida J, Ida K, Suginami H, Iwata H. Microencapsulated feeder cells as a source of soluble factors for expansion of CD34(+) hematopoietic stem cells. *Biomaterials*, 2007, **28**, 4795-4805.
17. Gronthos S, Chen S, Wang CY, Robey PG, Shi S. Telomerase accelerates osteogenesis of bone marrow stromal stem cells by upregulation of CBFA1, osterix, and osteocalcin. *J. Bone Miner. Res.*, 2003, **18**, 716-722.
18. Milona MA, Gough JE, Edgar AJ. Expression of alternatively spliced isoforms of human Sp7 in osteoblast-like cells. *BMC Genomics*, 2003, **4**, 43.
19. Flynn DM, Nijjar S, Hubscher SG, de Goyet Jde V, Kelly DA, Strain AJ, Crosby HA. The role of Notch receptor expression in bile duct development and disease. *J. Pathol*., 2004, **204**, 55-564.
20. Haÿ E, Lemonnier J, Modrowski D, Lomri A, Lasmoles F, Marie PJ. N- and E-cadherin mediate early human calvaria osteoblast differentiation promoted by bone morphogenetic protein-2. *J. Cell. Physiol*., 2000, **183**, 117-128.
21. Tulac S, Nayak NR, Kao LC, Van Waes M, Huang J, Lobo S, Germeyer A, Lessey BA, Taylor RN, Suchanek E, Giudice LC. Identification, characterization, and regulation of the canonical Wnt signaling pathway in human endometrium. *J. Clin.*

*Endocrinol. Metab.*, 2003, **88**, 3860-3866.

22. Huang YQ, Li JJ, Karpatkin S. Identification of a family of alternatively spliced mRNA species of angiopoietin-1. *Blood*, 2000, **95**, 1993-1999.

23. Reems JA, Torok-Storb B. Cell cycle and functional differences between $CD34^{+}/CD38^{hi}$ and $CD34^{+}/38^{lo}$ human marrow cells after in vitro cytokine exposure. *Blood*, 1995, **85**, 1480-1487.

24. Hao QL, Shah AJ, Thiemann FT, Smogorzewska EM, Crooks GM. A functional comparison of $CD34^{+}CD38^{-}$ cells in cord blood and bone marrow. *Blood*, 1995, **86**, 3745-3753.

25. Breems DA, Blokland EA, Neben S, Ploemacher RE. Frequency analysis of human primitive haematopoietic stem cell subsets using a cobblestone area forming cell assay. *Leukemia*, 1994, **8**, 1095-1104.

26. Ploemacher RE, van der Sluijs JP, Voerman JS, Brons NH. An in vitro limiting-dilution assay of long-term repopulating hematopoietic stem cells in the mouse. *Blood*, 1989, **74**, 2755-2763.

27. Androutsellis-Theotokis A, Leker RR, Soldner F, Hoeppner DJ, Ravin R, Poser SW, Rueger MA, Bae SK, Kittappa R, McKay RD. Notch signalling regulates stem cell numbers in vitro and in vivo. *Nature*, 2006, **442**, 823-826.

28. Digirolamo CM, Stokes D, Colter D, Phinney DG, Class R, Prockop DJ. Propagation and senescence of human marrow stromal cells in culture: a simple colony-forming assay identifies samples with the greatest potential to propagate and differentiate. *Br. J. Haematol.*, 1999, **107**, 275-281.

29. Javazon EH, Colter DC, Schwarz EJ, Prockop DJ. Rat marrow stromal cells are more sensitive to plating density and expand more rapidly from single-cell-derived

colonies than human marrow stromal cells. *Stem Cells*, 2001, **19**, 219-225.

30. Kawano Y, Kobune M, Yamaguchi M, Nakamura K, Ito Y, Sasaki K, Takahashi S, Nakamura T, Chiba H, Sato T, Matsunaga T, Azuma H, Ikebuchi K, Ikeda H, Kato J, Niitsu Y, Hamada H. Ex vivo expansion of human umbilical cord hematopoietic progenitor cells using a coculture system with human telomerase catalytic subunit (hTERT)-transfected human stromal cells. *Blood*, 2003, **101**, 532-540.
31. Kiyono T, Foster SA, Koop JI, McDougall JK, Galloway DA, Klingelhutz AJ. Both Rb/p16INK4a inactivation and telomerase activity are required to immortalize human epithelial cells. *Nature*, 1998, **396**, 84-88.
32. Terai M, Uyama T, Sugiki T, Li XK, Umezawa A, Kiyono T. Immortalization of human fetal cells: the life span of umbilical cord blood-derived cells can be prolonged without manipulating p16INK4a/RB braking pathway. *Mol. Biol. Cell*, 2005, **16**, 1491-1499.
33. Ducy P, Zhang R, Geoffroy V, Ridall AL, Karsenty G. Osf2/Cbfa1: a transcriptional activator of osteoblast differentiation. *Cell*, 1997, **89**, 747-754.
34. Nakashima K, Zhou X, Kunkel G, Zhang Z, Deng JM, Behringer RR, de Crombrugghe B. The novel zinc finger-containing transcription factor osterix is required for osteoblast differentiation and bone formation. *Cell*, 2002, **108**, 17-29.
35. Mancini SJ, Mantei N, Dumortier A, Suter U, MacDonald HR, Radtke F. Jagged1-dependent Notch signaling is dispensable for hematopoietic stem cell self-renewal and differentiation. *Blood*, 2005, **105**, 2340-2342.
36. Amos TA, Gordon MY. Sources of human hematopoietic stem cells for transplantation--a review. *Cell Transplant*, 1995, **4**, 547-569.
37. Rocha V, Gluckman E; Eurocord and European Blood and Marrow Transplant

Group. Clinical use of umbilical cord blood hematopoietic stem cells. *Biol. Blood Marrow Transplant.*, 2006, **12**(1 Suppl 1), 34-41.

38. Hofmeister CC, Zhang J, Knight KL, Le P, Stiff PJ. Ex vivo expansion of umbilical cord blood stem cells for transplantation: growing knowledge from the hematopoietic niche. *Bone Marrow Transplant.*, 2007, **39**, 11-23.

39. Sutherland HJ, Eaves CJ, Lansdorp PM, Thacker JD, Hogge DE. Differential regulation of primitive human hematopoietic cells in long-term cultures maintained on genetically engineered murine stromal cells. *Blood*, 1991, **78**, 666-672.

40. Tsuji T, Ogasawara H, Aoki Y, Tsurumaki Y, Kodama H. Characterization of murine stromal cell clones established from bone marrow and spleen. *Leukemia*, 1996, **10**, 803-812.

# CHAPTER 2

# Microencapsulated feeder cells as a source of soluble factors for expansion of $CD34^+$ hematopoietic stem cells

## INTRODUCTION

Umbilical cord blood (UCB) collected from a newborn baby is accepted as one of the promising sources of hematopoietic stem cells (HSCs) for transplantation [1]. The first UCB cell transplantation was performed by Gluckman et al. in 1989 [2]. UCB cell recipients have been limited to children with an average weight of 20 kg, as the major disadvantage of UCB cell transplantation is the low cell dose, which results in slower time to engraftment and higher rates of engraftment failure than occur with bone marrow transplantation. Numerous efforts have been made to expand HSCs *ex vivo* to improve engraftment time and reduce the graft failure rate in the recipients, particularly in developing this therapy for adult patients [3-5]. *Ex vivo* manipulation of HSCs dates back to the development of Dexter-type culture techniques, which identified the benefits of stroma for the maintenance of hematopoietic colony-forming units [6]. At the moment, the co-culture of UCB cells with murine stromal cells, such as M2-10B4 [7], MS-5 [8], OP9 [9,10], or HESS-5 [11, 12], is the currently accepted method for

expansion of HSCs.

In these co-culture systems, the stromal cells are generally considered to provide signal transductions through two major mechanisms to promote the expansion of HSCs. First, stromal cells secrete various soluble factors, such as growth factors and cytokines, that stimulate the proliferation and differentiation of HSCs, and provide niche as an appropriate environment for the proliferation and maintenance of HSCs. Secondly, co-culturing with stromal cells provides direct cell-cell contact, which plays an important role in HSC proliferation and differentiation.

Use of the xenogeneic stromal cells to expand HSCs in the clinical setting, however, has encountered several obstacles. Public heath officials are concerned about zoonosis and other unknown infectious diseases caused by contamination of xenogeneic feeder cells and concerned about pathogens which they carry, such as bovine spongiform encephalopathy (BSE) and porcine endogenous retrovirus (PERV) [13]. Furthermore, rejection or unexpected reactions against transplanted HSCs are shown to be caused by xenogeneic cell debris or proteins and polysaccharide derived from stromal cells [14]. Thus, the development of a co-culture system free from contamination of feeder cells or their debris is highly desired.

Conditioned media (CM) of the feeder cells has been examined to avoid the risks pointed above [15-17]. Although sufficient amounts of essential bioactive substances exist in CM for HSCs proliferation at the start of the culture, the cultured HSCs eventually consume the nutrients, and thus the efficacy of CM decreases with time. For more efficient proliferation of HSCs, the culture medium supplemented with CM should be frequently changed or a continuous supply of bioactive substances should be included in the UCB cell culture system.

In this chapter, efficacy of microencapsulated feeder cells was examined as a continuous supply unit of bioactive substances as shown in Scheme 2-1. Spherical aggregates of feeder cells were enclosed into agarose gel microcapsules and then added to the culture flask to co-culture with UCB cells. Agarose gel is permeable to various chemicals and low molecular proteins, such as amino acids, glucose and growth factors [18-20]. Agarose gel also can inhibit contact between feeder cells and UCB cells [21,22]. This novel culture system to expand HSC using the encapsulated feeder cells is described.

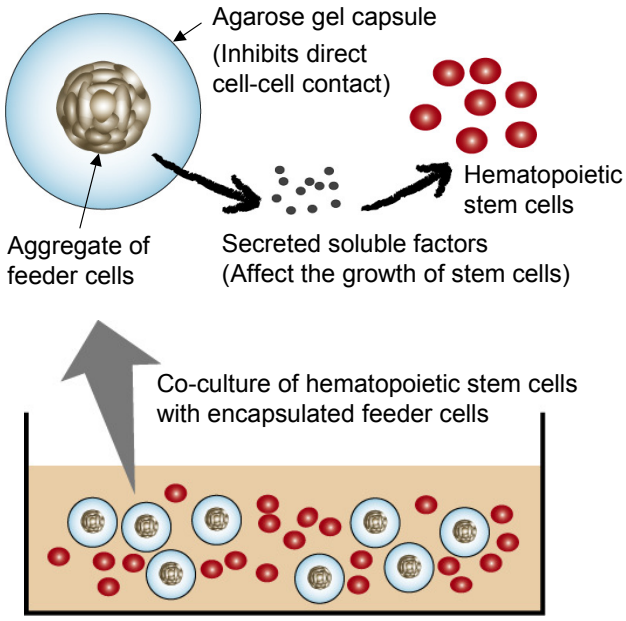


***Scheme 2-1***. Schematic representation of a co-culture system of $CD34^+$ cells with microencapsulated feeder cells. Cell aggregates, which are formed by the hanging drop method, are enclosed into agarose gel microcapsules. Soluble factors, such as growth factors and cytokines, are secreted from feeder cells and permeate through the agarose gel into the culture medium. $CD34^+$ cells are expected to proliferate and differentiate in response to those factors.

# EXPERIMENTAL

### *Cytokines and monoclonal antibodies*

A mixture of recombinant human (rh) stem cell factor (SCF), rh-thrombopoietin (TPO) and rh-Flt3 ligand (StemSpan CC110) was purchased from StemCell Technologies Inc (Vancouver, Canada). Monoclonal antibodies used for cell surface markers analyses by the flow cytometry are as follows: fluorescein isothiocyanate (FITC)–conjugated anti-human CD34 (clone 581) and allophycocyanin (APC)-conjugated anti-human CD45 (clone HI30), purchased from BD Pharmingen (CA, USA), and phycoerythrin (PE)-conjugated anti-human CD38 (clone HB7), purchased from Becton Dickinson (CA, USA).

### *Culture of murine stromal cell line and human mesenchymal stem cell line*

Two cell lines, HESS-5 and MSC-3, were used as feeder cells. HESS-5 was established from murine bone marrow as hematopoiesis-supportive stromal cells [11, 12]. HESS-5 cells were maintained in minimal essential medium alpha (MEM-alpha; Invitrogen Corp., CA, USA) supplemented with 10% horse serum (JRH Biosciences, CA, USA), 100 U/mL of penicillin and 100 μg/mL of streptomycin (Invitrogen) at 37 °C under 5% $CO_2$ in a humidified atmosphere, and subcultured at 5–8 × $10^3$ per $cm^2$ every three to four days.

MSC-3 was a human bone marrow-derived immortalized MSC clone established by Okamoto *et al*. [23] that supports the proliferation of HSCs as described in the previous chapter. MSC-3 was kindly donated by Dr. Aoyama of the Institute for Frontier Medical Sciences, Kyoto University. MSC-3 cells were maintained in

Dulbecco's Modified Essential Medium (DMEM; Invitrogen) supplemented with 10% fetal bovine serum (BIOWEST, France), 100 U/mL of penicillin and 100 μg/mL of streptomycin (Invitrogen) at 37 °C under 5% $CO_2$ in a humidified atmosphere, and subcultured at 5–8 × $10^3$ per $cm^2$ every 3 to 4 days.

***Microencapsulation of feeder cells***

Prior to microencapsulation of feeder cells, spherical cell aggregates were prepared by the hanging drop method as reported previously [24]. In brief, HESS-5 or MSC-3 cells were suspended in the respective maintaining media at a certain cell density, and 20 μL of the cell suspension were spotted on a lid of a multi tray (Asahi Techno Glass Corp., Tokyo, Japan). The lid was turned upside down to hang drops and statically cultured at 37 °C under 5% $CO_2$ in a humidified atmosphere for 3 days. After hanging, the cells formed a spherical aggregate in a drop. The drops containing the spherical cell aggregates were collected with a pipette and the cell aggregates were washed with Hanks' balanced salt solution (HBSS; Invitrogen).

The cell aggregates were enclosed into agarose gel microcapsules as reported previously [25]. In brief, low melting point agarose (Shimizu Shokuhin, LTD., Shizuoka, Japan) was suspended at a final concentration of 5% in 3 ml of serum-free minimum essential medium (Invitrogen) in a glass centrifuge tube, and heated in a microwave oven to dissolve agarose. The agarose solution was allowed to cool at 37 °C for 8 min before a suspension of spherical cell aggregates in approximately 0.1 ml of HBSS was added to the tube and mixed well with the agarose solution. Liquid paraffin (1.07162.1000; Merck, Germany), pre-incubated at 37 °C, was added into the tube. The tube was vigorously shaken such that small droplets of the agarose solution containing

cell aggregates formed in the liquid paraffin, and the tube was immediately immersed in an ice bath to induce gelation of the agarose solution. The suspension was washed three times with 15 ml of cold HBSS containing calcium and magnesium (HBSS (+); Invitrogen) to remove liquid paraffin from encapsulated cells. The microcapsules containing cell aggregates were selected using a Pasteur pipette under a stereoscopic microscope and subsequently incubated in the maintaining media overnight.

***Preparation of UCB cells***

Studies were approved by the institutional review board. Cord blood units were obtained from healthy donors, with their informed consent. The $CD34^+$ cell fraction, which is rich in HSCs, was isolated from fresh UCB as follows. Mononuclear cells were isolated by density gradient centrifugation using Lymphoprep (AXIS-SHIELD PoC AS, Oslo, Norway). After washing twice with Dulbecco's phosphate-buffered saline (DPBS; Nissui Pharmaceutical Co. Ltd., Tokyo, Japan), $CD34^+$ cells were isolated by magnetic beads (Direct CD34 Progenitor Cell Isolation Kit; Miltenyi Biotech GmbH, Bergisch Gladbach, Germany) in accordance with the manufacturer's instructions. Isolated $CD34^+$ cells were suspended into a cryopreservation solution containing bovine serum (Cellbanker; Nippon Zenyaku Kogyo Co., Ltd., Fukushima, Japan), and stocked in a liquid nitrogen tank until use.

***Preparation of conditioned medium (CM)***

For preparation of CM, $1.5 \times 10^5$ cells of HESS-5 or $3.0 \times 10^5$ cells of MSC-3 were seeded onto a 12-well tissue culture plate (BD Biosciences, NJ, USA). After incubation for 5–6 hours, the cells were washed three times with HBSS (+). The

medium was replaced with 2 mL per well of serum-free media for hematopoietic cell culture [StemPRO-34 SFM (Invitrogen) supplemented with 2 mM of L-alanyl-L-glutamine (GLUTAMAX I; Invitrogen)] and incubated for 3 days at 37 °C under 5% $CO_2$ in a humidified atmosphere. The supernatant was collected after culture and filtered through a 0.22 μm-filter (Millipore, MA, USA) to remove cell debris. The supernatant was diluted with an equal volume of a fresh serum-free medium to supply nutrients that were consumed while conditioning. Cytokines were then added at the following concentrations: 50 ng/ml SCF, 50 ng/ml TPO and 50 ng/ml Flt3 ligand (StemSpan CC110) (hereafter referred to as a conditioned medium, CM).

***Expansion of $CD34^+$ cells***

Three different culture conditions were utilized to expand $CD34^+$ cells as follows: culturing in CM, co-culturing with microencapsulated HESS-5 or MSC-3 cells in serum-free media (StemPro34-SFM), and co-culturing with microencapsulated HESS-5 or MSC-3 cells in CM.

For expansion of $CD34^+$ cells in CM, $5 \times 10^3$ of $CD34^+$ cells were plated in 2 ml of CM in each well of a 12-well tissue culture plate, and cultured at 37 °C under 5% $CO_2$ in a humidified atmosphere. Half of the medium was changed at day 4, and the $CD34^+$ cell progeny was harvested by pipetting at day 7 for analyses.

For co-culturing with feeder cells, aliquots of microcapsules were collected and washed with HBSS (+) twice, and seeded with $5 \times 10^3$ of $CD34^+$ cells in 2 ml of CM or the serum-free media supplemented with cytokines as mentioned above, onto a 12-well tissue culture plate. $CD34^+$ cells and encapsulated spheroids were co-cultured at 37 °C under 5% $CO_2$ in a humidified atmosphere. Half of the medium was changed at day 4

and the $CD34^+$ cell progeny was harvested at day 7 for analyses.

### *Flow cytometric analysis of $CD34^+$ cell progeny*

Immunophenotypic enumeration of the $CD34^+$ cell progeny was performed by flow cytometry [26, 27]. Collected cells (1–10 × $10^5$ cells) were suspended in 100 μL of DPBS with 0.1% FBS. The cell suspension was supplemented with 2 μL of the fluorescence dye-conjugated antibodies and incubated at 4 °C for 30 min to label surface antigens. Thawed cells were additionally costained with propidium iodide to exclude dead cells. Stained cells were washed twice with DPBS with 0.1% FBS, and subjected to flow cytometry analysis by FACSCalibur (BD Biosciences). For quantification of cell number, a 50 μL aliquot of a polystyrene fluorescent microsphere suspension (Flow-Count; Beckman Coulter, Inc., CA, USA) (containing 5 × $10^4$ particles) was added into the sample cell suspension prior to analysis. To reduce noise in counting the number of total nucleated cells, the region of blood cells was determined in a FSC - SSC cytogram and a $CD45^+$ gate. The CD34 and CD38 quadrants were determined on the basis of isotypic controls. $CD45^{bright}CD34^+$ cells were excluded as being non-specifically stained cells.

### *Colony-forming cell (CFC) assay*

Hematopoietic potency of the $CD34^+$ cell progeny was examined by the colony-forming cell (CFC) assay [28] and the cobblestone area forming-cell（CAFC) assay [29,30]. The CFC assay classifies multipotential progenitors, and lineage-restricted progenitors of the erythroid, granulocytic, monocyte-macrophage and megakaryocytic pathways by the morphological examination of each colony under a

light microscope. The progeny cells were suspended in a semi-solid methylcellulose medium (MethoCult GF H4434; StemCell Technologies) [Iscove's modified Dulbecco's medium with 1% methylcellulose, 30% fetal bovine serum, 1% bovine serum albumin, $10P^{-4P}$ M 2-mercaptoethanol, 2 mM L-glutamine, 50 ng/ml stem cell factor, 10 ng/ml GM-CSF, 10 ng/ml IL-3 and 3 U/ml erythropoietin] and seeded at 500 or 1000 cells per dish. The cells were incubated at 37 °C under 5% $CO_2$ in a humidified atmosphere. At day 14, the numbers of colony-forming units (CFU) were scored based on the morphology of colonies as follows: granulocytes/ macrophages (CFU-GM), erythroid cells (CFU-Erythroid), or granulocytes/ erythroid cells/ macrophages/ megakaryocytes (CFU-GEMM). At day 28, the dense colonies larger than 1 mm in diameter were scored as high-proliferative potential colony-forming cells (HPP-CFC). HPP-CFC and CFU-GEMM are multipotential progenitors and believed to be more primitive than the lineage-restricted CFU-GM and CFU-Erythroid.

***Cobblestone area forming-cell (CAFC) assay***

To quantify the number of stem cells, the CAFC assay by limiting dilution [29,30] was performed with minor modifications as follows. A confluent layer of HESS-5 cells was prepared on a 96-well tissue culture plate and irradiated (15 Gy of X-ray). Cultures were then serially diluted and single-cell suspensions were seeded in a long-term culture medium (MyeloCult H5100; StemCell Technology) [MEM-alpha with 12.5% horse serum, 12.5% fetal bovine serum, 0.2 mM *i*-inositol, 20 mM folic acid, $10^{-4}$ M 2-mercaptoethanol, 2 mM L-glutamine, and $10^{-6}$ M hydrocortisone]. The cells were seeded with 24 replicates at 2.5-fold dilutions (2–40 cells for thawed $CD34^+$ cells before co-culture and 320–5000 cells per well for $CD34^+$ cell progeny after

co-culture) and incubated at 37 °C under 5% $CO_2$ in a humidified atmosphere. Half of the culture medium was changed every week, and individual wells were scored as presence or absence of a cobblestone area at week 4. The frequency of CAFC in the seeded population was calculated by Poisson statistics.

***Statistical analysis***

Comparisons between two groups were calculated by Student's t-test. Comparisons among multiple groups were calculated by means of one-way analysis of variance (ANOVA), followed by Tukey's honestly significant difference (HSD) test. All of statistical calculations were performed using the software JMP ver.5.1.1.

## RESULTS

***Preparation of cell aggregates***

Spherical cell aggregates of HESS-5 and MSC-3 cells were prepared by the hanging drop method and aggregate characteristics were examined. Diameters of the formed cell aggregates were plotted against the number of cells initially incorporated into the drop (Figure 2-1). The slopes of regression lines for MSC-3 and HESS-5 were 0.34 and 0.26, respectively. The diameter of MSC-3 cell aggregates was nearly proportional to the one-third power of the seeding cell number as expected, but the diameter of HESS-5 was less than that expected, indicating that they formed more compact cell aggregates than the MSC-3 aggregates.

The amount of cytokines released from a microcapsule is expected to increase

with the increasing number of enclosed cells, thus the larger cell aggregates are predicted to be desirable for efficient supply of bioactive substances to UCB $CD34^+$ cells. However, cells within the core of a larger cell aggregate will eventually undergo necrosis due to an insufficient oxygen supply. Accordingly, the diameter of cell aggregates should be less than 300 μm to inhibit cell necrosis [18-20]. Based on these parameters and the regression lines shown in Figure 2-1, cell aggregates were prepared with $2.0 \times 10^4$ HESS-5 cells and $0.5 \times 10^4$ MSC-3 cells and used in the following experiments.

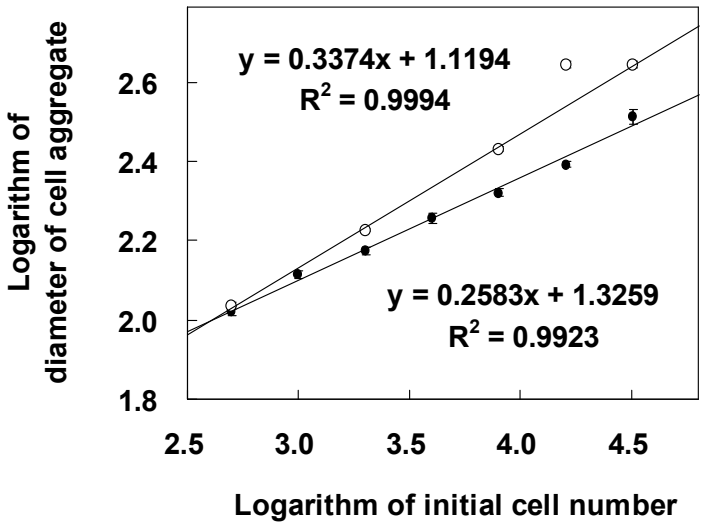


***Figure 2-1***. Diameters of cell aggregates formed under various seeding cell numbers. The sizes of cell aggregates were determined by microscopy at day 3 after preparation. Open circle, MSC-3; closed circle, HESS-5. Solid lines represent the regression lines fitted by the least-squares method.

***Microencapsulated cell aggregates***

The diameters of the microcapsules and cell aggregates immediately after encapsulation are listed in Table 2-1. The mean diameter of cell aggregates was 212 μm and 255 μm for HESS-5 and MSC-3 cells, respectively, both suitable sizes for maintenance of cell aggregates without cell necrosis occurring even at the core of aggregates.

The microencapsulated cell aggregates were then cultured in the maintaining media for 2 weeks and changes in morphology were observed (Figure 2-2). Young's modulus of 5% agarose hydrogel is about 500 kPa [31] and no mechanical disruption of the microcapsules was observed due to its sufficient mechanical strength. Cavities between cell aggregates and the agarose gel were observed and increased with time in the cultured HESS-5 cells, indicating compaction of HESS-5 aggregates. In comparison, MSC-3 aggregates maintained a similar size and no space was seen between the cell aggregates and the agarose gel capsules throughout the 2 weeks of observation.

***Table 2-1***. Diameters of cell aggregates and agarose microbeads.

| Feeder cell | Seeded cells, per drop | Diameter of capsule, μm | Diameter of cell aggregate, μm | Thickness of membrane, μm |
|---|---|---|---|---|
| HESS-5 | $2.0\times10^4$ | 343 (307-378) | 212 (208-215) | 66 (49-82) |
| MSC-3 | $0.5\times10^4$ | 358 (340-375) | 255 (249-260) | 52 (43-60) |

Each value represents mean size (95% confidence interval in parentheses). HESS-5 and MSC-3 cells were cultured by the hanging drop method for 3 days, and subsequently encapsulated into agarose microbeads as described in the text.

To examine cell viability in the microcapsules, cell aggregates were retrieved by tearing the agarose microcapsules with forceps under a microscope after 2 weeks of culture, and the trypan blue exclusion test was carried out for the cell aggregates. Stained cells, *i.e.* dead cells, in the cell aggregates were not found within either the HESS-5 or MSC-3 aggregates (data not shown).

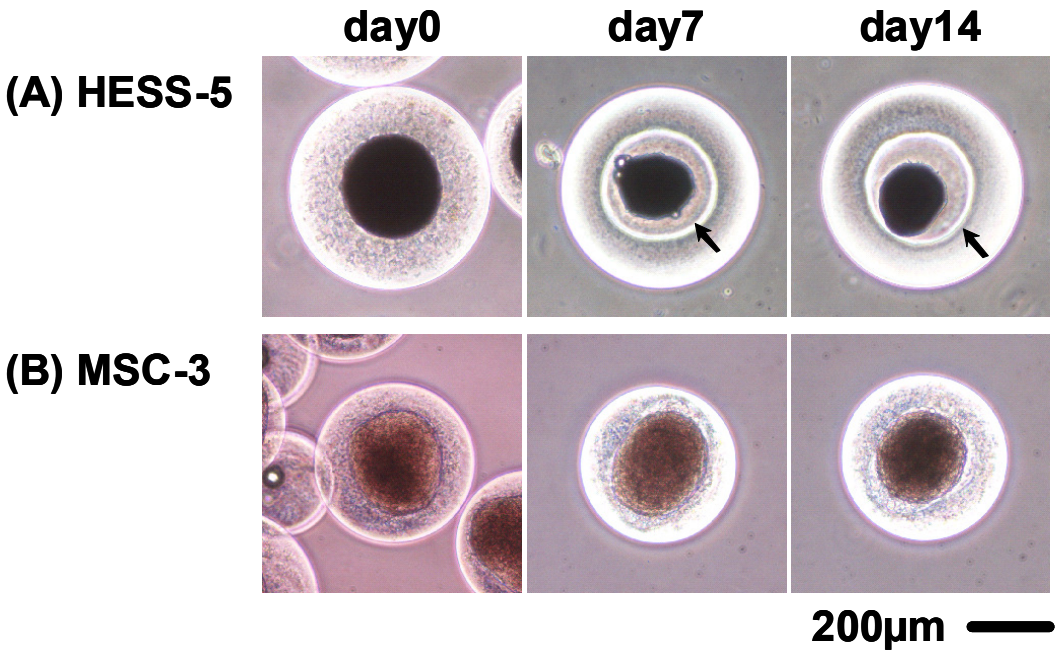


***Figure 2-2***. Microscopic images of encapsulated cell aggregates. Encapsulated cell aggregates of HESS-5 (A) and MSC-3 (B) were cultured for 2 weeks in the respective maintaining media. One week after encapsulation, almost all of the HESS-5 aggregates shrank in microcapsules, and a cavity was observed between the agarose hydrogel layer and the cell aggregate as indicated by arrows. In comparison, no cavity was observed in microcapsules containing MSC-3 aggregates, through 2 weeks (B). Scale bar is 200 μm.

***Optimization of number of microencapsulated feeder cells***

Feeder cells in the microcapsules release bioactive substances that stimulate proliferation and differentiation of $CD34^+$ cells. On the other hand, they also consume nutrients and release waste into the culture medium, and consumption of nutrients and accumulation of waste exert harmful effects on $CD34^+$ cells. $CD34^+$ cells were next co-cultured with different numbers of microencapsulated feeder cells to determine their optimal number for $CD34^+$ cell proliferation. Total cell numbers of the $CD34^+$ progeny were measured after seven days (shown in Figure 2-3). With the microencapsulated HESS-5 cells, application of 35 microcapsules to a well containing $1.5 \times 10^4$ $CD34^+$

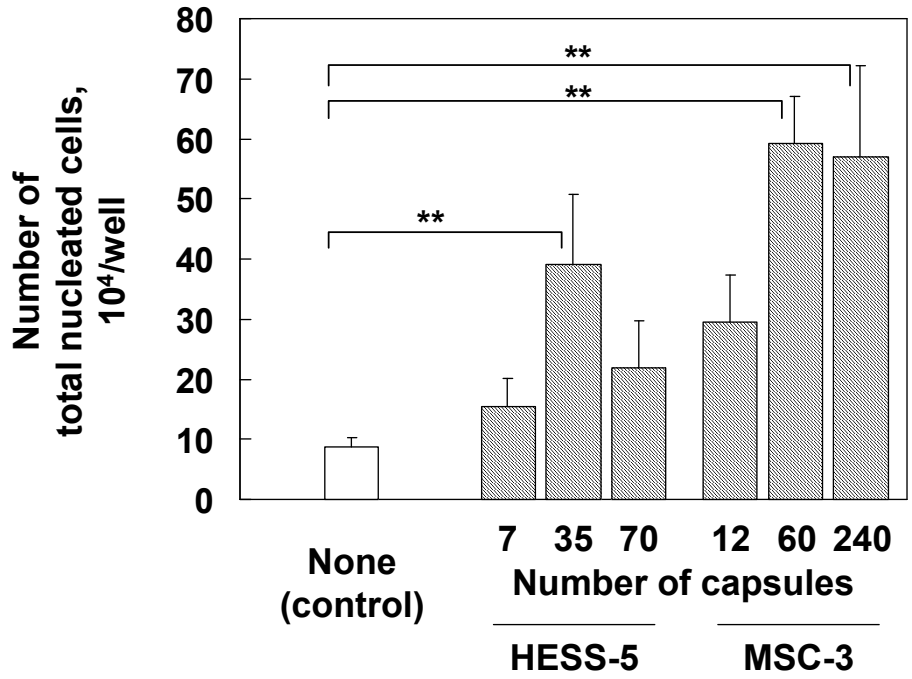


***Figure 2-3*** Dependence of total cell expansion on the number of microencapsulated feeder cells. None: cultured in StemPRO-34 SFM as a control. Double asterisks denote significant difference ($p < 0.05$) between two groups.

cells gave maximum cell proliferation. Thirty five microencapsulated HESS-5 were used for the following experiments. Although total cell number of the progeny increased with increasing number of microencapsulated MSC-3, no clear improvement was observed between 60 and 240 microcapsules. As mentioned above, existence of excess feeder cells might harmful effects on $CD34^+$ cells. Thus, 60 microcapsules were employed for MSC-3 cells for the following experiments. In this experiment, media were changed at day 4. Compared with the cell number at day 4, the cell number at day 7 increased (data not shown). Therefore, production of bioactive substances seemed to be lasted for at least 4 days. There was no data on the results after a week, but it is likely that the production was lasted for 7 days because the cell aggregates were kept alive for 2 weeks without any morphological changes as described above.

***Culture of $CD34^+$ cells***

Four different culture conditions were examined for optimal expansion of UCB cells as determined by an increase in total cell number after seven days. $CD34^+$ cells were cultured in StemPro-34 SFM, cultured in CM, co-cultured with microencapsulated HESS-5 or MSC-3 cells in StemPro-34 SFM, or co-cultured with microencapsulated of HESS-5 or MSC-3 cells in CM. The latter three culture conditions resulted in a significant increase of total cell number (142-, 78-, and 194-fold for HESS-5, and 126-, 118-, and 141-fold for MSC-3, respectively), compared with cultures in StemPro-34 SFM without CM or microencapsulated cells (17.2-fold), as shown in Figure 2-4. These results indicate that co-culturing with HESS-5 and MSC-3 cells promotes effective $CD34^+$ cell proliferation, likely due to the secretion soluble factors that can stimulate proliferation of UCB cells. The other interesting finding is that an additive effect of

CM and microencapsulated cells was observed for the conditions of co-culturing with microencapsulated HESS-5 cells in CM. Cells in this culture condition grew much more effectively than those in CM alone or microencapsulated HESS-5 cells in StemPro-34 SFM alone.

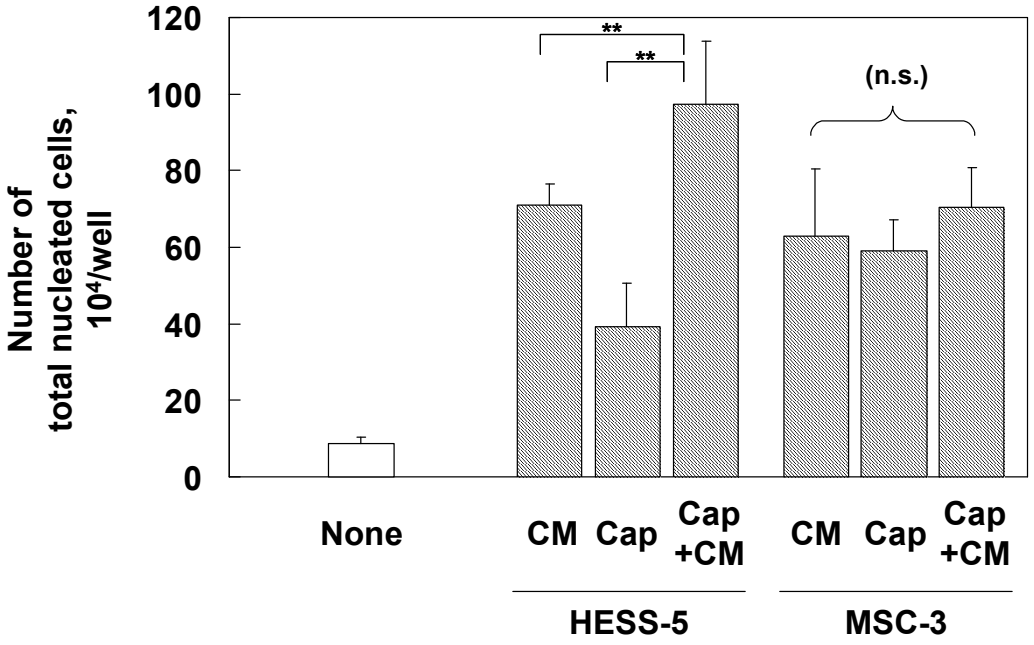


***Figure 2-4.*** Expansion of cells under various conditions. None: cultured in StemPRO-34 SFM as a control. CM: cultured in conditioned medium. Cap: cultured with microencapsulated cell aggregates in StemPRO34-SFM. Cap+CM: cultured with microencapsulated cell aggregates in CM. Panels represent the means of the numbers of total blood cells. Bars represent standard errors [n = 8 (35 HESS-5 capsules); n = 7 (60 MSC-3 capsules); n = 3 (other groups)]. All of experimental groups demonstrated significant cell expansion against the negative control (None). In experiments using HESS-5, asterisks denote significant difference between two groups evaluated by ANOVA and the following HSD test (**; $p < 0.05$). For the case of MSC-3, all of groups demonstrated significant expansion against control, but no significant difference was seen between experimental groups by ANOVA.

Figure 2-5 shows the representative results of flow cytometric analysis of the $CD34^+$ cell progenies after seven days culture under different conditions. Although most of cell progenies belonged to the $CD34^-$ cell population, $CD34^+$ cells evidently existed in all of these culture conditions. In particular, $CD34^+CD38^-$ cells, scarcely detected in

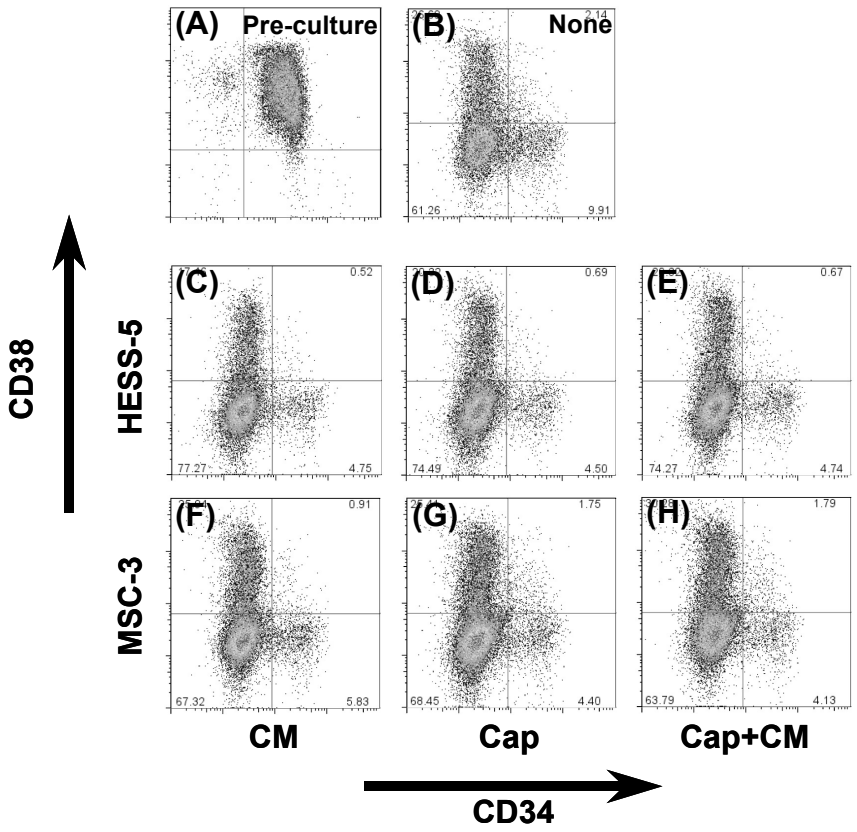


***Figure 2-5.*** Flow cytometric analyses of $CD34^+$ progeny. Each panel shows representative cytograms of CD45 positive-gated cells for CD34 and CD38. The quadrant regions were determined on the basis of isotypic controls. (A) Pre-cultured $CD34^+$ cells, (B) cultured in StemPRO-34 SFM, (C) in CM alone (HESS-5 CM) (D) with microencapsulated HESS-5 cells, (E) with microencapsulated HESS-5 cells in CM (HESS-5 CM), (F) in CM alone (MSC-3 CM), (G) with microencapsulated MSC-3 cells, (H) with microencapsulated MSC-3 cells in CM (MSC-3 CM).

the initial $CD34^+$ cells, were clearly seen after culturing and consisted of more than 4% of total cells. These results indicate that $CD34^+CD38^-$ cells, expected to contain the early primitive HSCs, proliferated well in all of these conditions.

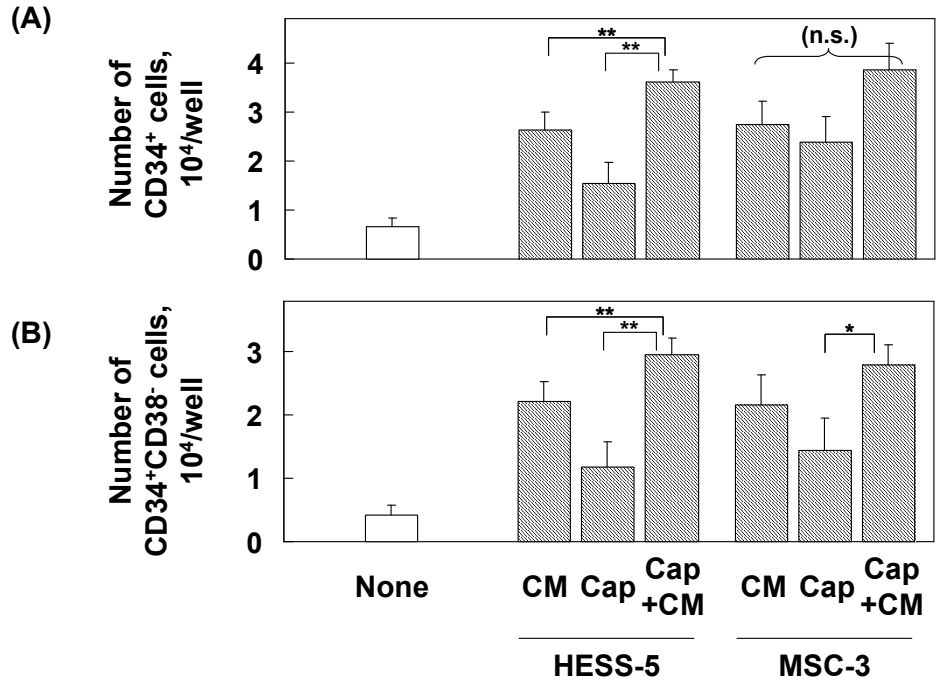


***Figure 2-6.*** Expansion of $CD34^+$ cells and $CD34^+CD38^-$ cells. None: cultured in StemPRO-34 SFM; CM: cultured in conditioned medium; Cap: cultured with microencapsulated cell aggregates in StemPRO-34 SFM; Cap+CM: cultured with microencapsulated cell aggregates in CM. Panels represent the means of the numbers of $CD34^+$ cells and $CD34^+CD38^-$ cells. Bars represent standard errors [n=5 (CM and Cap+CM of HESS-5); n=8 (Cap of HESS-5 and None); n=4 (CM of MSC-3); n=7 (Cap of MSC-3); n=3 (Cap+CM of MSC-3)]. All of experimental groups demonstrated significant cell expansion against negative control (None). 'n.s.' denotes no significant difference among 3 groups by ANOVA, and an asterisk denotes $p < 0.05$ between two groups and double asterisks denote $p < 0.1$ by ANOVA and the following HSD test.

Figure 2-6 summarizes the total amount of $CD34^+$ cells and $CD34^+CD38^-$ cells in the $CD34^+$ cell progenies after 7 days in various culture conditions. Both the $CD34^+$ cells and $CD34^+CD38^-$ cells expanded more effectively when cultured either with CM alone or with microencapsulated feeder cells supplemented with/without CM than with StemPro-34 SFM alone. The remarked additive effects of microencapsulated HESS-5 cells along with CM were observed, with a significant increase of $CD34^+$ cell and $CD34^+CD38^-$ cell numbers.

***Hematopoietic functions of progeny of $CD34^+$ cells***

Hematopoietic potency of the $CD34^+$ progeny was examined by the CFC assay and the CAFC assay. Results of the CFC assay are summarized in Figure 2-7. The number of CFU-GEMM, erythroids and GM was significantly larger for cultures in CM and with microencapsulated HESS-5 in CM than those in the culture with microencapsulated HESS-5 alone. For other colony types, the number of colonies tended to increase in three examined culture groups compared to control conditions, but no statistical differences were observed. Figure 2-8 includes the results of the CAFC assay, used to identify very primitive progenitor cells, such as HPP-CFC and CFU-GEMM, in a cell population. The very primitive progenitor cells were well maintained without decrease in all of three different culture conditions even after cell expansion for 7 days.

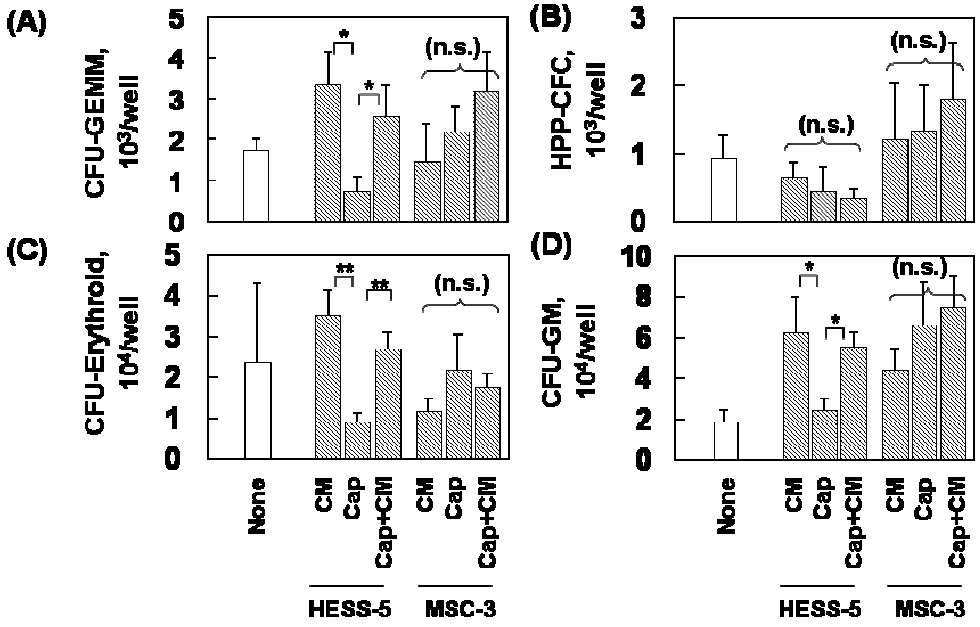


***Figure 2-7.*** Hematopoietic functions of the $CD34^+$ cell progeny after a 7-day culture. None: cultured in non-conditioned medium; CM: cultured in conditioned medium; Cap: cultured with microencapsulated cell aggregates in non-conditioned medium; Cap+CM: cultured with microencapsulated cell aggregates in CM. (A-D): Colony forming units (CFU) were determined by using the semi-solid methylcellulose medium. The number of CFU was counted in duplicate under each condition. Values represent the mean number of CFU per culture well and standard errors [n=5 (HESS-5); n=3 (MSC-3)]. Colonies were classified by morphology as follows: (A) CFU-GEMM (granulocyte/erythroid/ macrophage/megakaryocyte), (B) HPP-CFU (high-proliferative potential colony-forming cell), (C) CFU-Erythroid, (D) CFU-GM (granulocyte/ macrophage). 'n.s.' denotes no significant difference among 3 groups by ANOVA and an asterisk denotes $p < 0.05$ between two groups and double asterisks denote $p < 0.1$ by ANOVA and the following HSD test.

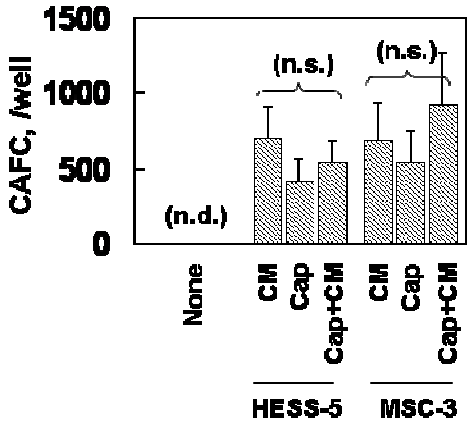


***Figure 2-8.*** Hematopoietic functions of the $CD34^+$ cell progeny after a 7-day culture. None: cultured in non-conditioned medium; CM: cultured in conditioned medium; Cap: cultured with microencapsulated cell aggregates in non-conditioned medium; Cap+CM: cultured with microencapsulated cell aggregates in CM. The number of cobblestone area forming-cell (CAFC) was calculated by limiting dilution. Values represents the mean number of CAFCs per culture well and standard error [n=5 (HESS-5); n=3 (MSC-3)]. 'n.s.' denotes no significant difference among 3 groups by ANOVA

# DISCUSSION

Various stromal cell lines established from the mouse, such as MS-5, OP9 and HESS-5, have been examined and credited with the ability to expand HSCs. However, it is difficult to rationalize the use of xenogeneic stromal cells in direct contact with HSCs in a clinical setting, due to the possibility of contamination of xenogeneic feeder cells with pathogens, which feeder cells carry [13]. To reduce the possibility of pathogen transmission, a unique co-culture system using a transwell membrane insert was reported for expansion of HSCs [12]. In this culture system, HSCs were separated from stroma HESS-5 cells by a porous membrane. HESS-5 cells feed various soluble bioactive substances to HSCs and provide growth stimuli, such as Notch signaling, to HSCs via direct cell-cell contact through filopodia extended from the membrane. Although this method is effective in expanding HSCs, public heath official remain cautious regarding contamination of xenogeneic pathogens through direct cell-cell contact or cell membrane fragments, and this approach has yet to be utilized for human patients. In addition, scaling up this culture system has proven to be difficult. Conditioned media (CM) of the feeder cells has also been previously examined to expand HSCs [15-17]. It is not as efficient, however, as co-culture with feeder cells. Various reasons are attributed to this difference. For example, stimuli afforded to HSCs through direct cell-cell contact are essential in supporting proliferation of HSCs, and although CM contains sufficient amounts of essential bioactive substances for HSC proliferation at the onset of culture, the efficacy of CM decreases with time as the nutrients are consumed by HSC cells. Thus, the frequency of media exchange has emerged as a key variable for maintaining optimal proliferation during *ex vivo*

expansion. These methodologies led us to develop a new culture system reported in this paper, that is, co-culture of HSCs with microencapsulated feeder cells in CM. The method proposed in this chapter addresses the HSC consumption of the limited supply of CM bioactive substances, by co-culturing with microencapsulated feeder cells that continuously supply the required nutrients.

When HESS-5 cells were employed as feeder cells, HSCs co-cultured with the microencapsulated cells in CM exhibited increased total cell number, more effective increase of $CD34^+$ cells and $CD34^+CD38^-$ cells, and maintenance of various progenitor cells, such as CFU-GEMM, GM and erythroid, as shown in Figure 2-7. It is known that the cell-cell interaction of hematopoietic stem cells with the niche cells is important for their self-renewal [32]. A calcium sensing receptor, expressed by hematopoietic stem cells, regulates the niches and can be targeted to increase stem cell number [33]. In this experimental setup, however, direct contact between HSCs and feeder cells could be not realized. Therefore, it is considered that the hematopoietic stem cells are expected to differentiate into progenitor cells during culture. Number of progenitor cells is believed to be an important parameter for success cell therapy. However, it recently claimed that the most important parameter in cell transplantation is the dose of total blood cells [1]. Therefore, the development of the method that can expand $CD34^+$ progenitor cells and concomitantly maintain early stem cells is importance for clinical application of UCB. Together this indicates that the combination of CM and microencapsulated HESS-5 cells is promising for clinical-scale *ex vivo* expansion of UCB.

The trend in stem cell research is to develop culture systems absolutely animal product-free. In this chapter, two cell lines, HESS-5 established from murine

bone marrow and MSC-3 established from human mesenchymal stem cells, were exmined. When the former cells are used for the clinical cell expansion, possibility of transmission of murine endogenous virus and microorgamisms to human patients should be carefully examined. Efficacy of polysaccharide microcapsules in protection of human recipients from transmission animal pathogens has been studied in the field of xenotransplantation of pancreatic islets. Although no infection of microorgamisms or porcine endogenous retroviruses (PERV) to human patients was reported in the transplantation of microencapsulated porcine cells [34, 35], infection of PERVs remains still controversial. Mice carry murine leukemia virus (MuLV) known as endogenous retrovirus. *In vitro* and *in vivo* assays to demonstrate total avoidance of the possibility of pathogen transmission, including endogenous retroviruses should be carefully established.

It is important to find human-derived hematopoietic-supportive feeder cells to further reduce the risk of contamination by xenogeneic pathogens. Thus, a cell line, MSC-3, established from human MSCs, was also examined. Recently, several groups reported that mesenchymal stem cells (MSCs), identified from human bone marrow in 1999 by Pittenger et al. [36], act as effective feeder cells for *in vitro* expansion of HSCs. [15, 37, 38]. Primary MSCs, however, are not accepted as tractable feeder cells for clinical use, as they undergo differentiation over time and enter senescence by 2 months after isolation [39]. The immortalization of MSCs and their hematopoiesis-supporting ability has been examined [40, 41]. When $CD34^+$ cells were co-cultured with CM, Cap of MSC-3 and CM+Cap of MSC-3, total cell number, $CD34^+$ cells and $CD34^+CD38^-$ cells increased in these three experimental conditions, but no clear additive effect CM and Cap of MSC-3. Feeder cells continuously supply bioactive

substances, but also consume nutrients and accumulate waste in media, thus the positive and negative effects of feeder cells were likely cancelled each other when microencapsulated MSC-3 cells were used. Additive effect of CM and Cap feeder cells in the case of HESS-5 means that effective soluble factors produced, and mode of production of bioactive substances and waste by MSC-3 are different from those of HESS-5. The cause of this difference remains unsettled. As pointed by Wen-tao et al. [42], it is important to develop mathematical models to better understanding the cell growth and consumption of supply of CM bioactive substances in order to design and build an effective system for expansion of HSCs using microencapsulated feeder cells. At this point, sufficient experimental data have not been accumulated for quantitative analyses. More detail analyses are left for future works.

One critical issue to be carefully considered for the future clinical applications of microencapsulated feeder cells is that increasing the number of committed progenitor cells may actually be depleting the more primitive stem cells from the unmanipulated inoculums. A concern regarding *ex vivo* expansion technology is the ability to maintain functional hematopoietic repopulating cells. Two groups reported Phase I studies of clinical use of expanded UCB stem and progenitor cells. In both studies, the UCB unit was split and a fraction was infused, while the rest was expanded and infused after expansion [43]. Although little clinical information is currently available to clarify questions for clinical efficacy of expanded cells from UCB, transfusion of these mature progenitors might shorten the time to engraftment by bridging the pancytopenic period even when the method employed is feasible to expand the mature progenitors.

# CONCLUSION

In this chapter, a novel co-culture system using microencapsulated feeder cells was developed to expand hematopoietic stem cells (HSCs) from cord blood. Co-culture of hematopoietic stem cells with microcapsulated feeder cells resulted in the increase of the number of total nucleated cells, including $CD34^{+}CD38^{-}$ cells, and various hematopoietic progenitors, and sustained the number of very earlier phase progenitors. Moreover, the addition of CM to the co-culture system demonstrated a significant additive effect when HESS-5 cells were employed as feeder cells. Effective expansion of total cells and maintenance of primitive progenitor cells suggest that transfusion of the progeny might shorten the time to engraftment by bridging the pancytopenic period and support functional hematopoietic repopulation. The combination of CM and microencapsulated feeder cells is promising for clinical-scale *ex vivo* expansion of HSCs.

# REFERENCES

1. Rocha V, Gluckman E; Eurocord and European Blood and Marrow Transplant Group. Clinical use of umbilical cord blood hematopoietic stem cells. *Biol. Blood Marrow Transplant.*, 2006, **12**(1 Suppl 1), 34-41.
2. Gluckman E, Broxmeyer HA, Auerbach AD, Friedman HS, Douglas GW, Devergie A, Esperou H, Thierry D, Socie G, Lehn P, et al. Hematopoietic reconstitution in a patient with Fanconi's anemia by means of umbilical-cord blood from an HLA-identical sibling. *N. Engl. J. Med.*, 1989, **321**, 1174-1178.
3. Franke K, Pompe T, Bornhauser M, Werner C. Engineered matrix coatings to modulate the adhesion of $CD133^+$ human hematopoietic progenitor cells. *Biomaterials*, 2007, **28**, 836-843.
4. Jiang XS, Chai C, Zhang Y, Zhuo RX, Mao HQ, Leong KW. Surface-immobilization of adhesion peptides on substrate for ex vivo expansion of cryopreserved umbilical cord blood $CD34^+$ cells. *Biomaterials*, 2006, **27**, 2723-2732.
5. LaIuppa JA, McAdams TA, Papoutsakis ET, Miller WM. Culture materials affect ex vivo expansion of hematopoietic progenitor cells. *J. Biomed. Mater. Res.*, 1997, **36**, 347-359.
6. Dexter TM, Moore MA, Sheridan AP. Maintenance of hemopoietic stem cells and production of differentiated progeny in allogeneic and semiallogeneic bone marrow chimeras in vitro. *J. Exp. Med.*, 1977, **145**, 1612-1616.
7. Sutherland HJ, Eaves CJ, Lansdorp PM, Thacker JD, Hogge DE. Differential regulation of primitive human hematopoietic cells in long-term cultures maintained on genetically engineered murine stromal cells. *Blood*, 1991, **78**, 666-672.

8. Croisille L, Auffray I, Katz A, Izac B, Vainchenker W, Coulombel L. Hydrocortisone differentially affects the ability of murine stromal cells and human marrow-derived adherent cells to promote the differentiation of $CD34^{++}/CD38^{-}$ long-term culture-initiating cells. *Blood*, 1994, **84**, 4116-4124.

9. Nakano T, Kodama H, Honjo T. Generation of lymphohematopoietic cells from embryonic stem cells in culture. *Science*, 1994, **265**, 1098-1101.

10. Nakano T, Kodama H, Honjo T. In vitro development of primitive and definitive erythrocytes from different precursors. *Science*, 1996, **272**, 722-724.

11. Tsuji T, Ogasawara H, Aoki Y, Tsurumaki Y, Kodama H. Characterization of murine stromal cell clones established from bone marrow and spleen. *Leukemia*, 1996, **10**, 803-812.

12. Kawada H, Ando K, Tsuji T, Shimakura Y, Nakamura Y, Chargui J, Hagihara M, Itagaki H, Shimizu T, Inokuchi S, Kato S, Hotta T. Rapid ex vivo expansion of human umbilical cord hematopoietic progenitors using a novel culture system. *Exp. Hematol.*, 1999, **27**, 904-915.

13. Patience C, Takeuchi Y, Weiss RA. Infection of human cells by an endogenous retrovirus of pigs. *Nat. Med.*, 1997, **3**, 282-286.

14. Martin MJ, Muotri A, Gage F, Varki A. Human embryonic stem cells express an immunogenic nonhuman sialic acid. *Nat. Med*., 2005, **11**, 228-232.

15. Kögler G, Radke TF, Lefort A, Sensken S, Fischer J, Sorg RV, Wernet P. Cytokine production and hematopoiesis supporting activity of cord blood-derived unrestricted somatic stem cells. *Exp. Hematol*., 2005, **33**, 573-583.

16. Breems DA, Blokland EA, Siebel KE, Mayen AE, Engels LJ, Ploemacher RE. Stroma-contact prevents loss of hematopoietic stem cell quality during *ex vivo*

expansion of $CD34^+$ mobilized peripheral blood stem cells. *Blood*, 1998, **91**, 111-117.

17. Bilko NM, Votyakova IA, Vasylovska SV, Bilko DI. Characterization of the interactions between stromal and haematopoietic progenitor cells in expansion cell culture models. *Cell Biol. Int.*, 2005, **29**, 83-86.
18. Nilsson K, Scheirer W, Merten OW, Ostberg L, Liehl E, Katinger HW, Mosbach K. Entrapment of animal cells for production of monoclonal antibodies and other biomolecules. *Nature*, 1983, **302**, 629-630.
19. Chaikof EL. Engineering and material considerations in islet cell transplantation. *Annu. Rev. Biomed. Eng.*, 1999, **1**, 103-127.
20. Avgoustiniatos ES, Colton CK. Effect of external oxygen mass transfer resistances on viability of immunoisolated tissue. *Ann.NY Acad.Sci.*, 1997, **831**, 145-167.
21. Iwata H, Takagi T, Kobayashi K, Yang H, Ito F. Immunoisolative effectiveness and limitation of agarose in a bioartificial pancreas. *Transplant. Proc.*, 1994, **26**, 789.
22. Iwata H, Murakami Y, Ikada Y, Control of complement activities for immunoisolation, *Ann.NY Acad.Sci.*, 1999, **875**, 7-23.
23. Okamoto T, Aoyama T, Nakayama T, Nakamata T, Hosaka T, Nishijo K, Nakamura T, Kiyono T, Toguchida J. Clonal heterogeneity in differentiation potential of immortalized human mesenchymal stem cells. *Biochem. Biophys. Res. Commun.*, 2002, **295**, 354-361.
24. Moriyasu K, Yamazoe H, Iwata H. Induction dopamine releasing cells from mouse embryonic stem cells and their long-term culture. *J. Biomed. Mater. Res. A*, 2006, **77**, 136-147.
25. Yang H, Iwata H, Shimizu H, Takagi T, Tsuji T, Ito F. Comparative studies of in vitro and in vivo function of three different shaped bioartificial pancreases made of

agarose hydrogel. *Biomaterials*, 1994, **15**, 113-120.

26. Sutherland DR, Anderson L, Keeney M, Nayar R, Chin-Yee I. The ISHAGE Guidelines for $CD34^+$ cell Determination by Flow Cytometry. *J. Hematother. Stem Cell Res.,* 1996, **5**, 213-226.

27. Leuner S, Arland M, Kahl C, Jentsch-Ullrich K, Franke A, Höffkes HG. Enumeration of CD34-positive hematopoietic progenitor cells by flow cytometry: comparison of a volumetric assay and the ISHAGE gating strategy. *Bone Marrow Transplant.*, 1998, **22**, 699-706.

28. Lu L, Xiao M, Shen RN, Grigsby S, Broxmeyer HE. Enrichment, characterization, and responsiveness of single primitive CD34 human umbilical cord blood hematopoietic progenitors with high proliferative and replating potential. *Blood*, 1993, **81**, 41-48.

29. Ploemacher RE, van der Sluijs JP, Voerman JS, Brons NH. An in vitro limiting-dilution assay of long-term repopulating hematopoietic stem cells in the mouse. *Blood*, 1989, **74**, 2755-2763.

30. Sutherland HJ, Lansdorp PM, Henkelman DH, Eaves AC, Eaves CJ. Functional characterization of individual human hematopoietic stem cells cultured at limiting dilution on supportive marrow stromal layers. *Proc. Natl. Acad. Sci. U. S. A.*, 1990, **87**, 3584-3588.

31. Normand V, Lootens DL, Amici E, Plucknett KP, Aymard P. New insight into agarose gel mechanical properties. *Biomacromolecules*, 2000, **1**, 730-738.

32. Ballen K. Targeting the stem cell niche: squeezing blood from bones. *Bone Marrow Transplant*., 2007, **39**, 655-660.

33. Adams GB, Chabner KT, Alley IR, Olson DP, Szczepiorkowski ZM, Poznansky MC,

Kos CH, Pollak MR, Brown EM, Scadden DT. Stem cell engraftment at the endosteal niche is specified by the calcium-sensing receptor. *Nature*, 2006, **439**, 599-603.

34. Zhang L, Yu P, Bu H, Li S, Li Y, Cheng J. Porcine endogenus retrovirus transmission from pig cell line to mouse tissues but not human cells in nude mice. *Transplant. Proc.*, 2005, **37**, 493-495.

35. Irgang M, Sauer IM, Karlas A, Zeilinger K, Gerlach JC, Kurth R, Neuhaus P, Denner J. Porcine endogenous retroviruses: no infection in patients treated with a bioreactor based on porcine liver cells. *J. Clin. Virol.*, 2003, **28**, 141-154.

36. Pittenger MF, Mackay AM, Beck SC, Jaiswal RK, Douglas R, Mosca JD, Moorman MA, Simonetti DW, Craig S, Marshak DR. Multilineage potential of adult human mesenchymal stem cells. *Science*, 1999, **284**, 143-147.

37. Reese JS, Koc ON, Gerson SL. Human mesenchymal stem cells provide stromal support for efficient $CD34^+$ transduction. *J. Hematother. Stem Cell Res.*, 1999, **8**, 515-523.

38. Zhang Y, Chai C, Jiang XS, Teoh SH, Leong KW. Co-culture of umbilical cord blood $CD34^+$ cells with human mesenchymal stem cells. *Tissue Eng.*, 2006, **12**, 2161-2170.

39. Rubio D, Garcia-Castro J, Martín MC, de la Fuente R, Cigudosa JC, Lloyd AC, Bernad A. Spontaneous human adult stem cell transformation. *Cancer Res.*, 2005, **65**, 3035-3039.

40. Nishioka K, Fujimori Y, Hashimoto-Tamaoki T, Kai S, Qiu H, Kobayashi N, Tanaka N, Westerman KA, Leboulch P, Hara H. Immortalization of bone marrow-derived human mesenchymal stem cells by removable simian virus 40T antigen gene: analysis of the ability to support expansion of cord blood hematopoietic progenitor

cells. *Int. J. Oncol.*, 2003, **23**, 925-932.

41. Kobune M, Kawano Y, Ito Y, Chiba H, Nakamura K, Tsuda H, Sasaki K, Dehari H, Uchida H, Honmou O, Takahashi S, Bizen A, Takimoto R, Matsunaga T, Kato J, Kato K, Houkin K, Niitsu Y, Hamada H. Telomerized human multipotent mesenchymal cells can differentiate into hematopoietic and cobblestone area-supporting cells. *Exp. Hematol.*, 2003, **31**, 715-722.
42. Wen-tao Q, Ying Z, Juan M, Xin G, Yu-bing X, Wei W, Xiaojun M. Optimization of the cell seeding density and modeling of cell growth and metabolism using the modified Gompertz model for microencapsulated animal cell culture. *Biotechnol. Bioeng.*, 2006, **93**, 887-895.
43. Schoemans H, Theunissen K, Maertens J, Boogaerts M, Verfaillie C, Wagner J. Adult umbilical cord blood transplantation: a comprehensive review. *Bone Marrow Transplant.*, 2006, **38**, 83-93.

# CHAPTER 3

# High-throughput evaluation of quiescent hematopoietic progenitor cells using micro-multiwell plate

## INTRODUCTION

Over the past few decades, a considerable number of studies have been conducted to identify and quantify primitive hematopoietic progenitor cells (HPCs). Various assays, such as flow cytometry using specific antibodies against surface markers, a short-term colony assay, and a long-term culture assay in the presence of various cytokines, have been developed. Each assay has its merits and disadvantages. For example, the simplest and most time-saving method is flow cytometry using specific antibodies against surface markers, such as CD34, CD117, and CD133 antigens [1], but surface markers to specify HPCs have not been fully identified and correlated with their multipotency. A short-term colony assay [2] is accepted as a simple and suitable method for quantifying lineage-restricted cells; thus, it is inadequate for detecting primitive HPCs. Long-term coculture assays using stromal cells to determine long-term culture-initiating cells (LTC-ICs) [3] and cobblestone area-forming cells (CAFCs) [4,5] are often used to quantify the number of primitive HPCs; however,

these assays require several weeks for results and consume a large number of cells. Thus, in this chapter, developing a short-term, simpler method for evaluating the number of primitive HPCs was focused on. The other problem is that a relatively large number of cells are needed to carry out these assays. There are a number of trials, such as, microcontact printing and microplates, to reduce a cell number for cell-based assays [6-8].

Two improvements were made for high-throughput evaluation of HPC frequency in $CD34^+$ cells from human cord blood. One was the development of a microwell plate made of a silicone sheet to reduce the number of cells required for each assay and that also allows for easy observation under a fluorescence microscope. The other improvement was the introduction of 5-fluorouracil (5-FU) treatment of $CD34^+$ cells, which has been used for isolating stem cells [9-12]. The number of 5-FU resistant progenitor cells (FRPCs) was evaluated by culturing 5-FU–treated $CD34^+$ cells in a culture medium supplemented with various cytokines. A combination of 5-FU treatment and the microwell format can result in high-throughput assays for obtaining information about HPC frequency in $CD34^+$ cells.

## EXPERIMENTAL

### *Cytokines and monoclonal antibodies*

A mixture of recombinant human stem cell factor (SCF), rh-thrombopoietin (TPO), and rh-Flt3 ligand (FL) (StemSpan CC110) was purchased from StemCell Technologies Inc (Vancouver, Canada). Antibodies used for immunohistochemistry

were as follows: mouse anti-human CD45 monoclonal antibody (clone HI30, BD Pharmingen, San Diego, CA, USA), rabbit anti-murine N-cadherin polyclonal antibody (H-63, Santa Cruz Biotechnology, Santa Cruz, CA, USA), and Alexa Fluor 488 goat anti-mouse IgG (H+L) and Alexa Fluor 594 goat anti-rabbit IgG (H+L) (Invitrogen Corp., Carlsbad, CA, USA).

***Preparation of cord-blood–derived CD34$^+$ cells***

Studies were approved by the institutional review board. Umbilical cord blood units were obtained from healthy donors, with the parents' informed consent. The CD34$^+$ cell fraction that is rich in HPCs was isolated from fresh umbilical cord blood as previously reported [13]. In brief, mononuclear cells were collected by density gradient centrifugation using Lymphoprep (AXIS-SHIELD PoC AS, Oslo, Norway). After two washes with Dulbecco's phosphate-buffered saline $Ca^{2+}Mg^{2+}$ free (DPBS(-); Nissui Pharmaceutical Co. Ltd., Tokyo, Japan), CD34$^+$ cells were isolated using magnetic beads (Direct CD34 Progenitor Cell Isolation Kit; Miltenyi Biotec GmbH, Bergisch Gladbach, Germany) in accordance with the manufacturer's instructions. Isolated CD34$^+$ cells were cryopreserved using a cryopreservation solution containing bovine serum (Cellbanker, Nippon Zenyaku Kogyo Co., Ltd., Fukushima, Japan) until use.

***Culture of murine stromal cell line***

A murine stromal cell line, HESS-5, was used as a hematopoiesis-supportive stromal cell line and was kindly donated by Dr. T. Tsuji (Tokyo University of Science) [14]. HESS-5 was maintained in the minimal essential medium alpha (MEM-alpha; Invitrogen) supplemented with 10% horse serum (JRH Biosciences, Lenexa, KS, USA),

100 U/mL of penicillin and 100 μg/mL of streptomycin (Invitrogen) at 37 °C under 5% $CO_2$ in a humidified atmosphere, and subcultured at 5–8 × $10^3$ per $cm^2$ every 3 to 4 d.

***Preparation of a microwell plate***

A schematic illustration of the preparation of a microwell plate is shown in Scheme 3-1. A silicone rubber sheet (thickness 0.5 mm; AS ONE Corp., Osaka,

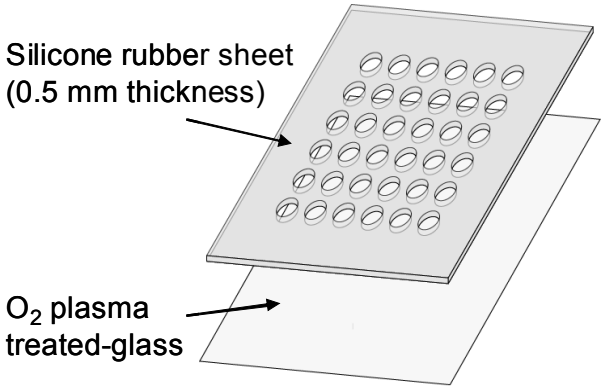


***Scheme 3-1***. Preparation of a microwell plate. A silicone rubber sheet with 6 × 6 wells was stuck to the oxygen plasma-treated glass slide.

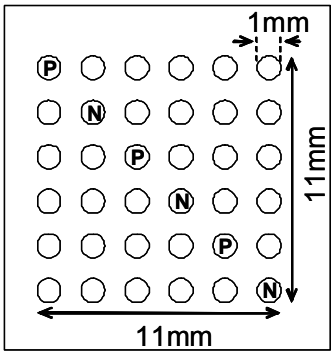


***Scheme 3-2***. Layout of a microwell sheet. The diameter of the well is 1 mm, and the distance between wells is also 1 mm. Positive (P) and negative (N) control spots were alternately placed on a diagonal line. Positive spots were inoculated with 100 $CD34^+$ cells, and negative spots were without $CD34^+$ cells.

Japan) was used to make microwells 1 mm in diameter and arrayed 6 × 6 at intervals of 1 mm (Scheme 3-2), and then sterilized in a dry oven (180 °C, 4 h). The fabricated rubber sheet was bonded to a glass substrate (Cover glass No. 5, 24 mm × 26 mm, thickness 0.5 mm; Matsunami Glass Ind., Ltd. Osaka, Japan), which was treated by oxygen plasma (5 Pa, 30 W, 60 sec) to remove stain and to increase hydrophilicity.

***Coculture of CD34$^+$ cells on a microwell plate***

The culture scheme for the primitive HPCs is shown in Scheme 3-3. A certain number of CD34$^+$ cells was suspended with HESS-5 cells ($7 \times 10^4$ cells/mL) in a culture medium, MyeloCult H5100 (StemCell Technologies Inc.; MEM-alpha containing 12.5% horse serum, 12.5% fetal bovine serum, 0.2 mM *i*-inositol, 16 μM folic acid, 0.1 mM 2-mercaptoethanol, and 2 mM L-glutamine) supplemented with 1 μM hydrocortisone (Sigma-Aldrich, St. Louis, MO, USA), 100 U/mL penicillin, and 100 μg/mL streptomycin (Invitrogen). The cell suspension was applied at 500 nL per well, and each well contained HESS-5 (350 cells/well) and certain numbers of CD34$^+$ cells (64, 32, 16, and 8 cells/well). Three wells containing 100 of CD34$^+$ cells and three wells without CD34$^+$ cells were used as positive and negative wells, respectively. Each culture was performed in duplicate. The microwell plate was placed in a Petri dish 5 cm in diameter and incubated overnight at 37 °C under 5% $CO_2$ in a humidified atmosphere to settle cells in the wells. Then, 2.5 mL of a selection medium, MyeloCult H5100 supplemented with 10 mg/mL 5-FU (Nacalai Tesque, Kyoto, Japan), was added to cover a whole plate to select for FRPCs. After a 2-day culture, the medium was changed to the expansion medium, MyeloCult H5100 supplemented with 50 ng/mL SCF, 50 ng/mL TPO, and 50 ng/mL FL. The medium was changed every 3 d.

After a 10-day expansion period, the culture was immunostained for quantification of proliferation of cells. The frequency of FRPCs in the seeded cell population was calculated by the numbers of the wells lacking expanded cells using Poisson statistics.

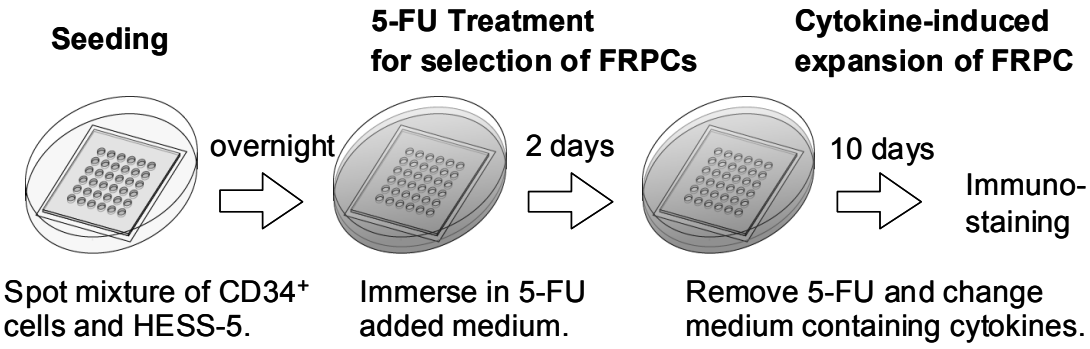


***Scheme 3-3***. The scheme of the cell culture. $CD34^+$ cells isolated from human cord blood were seeded together with HESS-5 onto a microwell plate. After cell adherence, the plate was immersed in a medium supplemented with 5-FU to remove proliferating cells and enrich 5-FU-resistant progenitor cells (FRPCs). FRPCs were expanded in a medium supplemented with cytokines for 10 d. After culture, the silicone sheet was removed and the cells were immunohistochemically stained to detect FRPC progeny cells

***Immunostaining of the culture***

A silicone rubber sheet was removed after the 10-day expansion culture period. The glass plate with cell spots was fixed with 4% paraformaldehyde (Nacalai Tesque) in DPBS for 30 min at 4 °C, rinsed with DPBS, and then permeabilized by treatment with 0.2% TritonX-100 in DPBS for 15 min at room temperature three times,

followed by immersion in 2% skim milk blocking solution for 30 min at room temperature to minimize nonspecific antibody binding. The plate was incubated overnight at 4 °C with primary antibodies: mouse anti-human CD45 monoclonal antibody (diluted to 1:250) to selectively label the progeny of human HPC, and rabbit anti-N-cadherin polyclonal antibody (1:250) to selectively label HESS-5. The plate was washed with 0.05% Tween-20 in DPBS (Wako) for 15 min three times and then was incubated with secondary antibodies, Alexa Fluor 488 goat anti-mouse IgG (1:250) and Alexa Fluor 594 goat anti-rabbit IgG (1:250), for 2 h at room temperature under dark. After washing with 0.05% Tween-20 three times, the plate was enclosed under a cover glass using a light anti-fade reagent (VectaShield, Vector Laboratories, Burlingame, CA, USA). Microscopic images were obtained under a fluorescence microscope (IX71, Olympus, Tokyo, Japan) or a fluorescence stereomicroscope (Leica Microsystems, Tokyo, Japan) for quantification. Fluorescence intensity of each spot was quantified using ImageJ (ver. 1.37, distributed by NIH). Numbers of $CD45^+$ cells were estimated from green fluorescence intensities from microwells. Values were normalized to the average intensity of positive control wells of each plate.

***Cobblestone area-forming cell assay***

The CAFC assay [4,5] was done with minor modifications, as follows. A confluent layer of HESS-5 cells was prepared on a 96-well tissue culture plate and irradiated by X-ray at a dose of 15 Gy to stop proliferation. $CD34^+$ cells were then serially diluted, and single-cell suspensions were seeded in MyeloCult H5100 supplemented with 1 μM hydrocortisone, 100 U/mL penicillin, and 100 μg/mL streptomycin. $CD34^+$ cells without 5-FU treatment were seeded at 100 μL per well with

24 replicates at 2-fold dilutions (40, 20, 10, 5, 2.5 cells/well) and incubated at 37 °C under 5% $CO_2$ in a humidified atmosphere. Half of the culture medium was changed every week, and individual wells were scored by visual inspection for the presence or absence of a cobblestone area at week 5. The frequency of CAFCs in the seeded population was calculated by using Poisson statistics.

***Statistical analysis***

Differences between the two groups were estimated by Student's t-test. $P < 0.05$ was considered statistically significant. All statistical calculations were performed using JMP ver.5.1.1 (SAS Institute, NC, USA).

## RESULTS

***Coculture of $CD34^+$ cells on a microwell plate***

$CD34^+$ cells and HESS-5 cells applied in microwells were cultured in the presence of 5-FU for 2 d, and then were expanded in a medium supplemented with SCF, TPO, and FL for 10 d. After expansion culture, wells contained different numbers of FRPC progeny cells, as shown in Figure 3-1. HESS-5 cells, which adhere on the glass plate, could be easily differentiated from FRPC progeny, and cells derived from FRPCs could be easily identified. Thus, FRPC frequency could be qualitatively estimated under a phase-contrast microscope. For more precise visualization of FRPC progeny, cells were immunohistochemically stained using antibodies against human CD45 and N-cadherin. CD45 is a membrane protein known as the leukocyte common antigen and

is widely expressed in leukocytes, but exhibits low expression in primitive HPCs. N-cadherin is reported as a key protein of the stem cell niche and is expressed on stromal cells [15, 16]. Figure 3-2(A) shows a plate after immunohistochemical staining for CD45 (green) and N-cadherin (red). Figures 3-2(B) and 3-2(C) show representative images of wells observed under a fluorescence microscope. HESS-5, hematopoiesis-supportive cells, expressed N-cadherin. Some wells contained a number of $CD45^+$ cells derived from FRPCs (Fig. 3-2(B)). Other wells did not contain any $CD45^+$ cells (Fig. 3-2(C)). These results indicate that the former well contained FRPCs but that the latter did not.

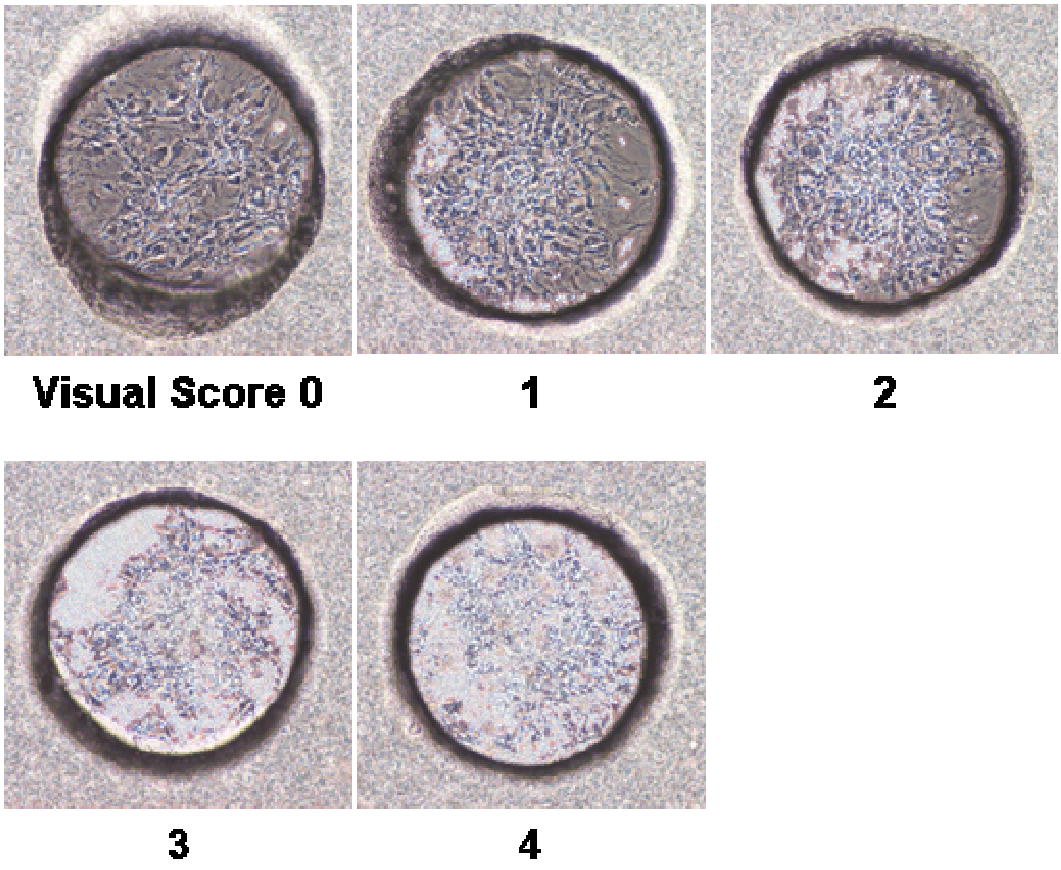


***Figure 3-1***. Representative phase-contrast microscopic images of wells containing FRPC progeny, which could be easily discriminated from HESS-5 cells based on the round-shaped morphology.

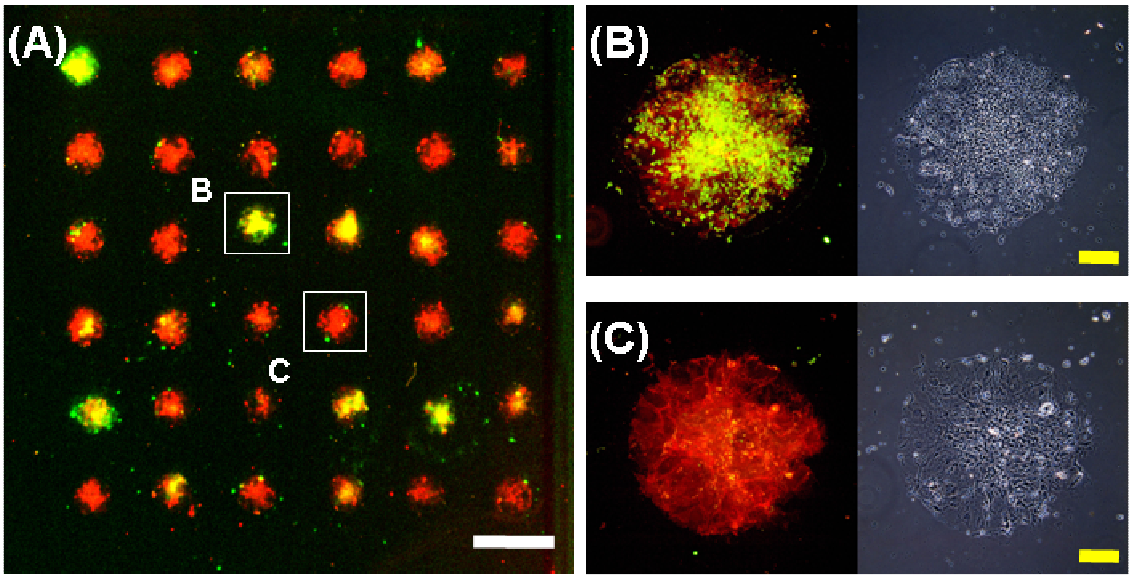


***Figure 3-2***. Representative microscopic images of wells containing FRPC progeny after coculture. (A) A fluorescent image of a representative microwell plate (bar = 2 mm). Cells on the plate were co-stained with anti-human CD45 (green) for the progeny of $CD34^+$ cells and anti–N-cadherin (red) for HESS-5. (B) High-magnification images of a well containing a lot of FRPC progeny cells in a well seeded with 100 $CD34^+$ cells. (C) No progeny of $CD34^+$ cells were observed in the well seeded only with HESS-5 (Bars = 200 μm for (B) and (C)).

### *Frequency of FRPC in $CD34^+$ cells*

The frequency of FRPCs in $CD34^+$ cells isolated from human cord blood was determined by the limiting dilution method. Different numbers of $CD34^+$ cells were inoculated into each well and treated with 5-FU and expanded as mentioned above. Figure 3-3 shows representative images of plates after immunohistochemical staining observed under a fluorescence microscope. The microwells of each plate were

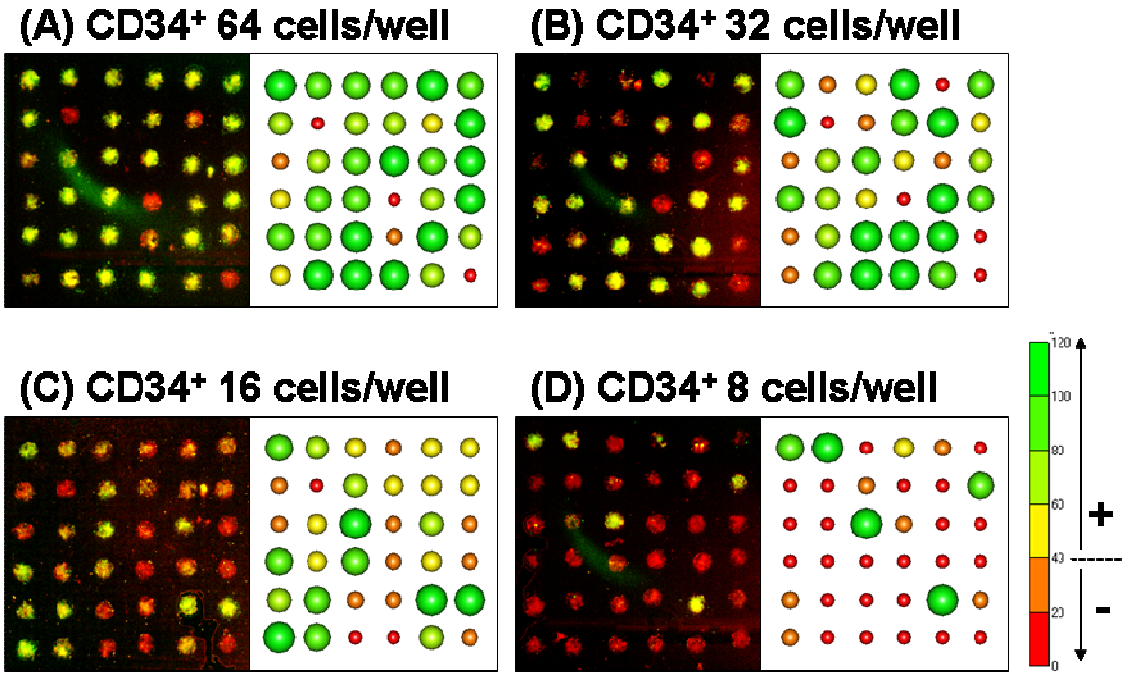


***Figure 3-3***. Fluorescent images of plates with different numbers of $CD34^+$ cells inoculated and their bubble-plot presentation for semi-quantitative expression of fluorescence intensities of the wells. Each left panel is a stereoscopic fluorescent microscopic image of the whole glass plate. The cells were immunostained with CD45 (green) and N-cadherin (red). Each right panel is a bubble plot of relative CD45 fluorescence intensity normalized to positive control wells. Green and yellow bubbles represent positive wells, and orange and red bubbles represent negative wells. The average numbers of inoculated $CD34^+$ cells were 64, 32, 16, and 8 cells per well for (A), (B), (C), and (D), respectively.

inoculated with 8, 16, 32, and 64 $CD34^+$ cells, respectively. Each spot exhibited a different green fluorescence intensity reflecting the numbers of FRPCs in a well. Fluorescence intensities of green and red for each spot were quantified using ImageJ.

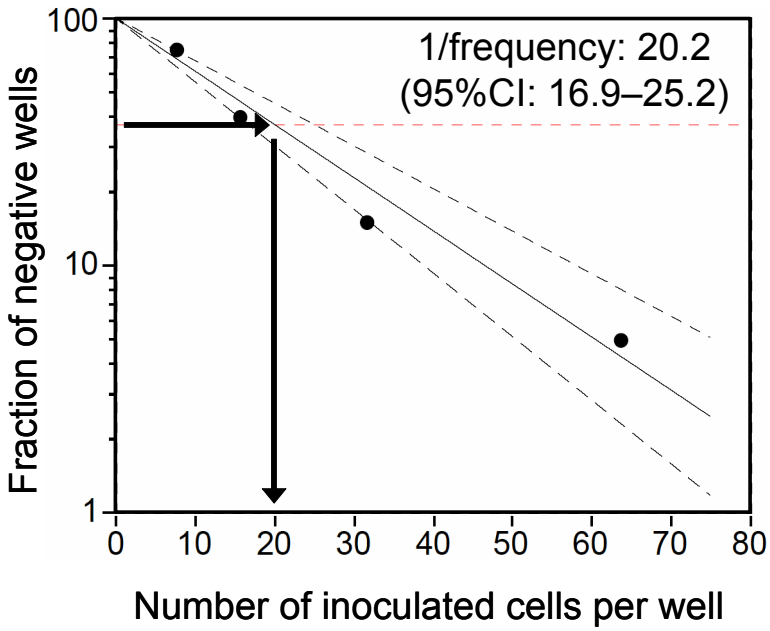


***Figure 3-4***. Plot of the fraction of negative spots as a function of the number of cells inoculated into the wells. The plain line represents the regression line estimated by the maximum likelihood method on the basis of Poisson statistics. Upper and lower dotted lines represent 95% confidence intervals.

Their intensities are schematically expressed in a bubble plot next to each plate in Figure 3-3, which includes a semi-quantitative scale for fluorescence intensities. A fluorescence intensity of 40 in arbitrary units was employed as a threshold for the existence of $CD45^+$ cells from FRPCs. Figure 3-3(A) shows a fluorescent image of a microwell plate, in which each well was inoculated with 64 $CD34^+$ cells except for the wells in a diagonal line, which were used as internal standards. The fluorescence intensities of 2 of 30 wells were less than 40. These 2 wells were identified as negative wells; *i.e.*, these wells were inoculated with $CD34^+$ cells, but those cells did not

***Table 3-1*** Summary of FRPC frequency *

| Cord blood lot # | Silicone microwell | 96-well multiplate |
|---|---|---|
| | **FRPC** | **CAFC ** (5 weeks)** |
| #1 | 20.2 ( 16.9–25.2 ) | 30.4 n.s. ( 23.5–42.8 ) |
| #2 | 50.0 ( 40.9–64.5 ) | 40.1 n.s. ( 24.3–71.4 ) |

* Each value represents the reciprocal number of HPC frequencies calculated by the limiting dilution assay (95% confidence intervals in parentheses). In a microwell plate, the number of wells of containing FRPCs derived from inoculated $CD34^+$ cells were counted using fluorescent images.

** CAFC frequency was evaluated by limiting dilution in a conventional long-term coculture method using a 96-well multiplate. 'n.s.' represents no significant difference with FRPC frequency. The significance level was calculated by comparing the regression slopes with the t-distribution.

contain FRPCs. When 8 $CD34^+$ cells were applied to wells, 24 out of 30 wells were regarded as negative (Figure 3-3(D)). The numbers of wells negative for FRPCs were plotted on semi-logarithmic graph paper as a function of the number of inoculated $CD34^+$ cells, and linear regression was done for the plots (Figure 3-4). The number of negative wells decreased with an increasing number of inoculated $CD34^+$ cells. The frequency of FRPCs was determined by the graphical method under the assumption that the frequency of the appearance of FRPCs in each well is expected to follow the predictions of Poisson statistics [3,5]. The value of the x-axis when the value of y-axis

is $e^{-1}$, or 0.37, is defined as the reciprocal of the frequency of FRPCs in a seeded $CD34^+$ cell population. In the case shown in Figure 3-3, the frequency of FRPCs was 1/20.2 (1/16.9 to 1/25.2, 95% confidence interval). The frequencies of FRPC in $CD34^+$ cells from different umbilical cord blood units are summarized in Table 3-1.

***Comparison with other methods***

To date, numbers of primitive HPCs have been estimated from numbers of CAFCs after long-term coculture of $CD34^+$ cells with stromal cells. When FRPC frequency was compared with the frequency of CAFCs for two lots of $CD34^+$ cells, both values were consistent with one another (Table 3-1).

## DISCUSSION

This assay consisting of two steps was developed for counting primitive HPCs. In the first step, $CD34^+$ cells isolated from human cord blood were treated with 5-FU to remove cells that actively proliferate, but enrich primitive HPCs. Treatment of peripheral blood mononuclear cells with 5-FU enriches primitive quiescent HPCs [9]. It has also been reported that HPCs can be purified by stimulation of target cells with c-kit and IL-3 in the presence of 5-FU. The 5-FU treatment has been used for isolating stem cells, such as hematopoietic stem cells and mesenchymal stem cells [10-12]. Thus, the 5-FU treatment of $CD34^+$ cells results in the enrichment of primitive HPCs.

In the second step, remaining cells were expanded on stromal cells in a culture medium supplemented with cytokines, FL, SCF, and TPO. Receptors for these

cytokines are known to be expressed on primitive HPCs [17-19]. Under the conditions, it is expected that HPCs would be well maintained and that early progenitors derived from HPCs would effectively proliferate. Differentiated cells would be removed during medium changes because only stem and progenitor cells attach to feeder HESS-5 cells. Moreover, primitive HPCs would be expected to survive after 5-FU treatment because primitive HPCs are believed to be in a quiescent state of the cell cycle [20,21]. In addition, cytokine treatment allows for functional analysis because expanded cells have receptors for cytokines. Therefore, the detection of FRPCs was predicted to be a functional indicator of the numbers of primitive HPCs.

To date, the frequency of primitive HPCs has been estimated from numbers of LTC-ICs [3] or CAFCs [4,5] after long-term coculture of $CD34^+$ cells with stromal cells. FRPC frequency was well correlated with CAFC frequency (Table 3-1). CAFC frequency, however, tended to be slightly higher than FRPC frequency. This slight difference might be due to the fact that FRPCs and CAFCs reflect different subpopulations containing HPCs. CAFCs are defined as cells that form the proliferating colony after long-term coculture with stromal cells and are rich in primitive HPCs [22]. However, the number of CAFCs does not reflect cells that can proliferate in response to cytokines. On the other hand, FRPCs are a cell subpopulation with the potential to proliferate in culture medium supplemented with cytokines. Thus, FRPC frequency tended to be slightly lower than CAFC frequency.

# CONCLUSION

In this chapter, the assay consisting of two steps was developed for counting primitive HPCs on a microwell plate. In the first step, $CD34^+$ cells isolated from human cord blood were treated with 5-FU to remove cells that actively proliferate, but enrich primitive HPCs. In the second step, remaining cells were expanded on stromal cells in a culture medium supplemented with cytokines, FL, SCF, and TPO. Under the conditions, early progenitors derived from HPCs would effectively proliferate. The 5-FU-resistant progenitor cells (FRPCs) was evaluated from the proliferation after these two steps. The frequency of detected FRPC was well correlated with HPC frequency determined conventional CAFC assay. A microwell plate to efficiently carry out the cell-proliferating assay was also developed. The cell number and the volume of medium can be reduced by using this newly developed microwell plate. Its use also allows easy observation of cells in wells under a fluorescence microscope. The combination of 5-FU treatment and the microwell format can realize a high-throughput assay for HPCs in $CD34^+$ cells.

# REFERENCES

1. Wognum AW, Eaves AC, Thomas. TE Identification and isolation of hematopoietic stem cells. *Arch. Med. Res.*, 2003, **34**, 461-475.
2. Broxmeyer HE. Colony assays of hematopoietic progenitor cells and correlations to clinical situations. *Crit. Rev. Oncol. Hematol.*, 1984, **1**, 227-257.
3. Sutherland HJ, Lansdorp PM, Henkelman DH, Eaves AC, Eaves CJ. Functional characterization of individual human hematopoietic stem cells cultured at limiting dilution on supportive marrow stromal layers. *Proc. Natl. Acad. Sci. U. S. A.*, 1990, **87**, 3584-3588.
4. Breems DA, Blokland EA, Neben S, Ploemacher RE. Frequency analysis of human primitive haematopoietic stem cell subsets using a cobblestone area forming cell assay. *Leukemia*, 1994, **8**, 1095-1104.
5. Ploemacher RE, van der Sluijs JP, Voerman JS, Brons NH. An in vitro limiting-dilution assay of long-term repopulating hematopoietic stem cells in the mouse. *Blood*, 1989, **74**, 2755-2763.
6. Mohr JC, de Pablo JJ, Palecek SP. 3-D microwell culture of human embryonic stem cells. *Biomaterials*, 2006, **27**, 6032-6042.
7. Moeller HC, Mian MK, Shrivastava S, Chung BG, Khademhosseini A. A microwell array system for stem cell culture. *Biomaterials*, 2008, **29**, 752-763.
8. Rosenthal A, Macdonald A, Voldman J. Cell patterning chip for controlling the stem cell microenvironment. *Biomaterials*, 2007, **28**, 3208-3216.
9. Rice A, Barbot C, Lacombe F, Dubosc-Marchenay N, Marit G, Hau F, Boiron JM, Reiffers J. 5-fluorouracil permits access to a primitive subpopulation of peripheral

blood stem cells. *Stem Cells*, 1993, **11**, 326-335.

10. Berardi AC, Wang A, Levine JD, Lopez P, Scadden DT. Functional isolation and characterization of human hematopoietic stem cells. *Science*, 1995, **267**, 104-108.
11. Bertolini F, Battaglia M, Soligo D, Corsini C, Curioni C, Lazzari L, Pedrazzoli P, Thalmeier K. "Stem cell candidates" purified by liquid culture in the presence of Steel factor, IL-3, and 5FU are strictly stroma-dependent and have myeloid, lymphoid, and megakaryocytic potential. *Exp. Hematol.*, 1997, **25**, 350-356.
12. Wang Z, Song J, Taichman RS, Krebsbach PH. Ablation of proliferating marrow with 5-fluorouracil allows partial purification of mesenchymal stem cells. *Stem Cells*, 2006, **24**, 1573-1582.
13. Fujimoto N, Fujita S, Tsuji T, Toguchida J, Ida K, Suginami H, Iwata H. Microencapsulated feeder cells as a source of soluble factors for expansion of CD34(+) hematopoietic stem cells. *Biomaterials*, 2007, **28**, 4795-4805.
14. Tsuji T, Ogasawara H, Aoki Y, Tsurumaki Y, Kodama H. Characterization of murine stromal cell clones established from bone marrow and spleen. *Leukemia*, 1996, **10**, 803-812.
15. Zhang J, Niu C, Ye L, Huang H, He X, Tong WG, Ross J, Haug J, Johnson T, Feng JQ, Harris S, Wiedemann LM, Mishina Y, Li L. Identification of the haematopoietic stem cell niche and control of the niche size. *Nature*, 2003, **425**, 836-841.
16. Calvi LM, Adams GB, Weibrecht KW, Weber JM, Olson DP, Knight MC, Martin RP, Schipani E, Divieti P, Bringhurst FR, Milner LA, Kronenberg HM, Scadden DT. Osteoblastic cells regulate the haematopoietic stem cell niche. *Nature*, 2003, **425**, 841-846.
17. Namikawa R, Muench MO, Roncarolo MG. Regulatory roles of the ligand for

Flk2/Flt3 tyrosine kinase receptor on human hematopoiesis. *Stem Cells*, 1996, **14**, 388-395.

18. Sharma S, Gurudutta GU, Satija NK, Pati S, Afrin F, Gupta P, Verma YK, Singh VK, Tripathi RP. Stem cell c-KIT and HOXB4 genes: critical roles and mechanisms in self-renewal, proliferation, and differentiation. *Stem Cells Dev.*, 2006, **15**, 755-778.
19. Kaushansky K Thrombopoietin and the hematopoietic stem cell. *Ann.NY Acad. Sci.*, 2005, **1044**, 139-141.
20. Hao QL, Thiemann FT, Petersen D, Smogorzewska EM, Crooks GM. Extended long-term culture reveals a highly quiescent and primitive human hematopoietic progenitor population. *Blood*, 1996, **88**, 3306-3313.
21. Cheng T, Rodrigues N, Shen H, Yang Y, Dombkowski D, Sykes M, Scadden DT. Hematopoietic stem cell quiescence maintained by p21cip1/waf1. *Science*, 2000, **287**, 1804-1808.
22. van Hennik PB, Verstegen MM, Bierhuizen MF, Limón A, Wognum AW, Cancelas JA, Barquinero J, Ploemacher RE, Wagemaker G. Highly efficient transduction of the green fluorescent protein gene in human umbilical cord blood stem cells capable of cobblestone formation in long-term cultures and multilineage engraftment of immunodeficient mice. *Blood*, 1998, **92**, 4013-4022.

# PART II

# ANALYSIS OF MICROENVIRONMENTAL RESPONSES OF MESENCHYMAL STEM CELLS BY USING FINE STRUCTURED SURFACES

# CHAPTER 4

# Supercritical $CO_2$-assisted embossing for studying cell behavior on microtextured surfaces

## INTRODUCTION

The chemical modification of biomedical material surfaces has been extensively studied in the context of controlling cell responses, such as adhesion, migration, proliferation, and differentiation, and also host inflammatory responses *in vivo* [1,2]. Recently, it has been reported that surface topography at the micro- and nanoscale levels also exerts various effects on cell behavior [3-7]. A greater understanding of the effects of surface topography on cell behaviors could lead to new opportunities for innovation in the design of biomaterials. Although many reports related to this subject were published, there have been still some difficulties in elucidating purely topographical effects on cell behavior [1]. Procedures, such as coating and etching [8], which have been frequently employed to prepare various surface microstructures, concomitantly alter surface chemical composition. Injection molding and hot embossing, which have been industrially used for thermoplastic polymers, seem to be easy methods for preparing a surface with unique topography

[9,10]. However, surface contamination with release reagents [11, 12] and oxidation during processing at high temperature bring uncertainty to any examination of the effects of surface topography on cell behaviors. Moreover, processing at high temperature gives rise to an unanticipated deformation of the substrates due to non-uniform cooling, resulting in a lower accuracy of fine surface structures [13]. A new processing method is needed to prepare micro- and nanoscale surface structures without these attendant problems.

In this chapter, supercritical $CO_2$-assisted embossing to prepare micro- and nanoscale surface structures was focused on [14, 15]. In supercritical $CO_2$-assisted embossing, a polymer surface is plasticized by dissolving supercritical $CO_2$ and thus can be embossed by a mold with a wide-scale, different pattern at a lower temperature than the glass transition temperature ($T$g). In addition, $CO_2$ gas released from the plasticized polymer surface flows along the interface between the mold and the substrate, thus allowing easy detachment of the polymer fabricate from the mold [16]. A release agent is not required in supercritical $CO_2$-assisted embossing. In this study, concave and convex microlenses and nanogrooves with three different scales were prepared on the surface of polycarbonate (PC) plates using supercritical $CO_2$-assisted embossing, and cell attachment and alignment on the surfaces were examined using mesenchymal stem cells (MSCs).

# EXPERIMENTAL

***Fabrication of fine structures***

PC plates with various micro- and nanopatterns were printed using a supercritical $CO_2$-assisted embossing machine. A vessel of the embossing machine was separated into two chambers by a partition (Scheme 4-1). An under pedestal could move between the two chambers through a partition like a syringe. A disk-shaped PC plate (diameter = 20 mm; thickness = 3 mm; bisphenol A type; Mw = 58,000; *T*g = 153 °C; Tsutsunaka Plastic Industry Co. Ltd., Osaka, Japan) was placed on top of the pedestal. A nickel mold was set on the ceiling of the upper chamber. Two nickel molds that were both micrometer scaled and lens shaped (ML-1 and ML-2) and three nanometer-scaled grooved nickel molds (NG-1, NG-2, and NG-3) were kindly donated

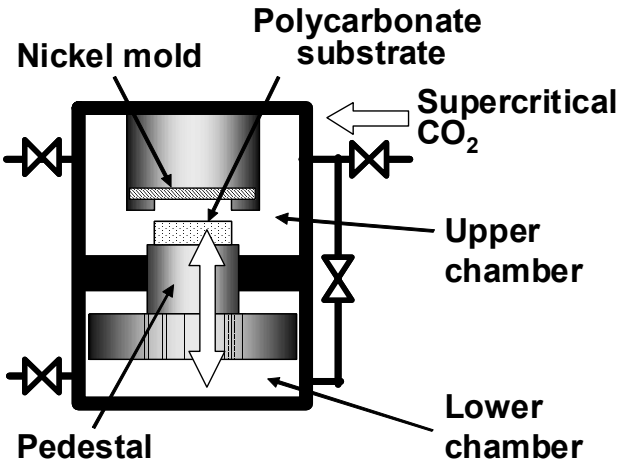


***Scheme 4-1***. Schematic illustration of embossing machine using supercritical $CO_2$.

by Hitachi Maxell, Ltd., Tokyo, Japan (Figs. 4-1 and 4-2). ML-1 and ML-2 molds have concave and convex microlenses, respectively. Microlenses were 10 μm in diameter and arrayed in a rectangular pattern. The groove widths of the NG-1, NG-2, and NG-3 molds were 483 ± 21, 553 ± 117, and 557 ± 140 μm, respectively; their ridge widths were 1050 ± 56, 1247 ± 61, and 1080 ± 30 μm, respectively; and their groove depths were 232.0 ± 0.9, 85.4 ± 9.0, and 57.6 ± 0.6 nm, respectively (means ± standard deviations for n = 4).

The molds and the PC plates were cleaned up by spraying fluorocarbon gas. Unfabricated PC plates were stored in a desiccator for at least one day before embossing. The upper chamber was filled with $CO_2$ gas to 10 MPa, and then the chamber temperature was increased to 100 °C to achieve the $CO_2$ supercritical condition. The *T*g of PC (153 °C) is reduced to approximately 100 °C by dissolving supercritical $CO_2$ [14,15]. The surface of the PC plate was plasticized by dissolution of $CO_2$ under the supercritical condition for 5 min. Then, $CO_2$ was released from the upper chamber, and immediately the pressure of the lower chamber was increased by introduction of the $CO_2$ gas to lift the pedestal. The PC plate was pressed to the nickel mold at 12000–15000 N for 30 sec at 100 °C. The micropattern was embossed onto the surface of the PC plate. $CO_2$ was completely released from both chambers, and the plate was detached from the mold.

***Microscopic analysis of surface topography***

Surface micropatterns on the PC plate were observed using a scanning electron microscope (SEM; S-2380N Natural SEM, Hitachi High-Technologies Corporation, Tokyo, Japan) for microlenses and a scanning probe microscope (SPM;

SPM-9500J3, Shimadzu Corp., Kyoto, Japan) for nanogrooves. Surface dimensions of micropatterns in 3 randomly selected fields for microlenses and 6 fields for nanogrooves were quantitatively determined using a laser 3D profile microscope (Type VK-8500, Keyence, Osaka, Japan) for microlenses and an SPM for nanogrooves, respectively.

***Surface atomic compositions***

Surface atomic compositions of the PC plates were characterized using an X-ray photoelectron spectrometer (XPS) (ESCA-850V; Shimadzu Corp., Kyoto, Japan) equipped with a Mg X-ray source to examine surface contamination and chemical changes during embossing. The take-off angle was 90 °, the operating pressure was lower than $1 \times 10^{-5}$ Pa, and Au ($4f_{7/2}$) at 83.8 eV was used as the standard peak.

***Cell culture***

Human bone-marrow–derived MSCs (Lonza, Basel, Switzerland) were maintained in Dulbecco's Modified Essential Medium (DMEM; Invitrogen Corp., CA, USA) supplemented with 10% fetal bovine serum (FBS; BIOWEST, France), 100 U/mL penicillin, and 100 μg/mL streptomycin (Invitrogen) at 37 °C under 5% $CO_2$ in a humidified atmosphere, and subcultured at $5 \times 10^3$ cells per $cm^2$ every 3 to 4 day. Cells at passages three through eight were used for experiments.

Prior to cell seeding, cells and the PC plates were pretreated as follows: MSCs were treated with 10 μg/mL mitomycin C (Wako Pure Chemical Industries, Ltd., Osaka, Japan) for 2 h to stop proliferation and then washed three times with Dulbecco's phosphate buffered-saline $Ca^{2+}Mg^{2+}$ free (DPBS(-); Nissui Pharmaceutical Co. Ltd.,

Tokyo, Japan). Fabricated plates were coated with 10 μg/mL fibronectin (Invitrogen) for 2 h at 37 °C and washed 5 times with DPBS(-). MSCs were seeded at $5 \times 10^3$ cells per $cm^2$ on fibronectin-coated plates and cultured for 4 days.

***Immunostaining***

Cells were stained with cytoskeletal fibrous actin (F-actin) for analysis of cell morphology and with vinculin to visualize focal adhesions. The cultures were fixed with 4% paraformaldehyde (Nacalai Tesque, Inc., Kyoto, Japan) for 15 min and permeabilized with 0.2% Triton-X (Wako) for 3 min. For vinculin staining, the cultures were blocked with 2% skimmed milk (Nacalai) for 1 h at room temperature, incubated with anti-mouse vinculin (Chemicon, CA, USA) (1:200 dilution; reactive with human vinculin) overnight at 4 °C, washed with 0.05% polyoxyethylene sorbitan monolaurate (Tween 20, Wako, Osaka, Japan) for 15 min three times at room temperature, and treated with Alexa-488 conjugated anti-mouse IgG (Invitrogen) (1:500 dilution) for 30 min at room temperature. The cultures were further treated with Alexa-594 conjugated phalloidin (Invitrogen) (1:40 dilution) for F-actin staining and with Hoechst 33342 (Dojindo, Kumamoto, Japan) (1:1000 dilution) for nuclear staining. The stained cultures were mounted on slides with a light anti-fade reagent (Vectashield, Vector Laboratories, CA, USA) and observed using a fluorescence inverted microscope (IX71, Olympus, Tokyo, Japan).

***Preparation of cultures for SEM observation***

The cultures for SEM observation were treated as follows. Cultures were fixed with 2% glutaraldehyde in PBS for 1 h and sequentially immersed in serially

diluted ethanol solutions (30, 50, 60, 70, 80, 90, 95, and 99.5%) and t-butyl alcohol four times for 10 min each to dehydrate. The samples were freeze-dried overnight with a freeze-dryer (FDU-830, EYELA, Tokyo, Japan) and then sputter-coated with Pt/Pd (E-1010 Ion sputter, Hitachi High-Technologies Corporation, Tokyo, Japan).

***Analysis of cell area and orientation angle***

Cell areas and orientation angles were quantified by analysis of immunostained images or low-magnification time-lapse phase-contrast images using Image J (ver 1.37, distributed by NIH). The orientation angle of an individual cell was determined as the angle between the longest axis of the cell that passes through the cell nucleus and the direction of the microlens grid or nanogroove. The distribution of cell orientation was estimated by a wrapped normal distribution as previously reported [17-19]. Briefly, the probability distribution function has been adapted from Fisher [20] for a periodicity of $\pi$ radians as follows:

$$f(\theta) = \frac{1}{\pi}\left(1 + 2\sum_{p=1}^{\infty} \rho^{p^2} \cos(2p(\theta - \pi))\right), \quad \text{(Eq. 4-1)}$$

$$\rho = \frac{1}{n}\sqrt{\left(\sum_{i=1}^{n} \cos 2\theta_i\right)^2 + \left(\sum_{i=1}^{n} \sin 2\theta_i\right)^2}, \quad \text{(Eq. 4-2)}$$

$$\mu = \tan^{-1}\left(\sum_{i=1}^{n} \sin 2\theta_i \Big/ \sum_{i=1}^{n} \cos 2\theta_i\right). \quad \text{(Eq. 4-3)}$$

where $\rho$ is the mean resultant length, and $\mu$ is the mean angle. These parameters were determined from a set of $n$ measured cell orientation angles, $\theta_i$. The angular standard deviation, $\sigma$, for the distribution was determined by the following equation:

$$\sigma = \frac{1}{2}\sqrt{-2\ln\rho}\,. \quad \text{(Eq. 4-4)}$$

### *Statistical analysis*

Significant differences between two groups were examined using the Student's t-test. A $p < 0.05$ was considered statistically significant. All statistical calculations were performed using the software JMP ver.5.1.1.

## RESULTS

### *Fabrication of substrata*

Micro- and nanostructures onto the surface of PC plates were embossed using supercritical $CO_2$-assisted embossing. Microscopic images of the molds and the cross-section images of formed micro- and nanostructures are shown in Figures 4-1 and 4-2. Dimensions of the surface structures were determined for three randomly selected fields and are summarized in Table 4-1. The standard deviations of each dimension for formed structures were 4.3% and 8.4% in coefficient of variation of the height for ML-1 and ML-2, respectively; they were 12.2%, 11.4%, and 7.4% in coefficient of variation of the groove depth for NG-1, NG-2, and NG-3, respectively. These smaller standard deviations suggest that uniform micro- and nanopatterned surfaces across the whole area of the PC plate surfaces were obtained.

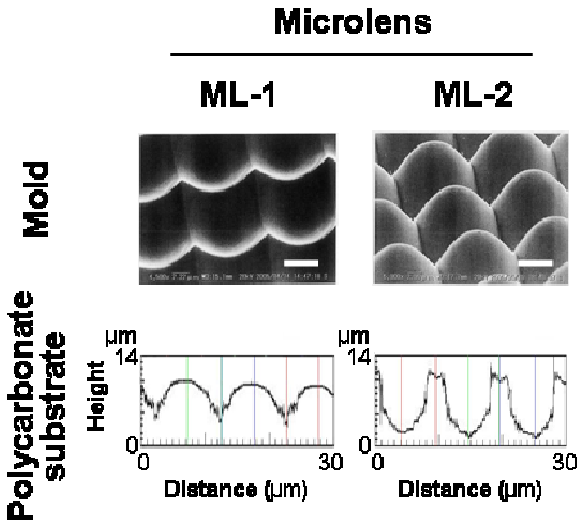


***Figure 4-1.*** The surface images of molds and the cross section of fabricated substrate. Upper panels show the surface images by SEM (bars = 5 μm) for microlenses or SPM (10 μm per square) for nanogrooves.

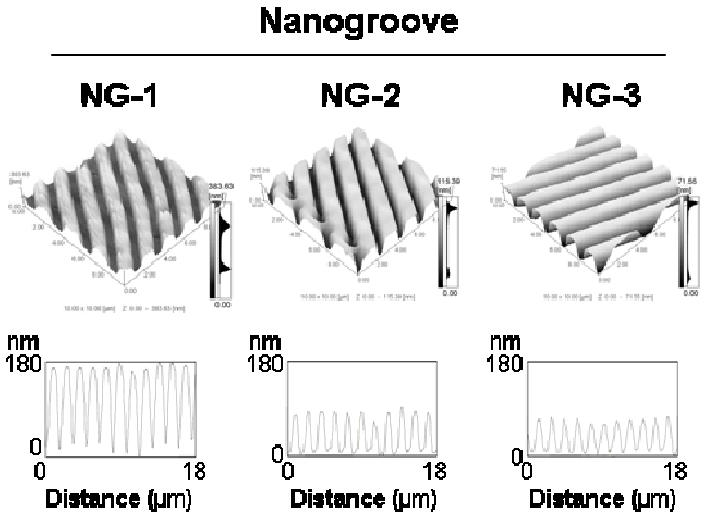


***Figure 4-2.*** The surface images of molds and the cross section of fabricated substrate. Lower panels show the cross section along the microlens grid or perpendicular to the nanogroove, captured by a laser 3D profile microscope.

***Table 4-1.*** Dimensions of the fabricated plates.*

| Name | Mold pattern | Dimensions of fabricated plate | | | | |
|---|---|---|---|---|---|---|
| | | Height | GL | | RMS | |
| ML-1 | Concave lens | 6.24 ± 0.27 | 10.34 ± 0.01 | | 1.31 ± 0.12 | (μm) |
| ML-2 | Convex lens | 6.31 ± 0.53 | 10.19 ± 0.42 | | 1.93 ± 0.29 | (μm) |
| | | GD | GW | RW | RMS | |
| NG-1 | Grooves | 199.3 ± 24.4 | 673 ± 160 | 867 ± 163 | 75.4 ± 14.3 | (nm) |
| NG-2 | Grooves | 83.0 ± 9.5 | 912 ± 48 | 648 ± 50 | 30.9 ± 4.2 | (nm) |
| NG-3 | Grooves | 56.4 ± 4.2 | 752 ± 79 | 763 ± 33 | 22.5 ± 1.9 | (nm) |

* GL = grid length, RMS = root-mean-square roughness; GD = groove depth; GW = groove width; RW = ridge width; and mean ± standard deviation (n = 3 for ML-1 and ML-2, respectively; n = 6 for NG-1, NG-2, and NG-3, respectively).

Surface atomic compositions of the printed surfaces were analyzed by XPS to assess chemical contamination and oxidation. The results are summarized in Table 4-2. Nickel, fluorine, and nitrogen, which are expected to be deposited on the surface from the mold, release reagents, and fingers of the researchers, respectively, were not detected. The carbon-to-oxygen ratios of the fabricated surfaces were almost equivalent to the theoretical ratio (C:O = 84.2:15.8) calculated from the PC molecular structure. These results suggest that the micro- and nanopatterned fabrication of plate was successfully embossed by supercritical $CO_2$-assisted embossing without the contamination of chemicals or oxidation. A combination of supercritical $CO_2$-assisted embossing of PC plates is suitable for preparing micro- and nanostructures on the surface for examining the effects of surface topography on cell behaviors.

***Table 4-2.*** Atomic contents of fabricated substrata determined by X-ray photoelectron spectroscopy.

| | Atomic contents (%) * | | | | |
|---|---|---|---|---|---|
| | C | O | N | F | Ni |
| Non-treated | 81.2 | 18.8 | n.d. | n.d. | n.d. |
| ML-1 | 84.7 | 15.3 | n.d. | n.d. | n.d. |
| ML-2 | 83.5 | 16.5 | n.d. | n.d. | n.d. |
| NG-1 | 82.2 | 17.8 | n.d. | n.d. | n.d. |
| NG-2 | 83.4 | 16.6 | n.d. | n.d. | n.d. |
| NG-3 | 85.5 | 14.5 | n.d. | n.d. | n.d. |

* 'n.d' denotes 'not detected'.

***Cell morphology***

MSCs are promising cells for cell therapy because they are multipotent stem cells that can differentiate into a variety of cell types [21] and support other stem cells as feeder cells [22, 23]. To investigate their behaviors on fabricated materials, MSCs were cultured on PC plates with different surface topographies for 4 days. Fig. 4-2 shows staining of F-actin and nucleus of the MSCs. Spreading areas and cell orientations were evaluated from the microphotographs and are summarized in Figs. 4-3 and 4-4. Spreading areas of MSCs cultured on microlenses ML-1 and ML-2 were reduced to 76% and 73% of the cell areas on non-treated PC substrates, respectively. The smaller spreading on the microlens might be due to the differences in cell attachment area on the substrate. MSCs elongated on nanogroove surfaces and tended to be aligned following the direction of the grooves, as clearly seen on NG-1 (Fig. 4-3).

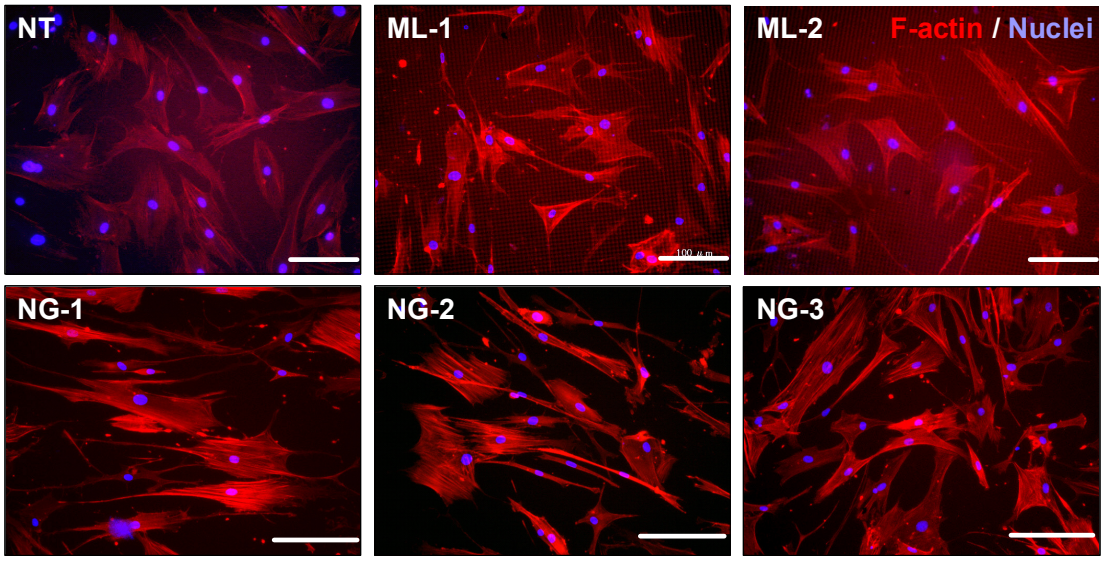


***Figure 4-2.*** Immunohistochemical images of MSCs cultured on fabricated polycarbonate substrata for 4 d. Cells were co-stained with F-actin for cytoskeleton (red) and nuclei (blue). NT: non-treated plate (bars = 100 μm). In the images of NG-1, NG-2, and NG-3, nanogrooves were parallel to the horizontal axis.

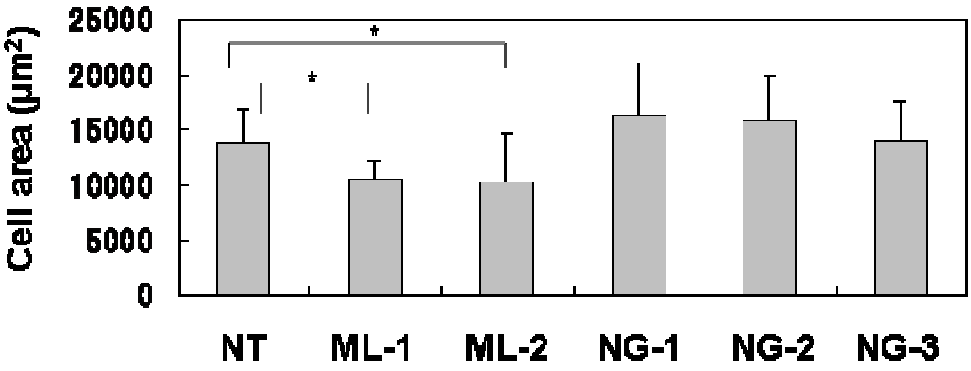


***Figure 4-3.*** The effect of nanogrooves on the cell area of individual cells cultured on fabricated substrata for 4 d. Values were obtained by image analysis (mean ± standard deviation; n = 4 independent cultures; more than 20 cells were measured in each culture). An asterisk denotes a significant difference between N.T. and a respective group ($p < 0.05$).

To quantify the alignment of cells on the nanogrooves, orientation angles of >100 individual cells were evaluated from F-actin–stained images. The histogram of the orientation angle distribution shown in Fig. 4-4 followed a normal distribution (see also EXPERIMENTAL Section). Fig. 4-4 included the angular standard deviations ($\sigma$), which were calculated using Equation (4-4). A smaller standard deviation indicates that the cells align along the specific direction. The angular standard deviations were decreased when the cells were cultured on a deeper nanogroove plate, such as NG-1 or NG-2.

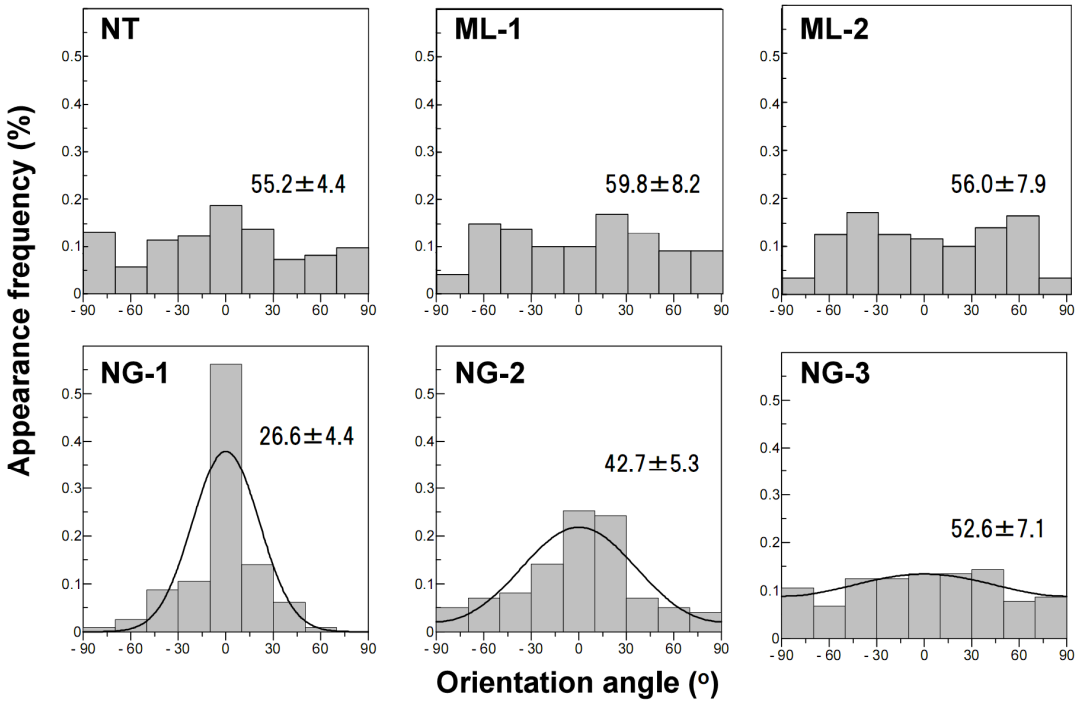


***Figure 4-4.*** The distribution of the orientation angles for individual cells cultured on the different substrata. The histogram shows the appearance frequency of each population. More than 100 cells were counted in each measurement. Curves represent the estimation from a wrapped normal distribution model [see Equation (4-1)]. The inlet values represent the averaged angular standard deviations (σ) of the estimated distribution (n=3).

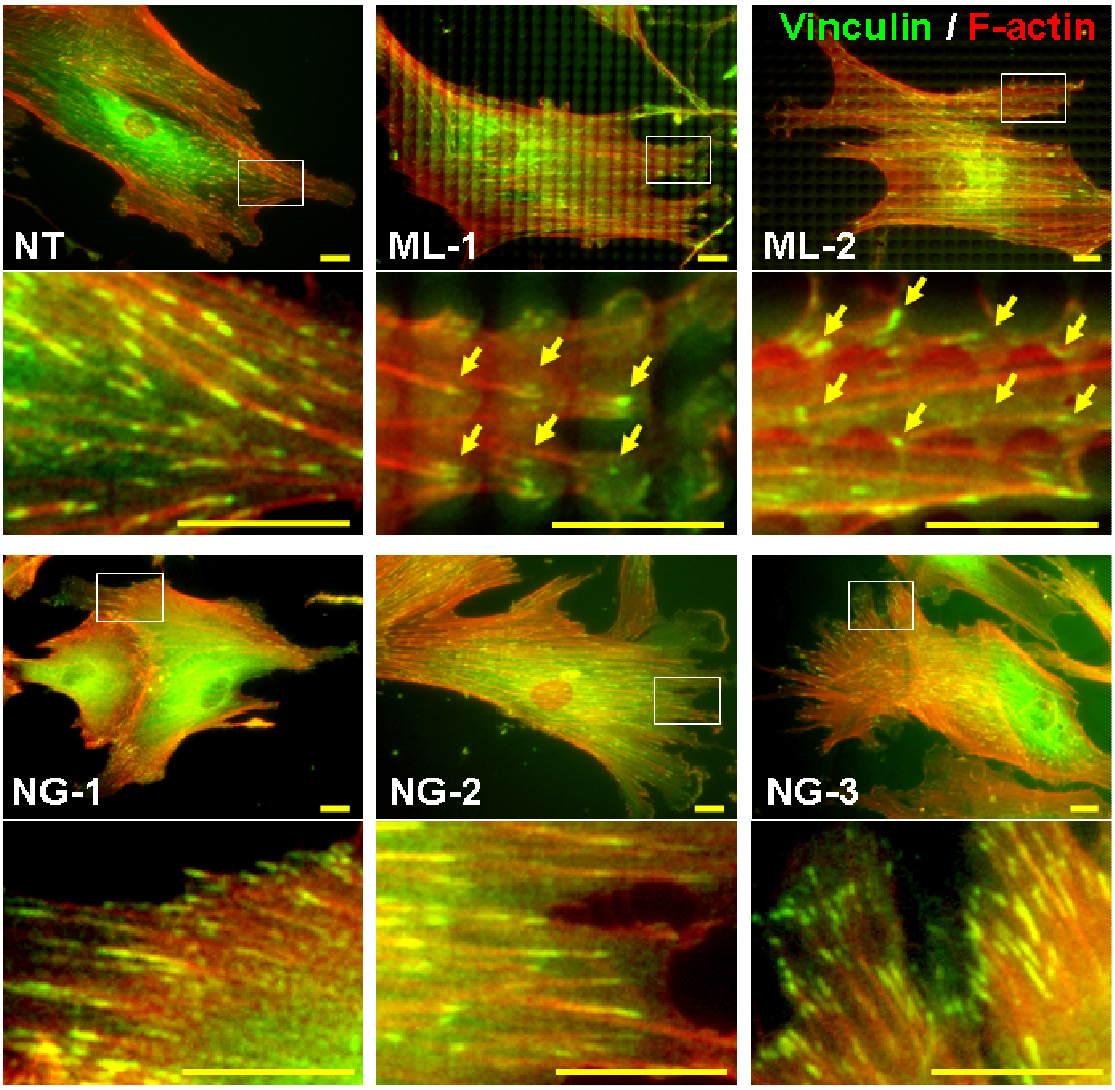


***Figure 4-5.*** Vinculin expression of MSCs cultured on fabricated substrata for 4 days. Cells were co-stained with anti-vinculin (green) and F-actin (red). NT: non-treated plate (bars = 20 μm). In the images of NG-1, NG-2, and NG-3, nanogrooves were parallel to the horizontal axis. The lower panels are high-magnification images of the white rectangular areas in the upper panels. Yellow arrows in the cells on the microlenses represent the point at which focal adhesions were expressed locally.

***Focal adhesion***

Vinculin, which is a membrane cytoskeletal protein that acts as a linker between the actin cytoskeleton and integrins or cadherins, localizes at focal adhesions. Fig. 4-5 shows immunohistochemical staining of vinculin for MSCs culture for 4 days on PC plates with different surface topographies. Vinculin was expressed more densely at the growing periphery of cells than in the area near the nucleus on the flat PC surface as shown in Fig. 4-5 (NT). Vinculin-positive areas were found on the top of the concave microlens ML-1, and on the rims of the convex microlens ML-2. These results suggest that focal adhesion plaques were formed on the projected area of the substrata. Results with SEM images also supported the location of lamellipodia on the projected area of the microlens (Fig. 4-6). Vinculin was expressed more densely in MSCs cultured on the nanogrooves than on the microlens, indicating that they attached to the nanogrooves more strongly than to the microlens.

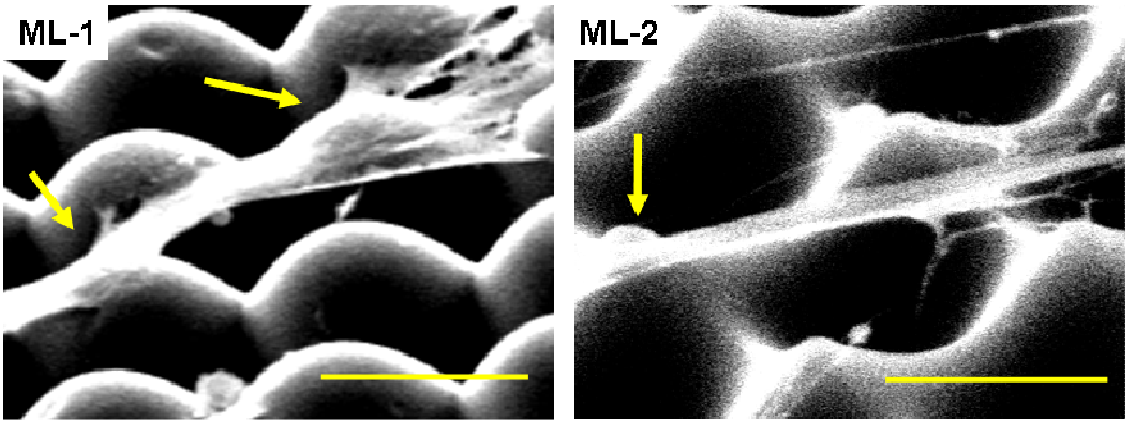


***Figure 4-6.*** SEM images of MSCs cultured on ML-1 and ML-2. Yellow arrows represent the point at which cells attached to the substrate (bars = 10 μm).

Differences in the size of the micropattern affected vinculin localization on the microlens and the nanogrooves (Table 4-1). The root-mean-square roughness of the microlenses (1.3–1.9 μm) was smaller than the extended cell size (50–100 μm in diameter) but as large as the size of focal adhesions (2–30 μm [24]). The available adhesion areas on the microlens were smaller than those on the non-treated plate, to which cells adhered at any place on the surface and could form larger focal adhesions. One other interesting observation is that focal adhesions aligned onto the ridges on NG-1 and NG-2. On the other hand, such alignment of focal adhesions was not observed in cells cultured on the non-treated plate or on NG-3.

## DISCUSSION

The combination of PC and the supercritical $CO_2$-assisted embossing process can achieve preparation of fine micro- and nanoscale surface structures without contamination with release reagents or chemical alternation. PC is mechanically rigid enough (flexural modulus = 2410 MPa) [25] to withstand the interfacial tension, and its high transmittance is adequate for observation of cells under a microscope in the visible light range [26]. Moreover, this embossing technology, without using a releasing agent and executing a chemical process, did not alter surface chemical components. In addition, the $CO_2$-assisted embossing process can be applicable to preparation of different-scaled surfaces, from nanostructures to microstructures. This fabrication process and substrata are suitable for evaluating pure effects of substrate topographies

on cell behaviors. Therefore, it can allow preparation of research tools for studying cell behaviors on biomaterial surfaces.

On micrometer grooves, cell behavior highly depends on the scale of grooves. They bridge micrometer grooves, which are as large as cells [27], whereas cells conform along the bottom of the nanoscale grooves [28]. When cells were cultured on the ML-1 plate in the current study, vinculin was expressed on the top area of each lens, which was about 2 μm in diameter. This observation implies that cells attach to the plate in the region within 100 μm of the top of each lens; each lens of ML-1 is hemispheric (radius = 5 μm), and cells bridge to the top of a neighbouring lens outside of the regions. On an ML-2 plate, cells attached to the corner of the convex lens, which was the highest region in the ML-2 and also approximately 2 μm × 2 μm. The sizes and pitches of the attachment regions in both of ML-1 and ML-2 were similar, resulting in similar cell spreading areas on both substrata. Gallant *et al.* showed that the force of adhesion depends on the available adhesion areas and levels of vinculin expression [29]. In keeping with their findings, it can be speculated that the narrow adhesion sites of the microlens prevented the formation of a focal adhesion large enough to support intracellular tension, preventing sufficient extension, as shown above.

In the observations of cell alignment on NG-1 and NG-2, vinculin was expressed along ridges and focal adhesions aligned at 1.5-μm intervals on both substrata. In addition, vinculin was expressed more densely on NG-3. Cells were attached to the top of the ridges via focal adhesions and bridged grooves with pitches of 1.5 μm. This result shows that the threshold height where cells bridged to grooves was approximately 100 nm, and it is consistent with the results using ML-1 described above. On the other hand, cell spreading in the microlens was smaller than that in nanogrooves. This

difference may be because of the smaller pitches of the nanogrooves compared to those of the microlenses, which resulted in wider spreading in nanogrooves. Teixeira *et al.* [6] reported that epithelial cells aligned parallel to grooves, which were 1.9 μm in ridge and 4.0 μm in pitch. Loesberg *et al.* [30] found that groove depths below 35 nm or ridge widths smaller than 100 nm did not result in fibroblast alignment. This difference among previous results and the results in this chapter may be attributed to differences in expression levels of cytoskeletal proteins and adhesion proteins in different cell types. Filopodial probing might cause the focal adhesion alignment as reported by Dalby *et al.* [31]. More detailed time-course studies on the formation and movement of focal adhesion are in progress.

## CONCLUSION

Supercritical $CO_2$-assisted embossing can produce fine substrates suitable for studies on the effects of the surface topography of synthetic materials on cell behaviors. MSCs attach to the top of each lens or the corner of a convex lens. On the grooves, cells attached to the tops of ridges through focal adhesions and align onto the ridges that are deeper than 90 nm.

# REFERENCES

1. Flemming RG., Murphy CJ, Abrams GA, Goodman SL, Nealey PF. Effects of synthetic micro- and nano-structured surfaces on cell behavior. *Biomaterials*, 1999, **20**, 573-588.
2. Lim JY, Donahue HJ. Cell sensing and response to micro- and nanostructured surfaces produced by chemical and topographic patterning. *Tissue Eng.*, 2007, **13**, 1879-1891.
3. Clark P, Connolly P, Curtis AS, Dow JA, Wilkinson CD. Topographical control of cell behaviour: II. Multiple grooved substrata. *Development*, 1990, **108**, 635-644.
4. Curtis A, Wilkinson C. Topographical control of cells. *Biomaterials*, 1997, **18**, 1573-1583.
5. Dalton BA, Walboomers XF, Dziegielewski M, Evans MD, Taylor S, Jansen JA, Steele JG. Modulation of epithelial tissue and cell migration by microgrooves. *J. Biomed. Mater. Res*., 2001, **56**, 195-207.
6. Teixeira AI, McKie GA, Foley JD, Bertics PJ, Nealey PF, Murphy CJ. The effect of environmental factors on the response of human corneal epithelial cells to nanoscale substrate topography. *Biomaterials*, 2006, **27**, 3945-3954.
7. Charest JL, García AJ, King WP. Myoblast alignment and differentiation on cell culture substrates with microscale topography and model chemistries. *Biomaterials*, 2007, **28**, 2202-2210.
8. Lee LJ. Polymer nano-engineering for biomedical applications. *Ann. Biomed. Eng.*, 2006, **34**, 75-88.
9. Giboz J, Copponnex T, Mélé P. Microinjection molding of thermoplastic polymers: A

review, *J. Micromech. Microeng*., 2007, **17**, R96-R109.

10. Charest JL, Bryant LE, Garcia AJ, King WP. Hot embossing for micropatterned cell substrates. *Biomaterials*, 2004, **25**, 4767-4775.
11. Yao D, Nagarajan P, Li L, Yi AY. A two-station embossing process for rapid fabrication of surface microstructures on thermoplastic polymers. *Polym. Eng. Sci.*, 2007, **47**, 530-539.
12. Becker H, Gärtner C. Polymer microfabrication technologies for microfluidic systems. *Anal. Bioanal. Chem*., 2008, **390**, 89-111.
13. Stutzmann N, Tervoort TA, Bastiaansen CWM, Feldman K, Smith P. Solid-State Replication of Relief Structures in Semicrystalline Polymers. *Adv. Mater.*, 2000, **12**, 557-562.
14. Ohshima M. Supercritical $CO_2$-Assisted Surface Coating Injection Molding. *In*: Lee S. editor. *Encyclopedia of Chemical Processing*., New York: Taylor & Francis Group, 2005, 2897-2906.
15. Nozaki SS, Ohshima M. A $CO_2$ assisted nanoimprinting and cold embossing. *Annual Technical Conference - ANTEC Conference Proceedings*., 2005; **5**, 2551-2555.
16. Wang Y, Liu Z, Han B, Huang Y, Zhang J, Sun D, Du J. Compressed-$CO_2$-assisted patterning of polymers. *J. Phys. Chem. B*, 2005, **109**, 12376-12379.
17. Dakin SC, Mareschal I, Bex PJ. Local and global limitations on direction integration assessed using equivalent noise analysis. *Vision Res.*, 2005, **45**, 3027-3049.
18. Bashur CA, Dahlgren LA, Goldstein AS. Effect of fiber diameter and orientation on fibroblast morphology and proliferation on electrospun poly(D,L-lactic-co-glycolic acid) meshes. *Biomaterials*, 2006, **27**, 5681-5688.
19. Agostinelli C. Robust estimation for circular data. *Comput. Stat. Data Anal.*, 2007,

**51**, 5867-5875.

20. Fisher NI. *Statistical analysis of circular data*., New York: Cambridge University Press, 1993.
21. Pittenger MF, Mackay AM, Beck SC, Jaiswal RK, Douglas R, Mosca JD, Moorman MA, Simonetti DW, Craig S, Marshak DR. Multilineage potential of adult human mesenchymal stem cells. *Science*, 1999, **284**, 143-147.
22. Fujimoto N, Fujita S, Tsuji T, Toguchida J, Ida K, Suginami H, Iwata H. Microencapsulated feeder cells as a source of soluble factors for expansion of CD34(+) hematopoietic stem cells. *Biomaterials*, 2007, **28**, 4795-4805.
23. Fujita S, Toguchida J, Morita Y, Iwata H. Clonal analysis of hematopoiesis-supporting activity of human mesenchymal stem cells in association with Jagged1 expression and osteogenic potential. *Cell Transplant.*, 2008; in press.
24. Goffin JM, Pittet P, Csucs G, Lussi JW, Meister JJ, Hinz B. Focal adhesion size controls tension-dependent recruitment of -smooth muscle actin to stress fibers. *J. Cell Biol*., 2006, **172**, 259-268.
25. DeLassus PT, Whiteman NF. Physical and mechanical properties of some important polymers. *In*: Brandrup J, Immergut EH, Grulke EA, editors. *Polymer Handbook, 4th Ed*., New York: Wiley-Interscience, 1999, V/159-169.
26. Yan M., Kim TW, Erlat AG., Pellow M, Foust DF, Liu J, Schaepkens M, Heller CM, Mcconnelee PA, Feist TP, Duggal AR. A transparent, high barrier, and high heat substrate for organic electronics. *Proceedings of the IEEE.*, 2005, **93**, 1468-1477.
27. Walboomers XF, Monaghan W, Curtis AS, Jansen JA. Attachment of fibroblasts on smooth and microgrooved polystyrene. *J. Biomed. Mater. Res*., 1999, **46**, 212-220.
28. Teixeira AI, Abrams G.A, Bertics PJ, Murphy CJ, Nealey PF. Epithelial contact

guidance on well-defined micro- and nanostructured substrates. *J. Cell Sci.*, 2003, **116**, 1881-1892.

29. Gallant ND, Michael KE, García AJ. Cell adhesion strengthening: contributions of adhesive area, integrin binding, and focal adhesion assembly. *Mol. Biol. Cell*, 2005, **16**, 4329-4340.

30. Loesberg WA, te Riet J, van Delft FC, Schön P, Figdor CG, Speller S, van Loon JJ, Walboomers XF, Jansen JA. The threshold at which substrate nanogroove dimensions may influence fibroblast alignment and adhesion. *Biomaterials*, 2007, **28**, 3944-3951.

31. Dalby MJ, Gadegaard N, Riehle MO, Wilkinson CD, Curtis AS. Investigating filopodia sensing using arrays of defined nano-pits down to 35 nm diameter in size. *Int. J. Biochem. Cell Biol.*, 2004, **36**, 2005-2015.

# CHAPTER 5

# Time-lapse observation of cell alignment on nanogrooved patterns

## INTRODUCTION

A large number of studies have examined the effects on cell behaviors of surface characteristics, such as wettability, electrostatic charges, and functional groups, [1, 2]. These studies have provided the basis for the development of materials for artificial organs, disposable medical devices, and cell culture substrates. In the last decade, the effects of surface micro- and nanotexture on cell adhesion and cell morphology have attracted much attention [3-7]. Substrates with fine grooves induce various cell responses, such as cell alignment and migration along the groove [8-10], and, moreover, differentiation of stem cells [11]. Most researchers have assessed cell alignments after cells have been fixed in formaldehyde, methanol, or glutaraldehyde. Although those static observations are useful for visualizing intracellular protein fibre alignment in detail, they provide scarce information about dynamic cell behaviors on surfaces with nanopatterns. Studies are needed on dynamic cell behaviors in an acute phase and are expected to give more detailed information on the mechanism of cell alignment on nanogrooved (NG) patterns.

In this chapter, NG patterns were printed on polycarbonate (PC) plates using supercritical $CO_2$-assisted embossing [12], and the dynamic behaviors of mesenchymal stem cells (MSCs) on NG patterns were observed under 5% $CO_2$ and at 37 °C using time-lapse microscopes. Time dependence of cell alignment, cell protrusion movements, and their remodelling were analyzed to infer the mechanism of the topographical effect of the substrate on cell responses.

## EXPERIMENTAL

### *Fabrication of the nanogrooved substrate*

An NG pattern (200 nm in the groove depth, 870 nm in the ridge width, and 670 nm in the groove width; Scheme 5-1) was printed on PC plates using a supercritical $CO_2$-assisted embossing machine, as described in Chapter 4. In brief, a vessel of the embossing machine was separated into two chambers by a partition. An under pedestal could move between the two chambers through a partition, like a syringe. A disk-shaped PC plate (diameter = 20 mm; thickness = 3 mm; bisphenol-A type; Mw = 58

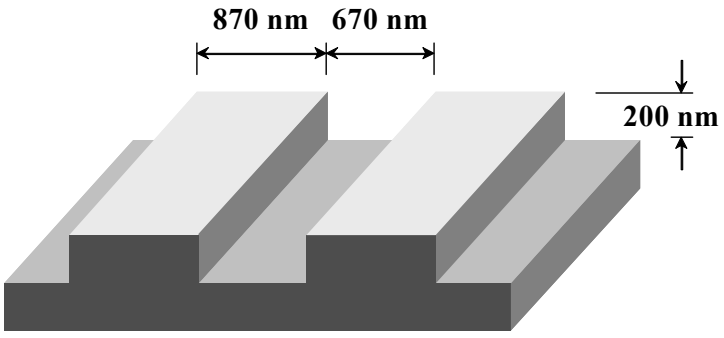


***Scheme 5-1.*** Dimension of the NG pattern.

000; *T*g = 153 °C; Tsutsunaka Plastic Industry Co. Ltd., Osaka, Japan) was placed on top of the pedestal. A nickel mold (supplied by Hitachi Maxell, Ltd., Tokyo, Japan) was set on the ceiling of the upper chamber.

The mold and the PC plate were cleaned up with the spraying of fluorocarbon gas. The upper chamber was filled with $CO_2$ gas to 10 MPa, and the chamber temperature was increased to 100 °C to achieve the $CO_2$ supercritical condition. The surface of the PC plate was plasticized by dissolution of $CO_2$ under the supercritical condition for 5 min. Then, $CO_2$ was released from the upper chamber, and immediately the pressure of the lower chamber was increased by introduction of the $CO_2$ gas to lift the pedestal. The PC plate was pressed to the nickel mold at 12 000–15 000 N for 30 sec at 100 °C. After stamping, $CO_2$ was completely released from both chambers, and the plate was detached from the mold.

***Cell culture***

Human bone marrow–derived MSCs (Lonza, Basel, Switzerland) were maintained in Dulbecco's Modified Essential Medium (DMEM; Invitrogen Corp., Carlsbad, CA, USA) supplemented with 10% foetal bovine serum (FBS; BIOWEST, France), 100 U/ml penicillin, and 100 μg/ml streptomycin (Invitrogen) at 37 °C under 5% $CO_2$ in a humidified atmosphere, and subcultured at $5 \times 10^3$ cells/cm$^2$ every 3 to 4 days. Cells at passages three through eight were used for experiments.

Prior to cell seeding, MSCs were treated with 10 μg/ml mitomycin C (Wako Pure Chemical Industries, Ltd., Osaka, Japan) for 2 h to stop proliferation and then washed three times with Dulbecco's phosphate buffered-saline $Ca^{2+}Mg^{2+}$ free (DPBS(-); Nissui Pharmaceutical Co. Ltd., Tokyo, Japan). PC plates were coated with 10 μg/ml

fibronectin (Invitrogen) for 2 h at 37 °C and washed 5 times with DPBS(-). MSCs were seeded at $5 \times 10^3$ cells/cm$^2$ on fibronectin-coated plates and cultured for 4 days.

***Time-lapse video microscopy***

For time-lapse imaging, $1.5 \times 10^4$ cells of MSCs, which were treated with 10 μg/ml mitomycin C and suspended in 300 μl of medium, were seeded onto a fibronectin-treated plate, placed in a 35-mm culture dish, and then statically incubated at 37°C under 5% $CO_2$ for 60 min for adhesion. Then, after addition of 2 ml medium, the dish was stored in a gas-tight container with capnophilic powder, which consists mainly of ascorbic acid (CulturePal; Corefront Corp., Tokyo, Japan), to maintain 5% $CO_2$ during observation. For analysis of cell orientation, cell images were captured every 2.5 min for 5 days using an inverted-phase contrast microscope (Cellwatcher; Corefront).

For visualization of cells under high magnification, a plate carrying MSCs was placed upside down with cells facing to a culture dish on a silicone spacer (thickness, 0.5 mm). Cells could be observed under high magnification with an inverted microscope (Biostation IM; Nikon Corp., Tokyo, Japan). For visualization of the extension of cell protrusions, cell images were recorded every 2.5 min for 7 h. For investigating filopodial movements, time-lapse images were captured every 4 sec for 2 h. Captured images were stacked by ImageJ (ver 1.39f, distributed by NIH).

***Quantification of orientation angle***

Cell orientation angles were quantified by analysis of immunostained images or low-magnification time-lapse phase-contrast images using Image J. The orientation angle of an individual cell was determined as the angle between the groove direction and the

direction of the longer axis of the approximated ellipse, which approximates to the cell shape (Scheme 5-2). The distribution of cell orientation was estimated by a wrapped normal distribution, as previously reported [13-15]. Briefly, the probability distribution function was adapted from Fisher [16] for a periodicity of $\pi$ radians as follows:

$$f(\theta) = \frac{1}{\pi}\left(1 + 2\sum_{p=1}^{\infty} \rho^{p^2} \cos(2p(\theta - \pi))\right), \quad \text{(Eq. 5-1)}$$

$$\rho = \frac{1}{n}\sqrt{\left(\sum_{i=1}^{n} \cos 2\theta_i\right)^2 + \left(\sum_{i=1}^{n} \sin 2\theta_i\right)^2}, \quad \text{(Eq. 5-2)}$$

$$\mu = \tan^{-1}\left(\sum_{i=1}^{n} \sin 2\theta_i \Big/ \sum_{i=1}^{n} \cos 2\theta_i\right), \quad \text{(Eq. 5-3)}$$

where $\rho$ is the mean resultant length and $\mu$ is the mean angle. These parameters were determined from a set of $n$ measured cell orientation angles, $\theta_i$. The angular standard deviation, $\sigma$, for the distribution was determined by the following equation:

$$\sigma = \frac{1}{2}\sqrt{-2\ln\rho}\,. \quad \text{(Eq. 5-4)}$$

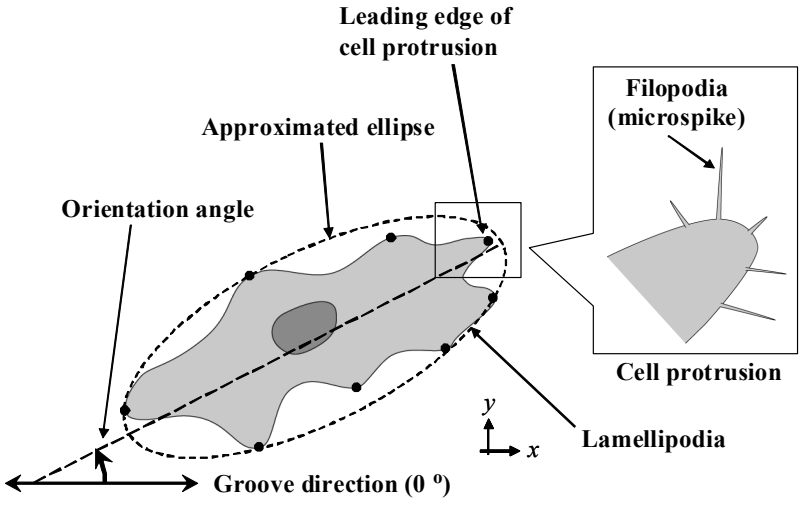


***Scheme 5-2.*** Terminologies used in this chapter.

***Tracking of cell protrusions***

The leading edges of cell protrusions were tracked through all of the captured images using the MTrackJ plug-in (ver 1.2.0) and Chemotaxis and Migration Tool plug-in (ver 1.01, distributed by ibidi GmbH, München, German) for ImageJ. The position of each leading edge was plotted in the coordinate axis, where the origin was the position where each edge first appeared and the x-axis was parallel to the grooves (see Scheme 5-2). Tracking was terminated when the tip of the cell protrusion disappeared or recording ended. The distribution of protrusions was quantitatively compared by the standard deviations of the angle between the vector of the end point of cell protrusion and x-axis calculated from Equation (5-4). From the start point to the end point of each leading edge, an accumulated distance and Euclidean distance were calculated as defined in Scheme 5-3. The velocity of a leading edge of a cell protrusion was defined as an accumulated distance of each edge divided by time (see Scheme 5-3). The directionality of a leading edge of a cell protrusion was defined as given in the following Equation (5-5):

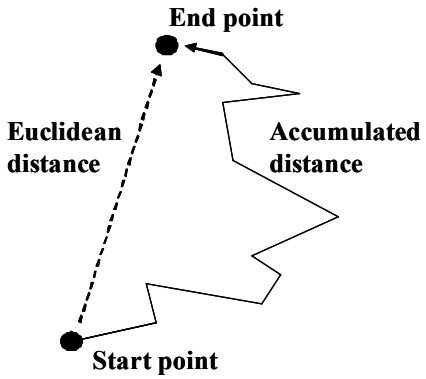


***Scheme 5-3.*** Schematic representation of accumulated distance and Euclidean distance of movements of the leading edge of the cell protrusion.

$$Directonality = \frac{Euclidean\ distance}{accumulated\ distance}. \quad \text{(Eq. 5-5)}$$

***Immunostaining***

Cells were stained with F-actin and vinculin. Cultures were fixed with 4% paraformaldehyde (Nacalai Tesque, Inc., Kyoto, Japan) for 15 min, permeabilized with 0.2% Triton-X (Wako) for 3 min, blocked with 2% skimmed milk (Nacalai) for 1 h at room temperature, and incubated with anti-mouse vinculin (Chemicon, CA, USA) (1:200 dilution) overnight at 4°C. They then were washed with 0.05% polyoxyethylene sorbitan monolaurate (Tween 20, Wako, Osaka, Japan) for 15 min three times at room temperature and treated with Alexa-594 conjugated phalloidin (Invitrogen) (1:40 dilution) for F-actin staining, Hoechst 33342 (Dojindo, Kumamoto, Japan) (1:1000 dilution) for nucleus staining, and Alexa-488 conjugated mouse anti-IgG (Invitrogen) (1:500 dilution) for vinculin staining, for 30 min at room temperature. Stained cultures were mounted on slides with a light anti-fade reagent (Vectashield, Vector Laboratories, Burlingame, CA, USA) and observed using a fluorescence inverted microscope (IX71, Olympus, Tokyo, Japan).

***Statistical analysis***

Comparisons between two groups were made using Student's t-tests. $P < 0.05$ was considered statistically significant. All statistical calculations were performed using the software JMP ver.5.1.1.

# RESULTS

## *Cell alignment*

In Chapter 4, when NG depth was more than 90 nm, contact guidance of MSC alignment on NG substrates was observed. In this chapter, NG plates with 200 nm in the groove depth, 870 nm in the ridge width, and 670 nm in the groove width were employed (Scheme 5-1). Dynamic cell behaviors on the NG plate were observed using

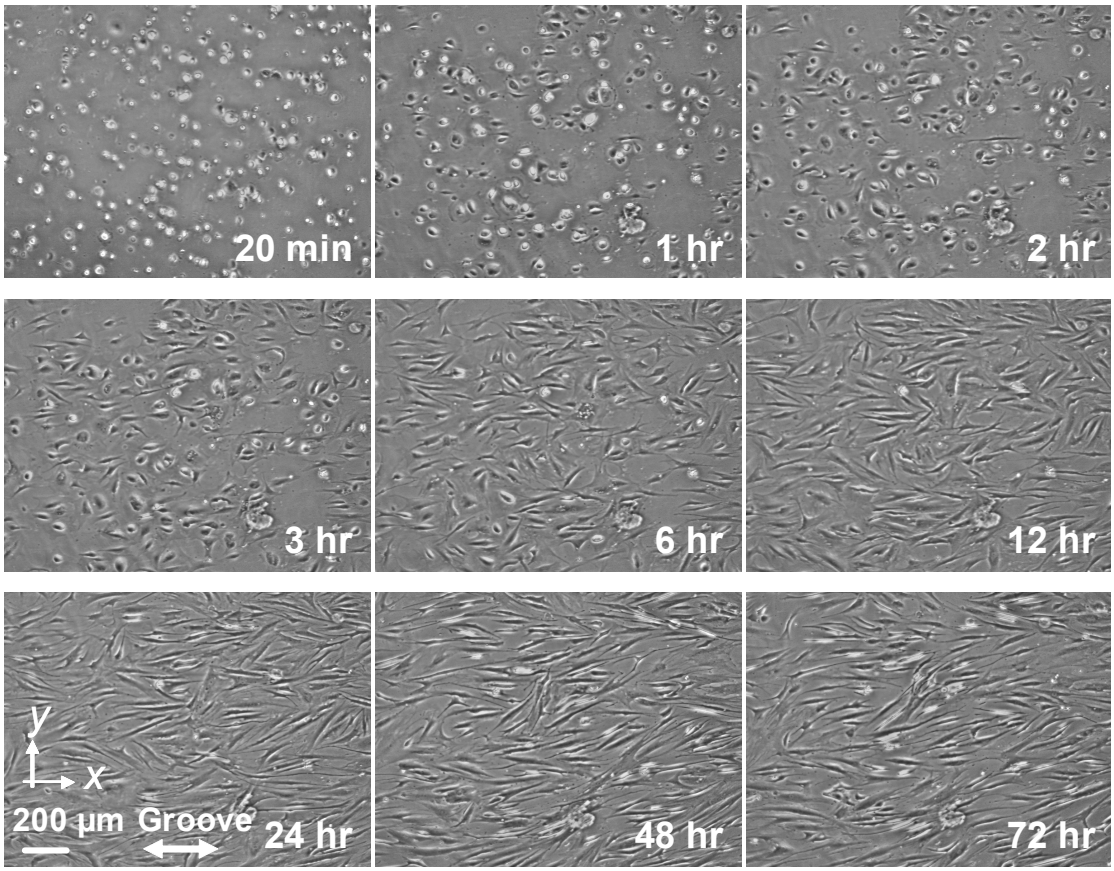


***Figure 5-1.*** Low-magnification time-lapse images of mesenchymal stem cells seeded on the nanogroove (NG) pattern. The NG lines were parallel to the x-axis. Recording under the time-lapse microscope started from 20 min post-seeding. Scale bar = 200 μm.

time-lapse microscopes. Cells on the NG plate started to align along the NG patterns just after cell seeding, as shown in Figure 5-1. Cells extended in parallel with the NG pattern and aligned with each other during the subsequent 24-h culture. Cell alignment was maintained for at least 4 days following this period (data not shown).

To express cell alignment quantitatively, the orientation angles of individual cells (n > 140 for each time point) against the groove direction were determined (see

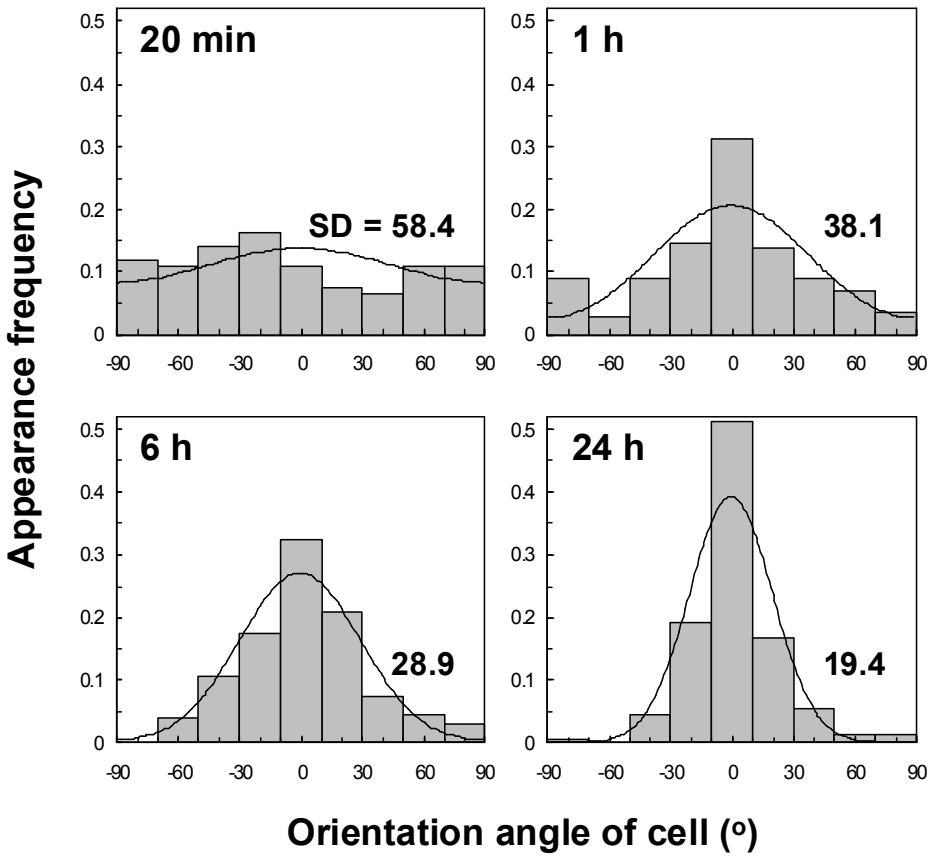


***Figure 5-2.*** Cell orientation angle against NG lines and the angular standard deviation. Histograms of cell orientation angle against NG lines at 20 min, 1 h, 6 h, and 24 h post-seeding. Each figure includes the angular standard deviation (SD) calculated from the wrapped normal distribution (see equation (5-4) in the text).

Scheme 5-2), and calculated the standard deviation, $\sigma$, of the distribution of the orientation angles at each time point using Equation (5-4). No specific orientation of cells in a specific direction was observed at 20 min after cell seeding, as shown in Figure 5-1. Figure 5-2 shows cell orientation more quantitatively by histograms and the angular standard deviation ($\sigma$). It was $\sigma$ = 58.4 at 20 min. After 1 h of culture, a clear peak at 0 degrees was observed in the histogram of the orientation angle distribution. This tendency became much clearer and the angular standard deviation decreased rapidly with time afterwards. Figure 5-3 shows the time course of values of the standard deviation, $\sigma$. The SD value sharply decreased with time during the initial several hours and was kept around 20 afterwards, indicating maintenance of cell alignment along the grooves.

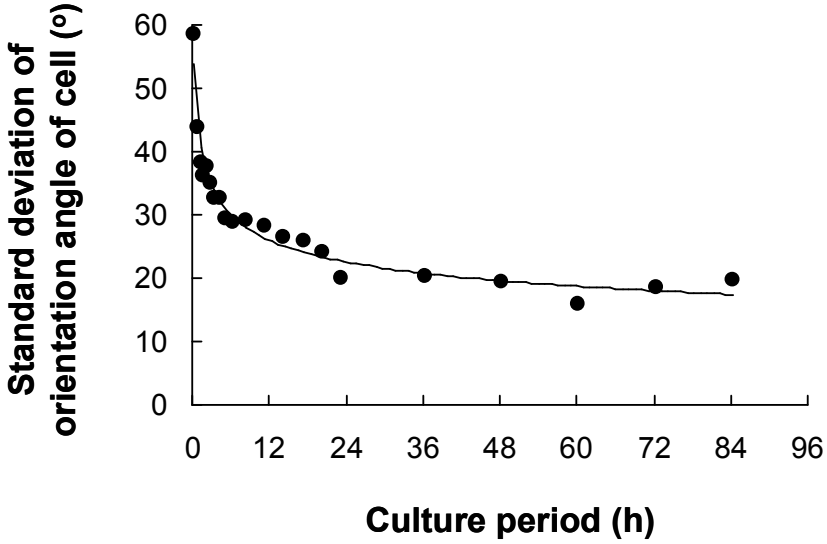


***Figure 5-3.*** Cell orientation angle against NG lines and the angular standard deviation. Time course of the angular standard deviation, SD.

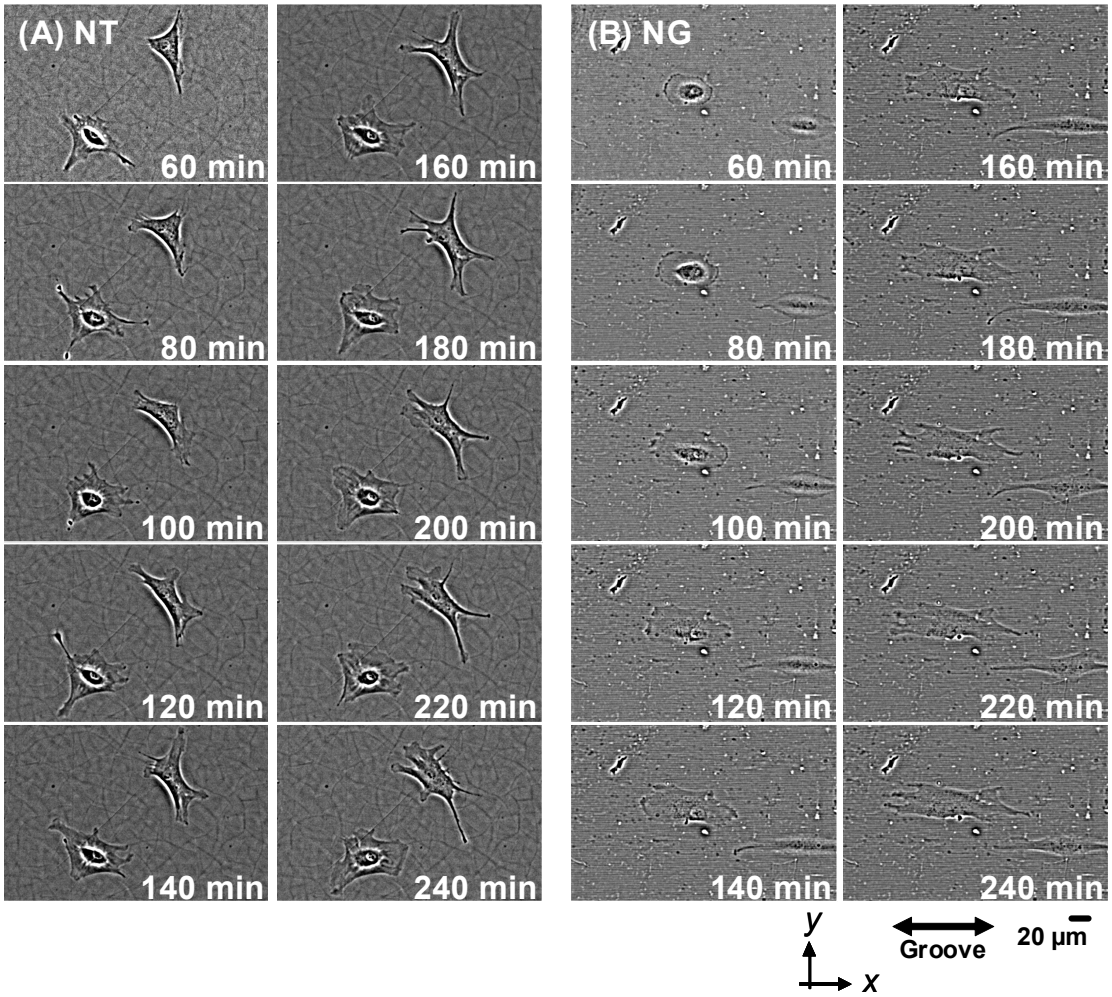


***Figure 5-4.*** Comparison of time-lapse images of MSCs seeded on a non-treated (NT) flat substrate and a nanogrooved (NG) substrate. (A) MSCs on a flat substrate, and (B) MSCs on the NG substrate. Cultures were incubated for 60 min after cell seeding at 37°C, 5% $CO_2$, and followed by recording under a time-lapse microscope every 2.5 min. Panels show images every 20 min. In NG images, the NG lines were parallel to the x-axis. Bar = 20 µm.

### *Cell protrusions*

To elucidate the mechanism of cell morphological changes, cell protrusions were focused (see Scheme 5-1). A cell protrusion is defined as a thicker protrusive structure in amoeboid cells, carrying lamellipodia, pseudopodia, filopodia (microspikes), and microvilli [17,18]. Figure 5-4(A) shows that cells extended their cell protrusions in all directions on a flat substrate. Lifetimes of the cell protrusions differed from one another, but no clear dependence of lifetime on direction was seen on the flat substrate. Figure 5-4(B), however, shows that cells extended cell protrusions in all directions

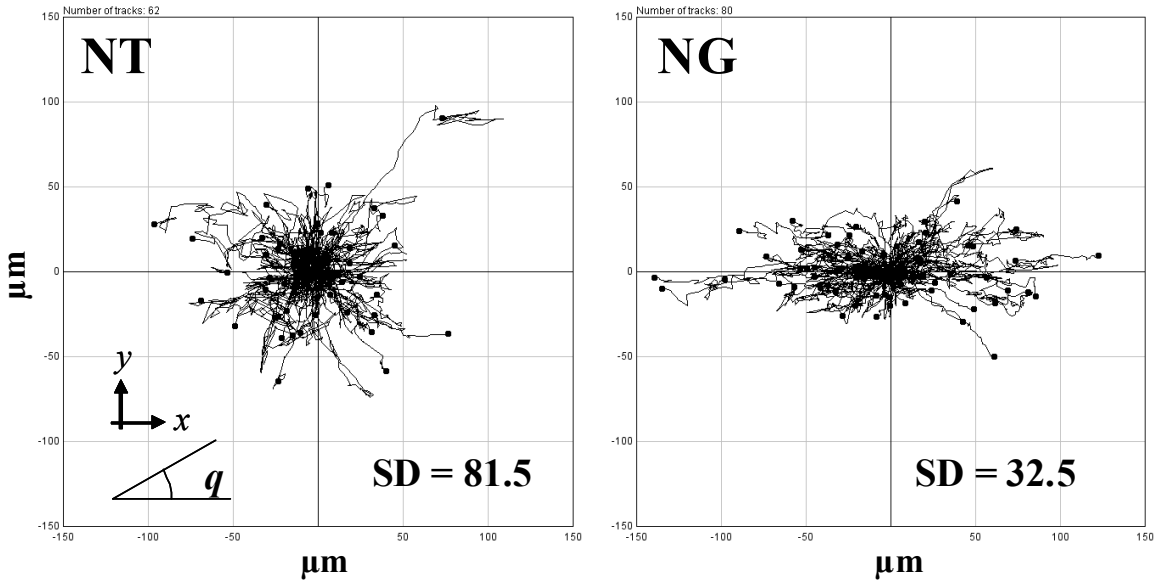


***Figure 5-5.*** Movements of leading edges of cell protrusions. Tracks of leading edges of cell protrusions of cells on the non-treated (NT) flat substrate and on the NG substrate (n = 8 cells, respectively). Start point of a leading edge of each cell protrusion was set at the origin of the coordinate axes, its location every 2.5 min was plotted, and a filled circle indicates its end point after observation. The values inserted represent the standard deviations (SDs) of angles between lines from the origin to filled circles and the x-axis.

equally on the NG plate, as seen on the flat substrate, but cell protrusions that extended in the groove direction remained longer than those that were perpendicular to the groove direction. Consequently, cells elongated and aligned along the groove direction.

To evaluate extension length and direction of cell protrusions more quantitatively, the leading edges of the cell protrusions were tracked every 2.5 min from 1 h to 7 h after cell seeding. Movements of the cell protrusions from the cells are shown in Figure 5-4. The trajectories of the leading edges of cell protrusions were plotted in Figure 5-5. The standard deviations of the angles of the cell protrusions against the groove direction were 32.5 on the NG plate buț 81.5 on the flat plate. Thus, the leading edges of the cell protrusions extended along the grooves on the NG plate. These results

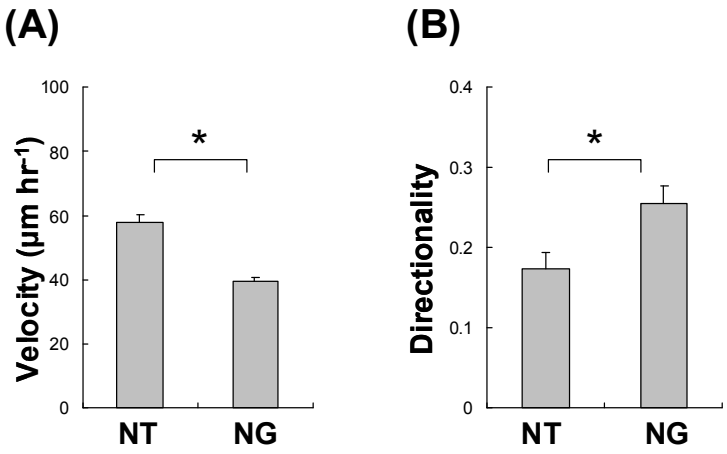


***Figure 5-6.*** (A) Average velocity of leading edges. The velocity of each leading edge was determined by dividing the contour length by observed time. Values were given as mean ± standard deviation for n = 62 protrusions for the flat substrate and 80 for the NG substrate, of 10 randomly selected cells, respectively). (B) Directionality of leading edge movement, which was defined as a ratio of Euclidean distance and accumulated distance. Asterisks represent a significant difference ($p < 0.05$) between two groups.

indicate that cells rapidly elongated along the NG patterns.

The averaged velocities and the directionality of edge movement of cell protrusions were determined as described in the Methods. Significant differences were observed in the velocities and the directions of movements of cell protrusions between cells cultured on non-treated (NT) plates and NG plates, as shown in Figures 5-6. A lower velocity of movements of cell protrusions observed on the NG plate (see Figure 5-6(A)) seems to reflect weaker adhesion of cell protrusions. Moreover, directionality was higher in the NG plate than on the NT. This outcome implies that the movement of the edge of cell protrusions on the NG plate would confine the movements of cell protrusion along the grooves because higher directionality indicates linear movement of cell protrusion.

***Focal adhesion points***

To give some insight into the anisotropic movements of cell protrusions, focal adhesion points under a cell protrusion onto the NG pattern were examined in detail by immunohistochemical staining of vinculin and actin filaments (Figure 5-7). Vinculin, which exists at focal adhesion points, was found only on the ridges of the NG pitches, as seen Figure 5-7(A). When the cell protrusions extended parallel to the groove direction, actin filaments attached to vinculin on the ridges and aligned parallel to the NG direction, as shown in Figure 5-7(A). A long area of focal adhesion is expected to be able to resist the contraction force generated by actin filaments. On the other hand, when cell protrusions extended perpendicular to the groove direction, vinculin aligned parallel to the NG direction, but vinculin staining was fragmented, as seen in Figure 5-7(B). Actin filaments did not align to a specific direction. The fragmented focal

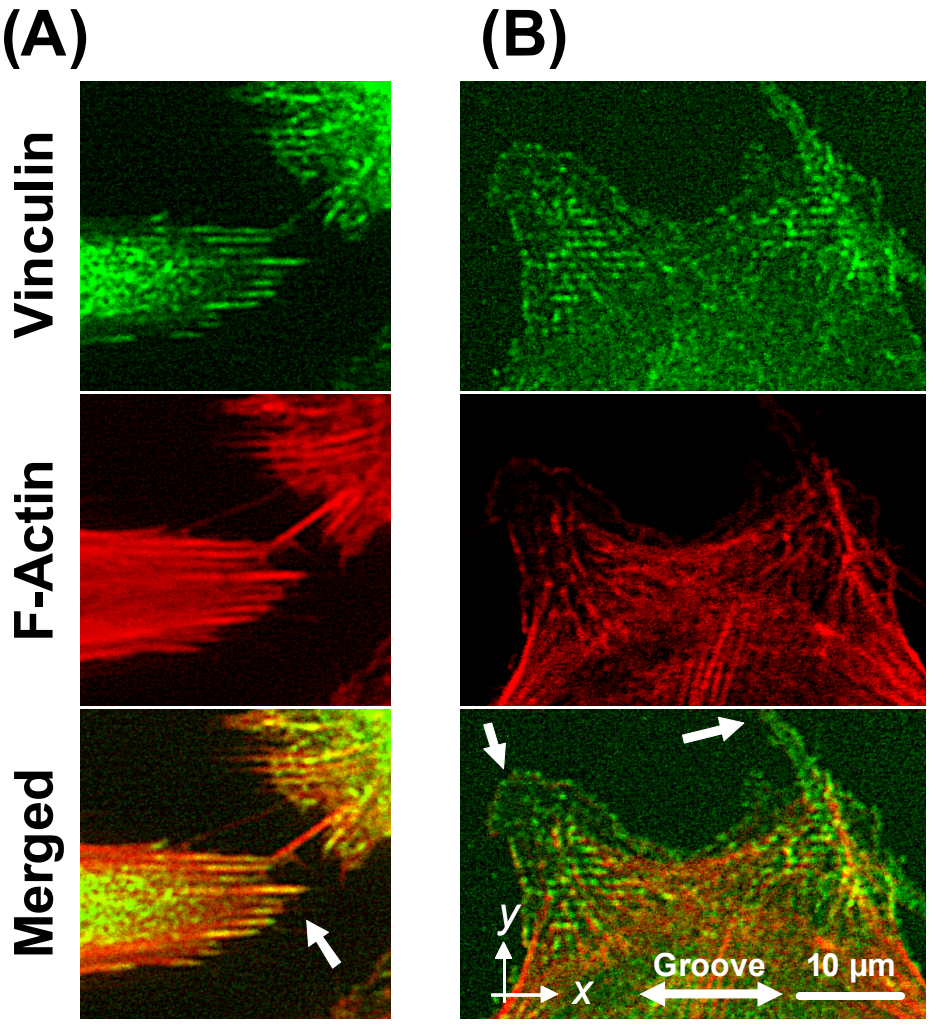


***Figure 5-7.*** Immunohistochemical staining of vinculin and actin filaments of MSCs after 4 days of culture on the NG substrate. (A) A cell protrusion extended parallel to the NG lines; (B) cell protrusions extended perpendicular to the NG lines. Vinculin was stained with Alexa-488 conjugated antibody (green) in photos in the top row and F-actin of the cytoskeleton was stained with Alexa-594 conjugated phalloidin (red) in photos in the middle row. Merged images are shown in the bottom row. Arrows indicate leading edges of cell protrusions. Bar = 10 μm.

adhesion indicated by vinculin staining is expected to be weaker than the long focal adhesion and thus be easily remodelled. These results suggest that the retraction phase of the cell protrusions plays a key role for the forming of cell contact guidance.

***Filopodial probing***

It has been reported that filopodia play a sensory or exploratory role when a cell migrates and extends [19]. The diameters of filopodia are 250 to 400 nm [20], smaller than the width of the ridge and the groove of the NG plate used in this chapter. Filopodia were expected to attach to the ridges and to reach the bottom of the grooves without difficulty. Filopodia movements were followed by a time-lapse microscope to visualize their role in cell alignment along the NG plate.

A representative cell protrusion was observed under high magnification (80-X objective lens) on a time-lapse microscope to see the dynamic features of the filopodia. Figures 5-8 and 5-9 show the representative movements of filopodia. Filopodia

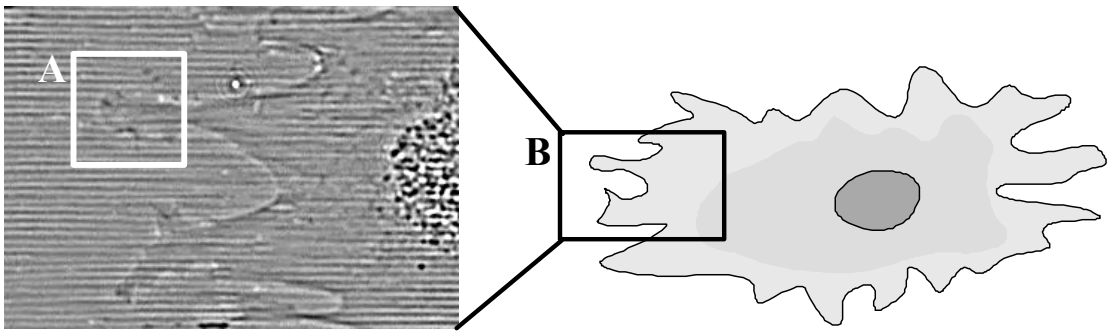


***Figure 5-8.*** Observation of filopodia under high magnification. Schematic representation of the observation area.

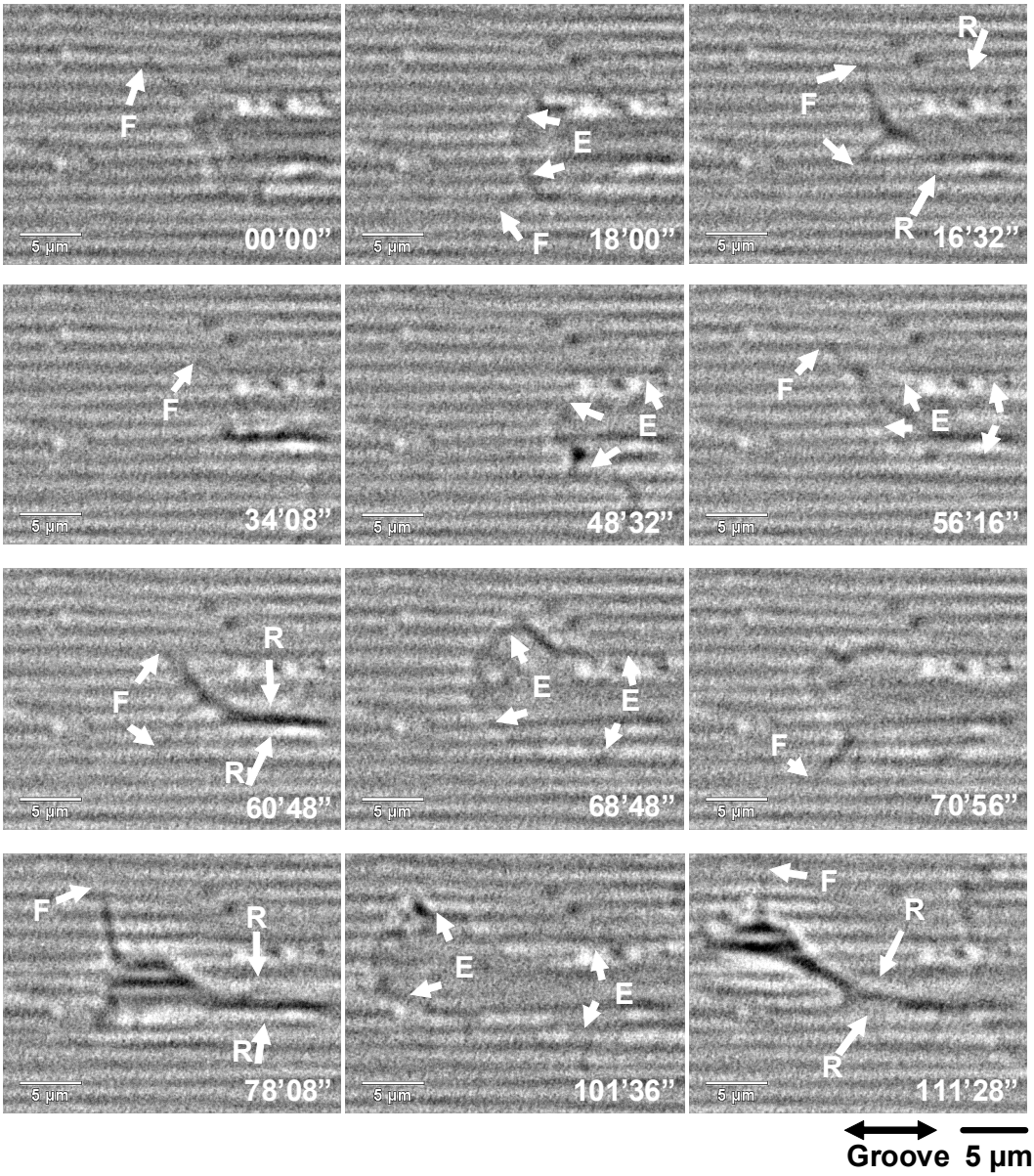


***Figure 5-9.*** Observation of filopodia under high magnification. . Pictures were captured with time-lapse microscopy every 4 sec. The extension and retraction of the leading edge of the cell protrusion and precession movements of representative filopodia on the NG substrate. Arrows in the figure indicate (F) filopodial probing, (E) extending cell protrusion, and (R) retracting cell protrusion. Scale bars = 10 µm.

indicated by arrows in the figure moved as if they were probing the surroundings of the cell protrusion. Then, some cell protrusions invaded the probed areas, as indicated by arrowheads. Cell protrusions that extended perpendicular to the NG direction retracted more easily than those parallel to the grooves (arrow, R), while, on a flat substrate, this repeated probing and retraction of the cell protrusion was rarely observed (data not shown). In these two cases, however, no difference in filopodia movements was observed. These results indicate that filopodia cannot distinguish topological differences or that filopodia can do so but that the retracting phase of cell protrusions is a major factor for cell alignment along the NG patterns.

## DISCUSSION

A large number of studies have examined the effects of surface topography on cell behaviors or contact guidance. Dalby *et al*. reported that filopodia of human fibroblasts can sense topography down to a pitch 35 nm in diameter and 50 nm in depth and that filopodial probing acts as an initial trigger for cell alignment in response to the topography of substrates [21]. Teixeira *et al*. employed human corneal epithelial cells [22]. In their study, they found that filopodia aligned along the grooves and that cells attached to the ridge and aligned along the NG pattern. From these findings, they speculated that filopodia sense differences in surface topography and induce cell alignment. In their other report, however, filopodia aligned perpendicular to the grooves [6]. They mentioned that these two contradictory results reflected a difference in culture media. Wójciak-Stothard *et al*. reported that filopodia extending perpendicular

to the groove direction were more frequently observed than those along the NG pattern, even though they were in cells that had aligned along the NG pattern [23].

The role of filopodial probing remains controversial. Most researchers assessed this relationship of filopodial movements and cell alignments after cells were fixed with formaldehyde, methanol, or glutaraldehyde. The examination by time-lapse microscopes of the kinetics of cell alignment and dynamic features of cell protrusions and filopodia would give more detailed insights into cell responses to surface topography and the roles of cell protrusions and filopodia in contact guidance of cells.

In this chapter, filopodia movements were fount to be isotropic: no specific direction was observed for their extension and retraction against the NG structure. This finding suggests that filopodia probing does not play a major role in cell alignment. On the other hand, anisotropy of cell protrusion movements was found, especially in their retraction phase. Cell protrusions perpendicular to the NG pattern retracted more rapidly than those parallel to the NG pattern. A model of cell alignment on the NG pattern from these observations was proposed (see Scheme 5-4). Cell protrusions isotropically extended, but some of those perpendicular to the NG pattern more rapidly retracted than those parallel to the NG pattern. These cell protrusion dynamics force a cell to be elongated and aligned along the NG pattern.

The model also derives support from the immunohistochemical results with vinculin and actin filaments at focal adhesion points under cell protrusions. When cell protrusions extended parallel to NG lines, both vinculin and actin filaments also aligned parallel to the NG lines. On the other hand, when cell protrusions extended perpendicular to the NG lines, vinculin staining was fragmented, and no clear alignment of actin filaments was observed, as seen in Figure 5-7. The former focal adhesion—the

long vinculin expression area—is expected to generate a stronger adhesion force than the fragmented vinculin expression area.

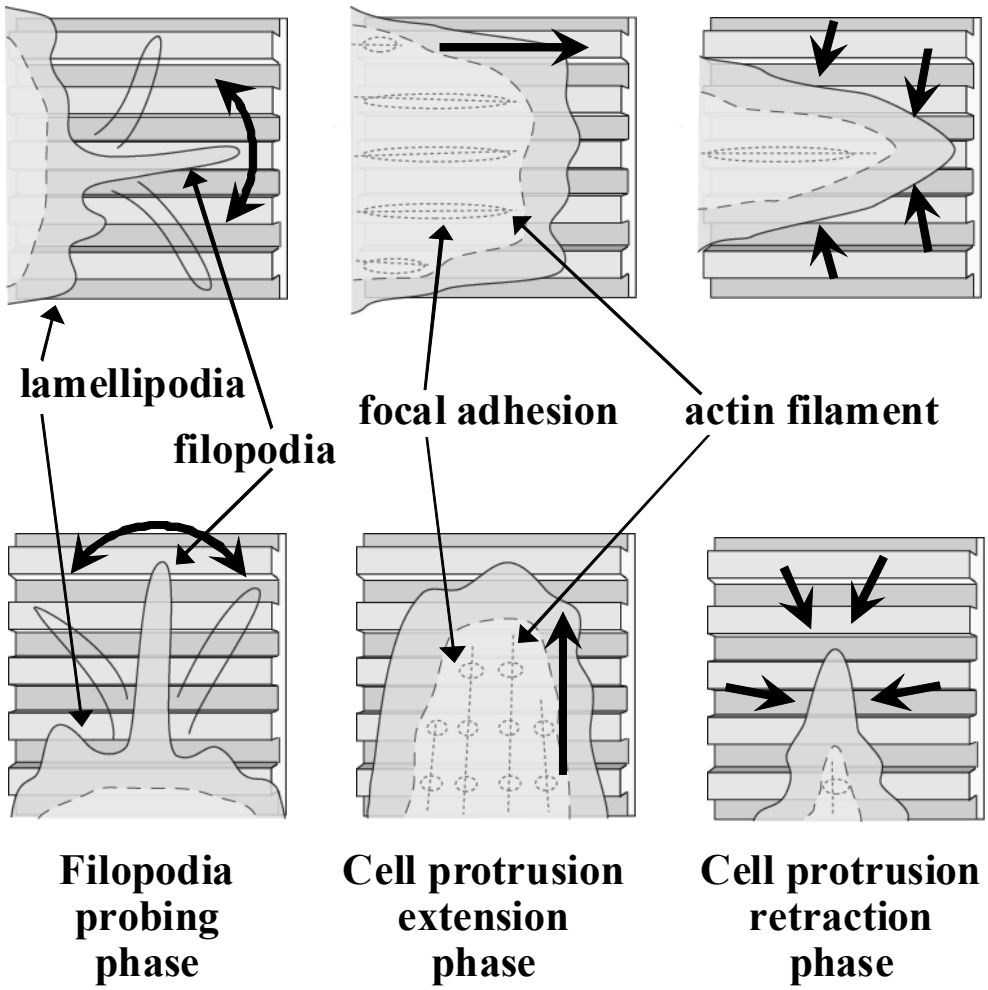


***Scheme 5-4.*** Model for cell alignment on the NG substrate. Filopodia movements are isotropic, that is, no specific direction was observed for their extension and retraction against the NG structure. This finding suggests that filopodia probing does not play a major role in cell alignment. Cell protrusions isotropically extended, but some of them that were perpendicular to the NG pattern more rapidly retracted than those parallel to the NG pattern. These cell protrusion dynamics force a cell to elongate and align along the NG pattern.

Although epithelial cells and fibroblasts have been used to examine cell responses to substrate topography [7], MSCs were used in this thesis. MSCs are multipotent stem cells that can differentiate into osteoblasts, adipocytes, chondrocytes, and other kinds of mesenchymal cells [24]. The morphology of MSCs is affected by some physico-chemical properties of cell culture substrates, which can determine cell fates, such as proliferation or differentiation direction [25-28]. As shown in this and previous studies, substrate topography can control MSC cell morphology, and their differentiation direction thus is also expected to be controlled by substrate topography. Studying the effects of substrate topography on MSC behavior in detail is therefore meaningful. In future studies, carefully examination of the effect of NG patterns on MSC differentiation should be performed.

# CONCLUSION

Living cells on an NG pattern were observed using time-lapse microscopes to clearly demonstrate the dynamic features of cell alignment along the NG pattern. Cell protrusions perpendicular to the NG pattern retracted more rapidly than those parallel to it. The anisotropic retraction of cell protrusions induces cell elongation and alignment along the NG pattern.

# REFERENCES

1. Witt D, Klajn R, Barski P, Grzybowski BA. Applications, properties and synthesis of ω-functionalized n-alkanethiols and disulfides - The building blocks of self-assembled monolayers. *Curr. Org. Chem.*, 2004, **8**, 1763-1797.
2. Navarro M, Aparicio C, Charles-Harris M, Ginebra MP, Engel E, Planell JA. Development of a biodegradable composite scaffold for bone tissue engineering: Physicochemical, topographical, mechanical, degradation, and biological properties. *Adv. Polym. Sci.*, 2006, **200**, 209-231.
3. Clark P, Connolly P, Curtis ASG, Dow JAT, Wilkinson CDW. Topographical control of cell behaviour: II. multiple grooved substrata. *Development*, 1990, **108**, 635-644.
4. Curtis A, Wilkinson C. Topographical control of cells. *Biomaterials*, 1997, **18**, 1573-1583.
5. Flemming RG, Murphy CJ, Abrams GA, Goodman SL, Nealey PF. Effects of synthetic micro- and nano-structured surfaces on cell behavior. *Biomaterials*, 1999, **20**, 573-588.
6. Teixeira AI, McKie GA, Foley JD, Bertics PJ, Nealey PF, Murphy CJ. The effect of environmental factors on the response of human corneal epithelial cells to nanoscale substrate topography. *Biomaterials*, 2006, **27**, 3945-3954.
7. Lim JY, Donahue HJ. Cell sensing and response to micro- and nanostructured surfaces produced by chemical and topographic patterning. *Tissue Eng.*, 2007, **13**, 1879-1891.
8. Dalton BA, Walboomers XF, Dziegielewski M, Evans MDM, Taylor S, Jansen JA, Steele JG. Modulation of epithelial tissue and cell migration by microgrooves. *J.*

*Biomed. Mater. Res.*, 2001, **56**, 195-207.

9. Su WT, Liao YF, Chu IM. Observation of fibroblast motility on a micro-grooved hydrophobic elastomer substrate with different geometric characteristics. *Micron*, 2007, **38**, 278-285.
10. Diehl KA, Foley JD, Nealey PF, Murphy CJ. Nanoscale topography modulates corneal epithelial cell migration. *J. Biomed. Mater. Res. A*, 2005, **75**, 603-611.
11. Charest JL, García AJ, King WP. Myoblast alignment and differentiation on cell culture substrates with microscale topography and model chemistries. *Biomaterials*, 2007, **28**, 2202-2210.
12. Fujita S, Ono D, Ohshima M, Iwata H. Supercritical $CO_2$-assisted embossing for studying cell behaviour on microtextured surfaces. *Biomaterials*, 2008, **29**, 4494-4500.
13. Dakin SC, Mareschal I, Bex PJ. Local and global limitations on direction integration assessed using equivalent noise analysis. *Vision Res.*, 2005, **45**, 3027-3049.
14. Bashur CA, Dahlgren LA, Goldstein AS. Effect of fiber diameter and orientation on fibroblast morphology and proliferation on electrospun poly(D,L-lactic-co-glycolic acid) meshes. *Biomaterials*, 2006, **27**, 5681-5688.
15. Agostinelli C. Robust estimation for circular data. *Comput. Stat. Data Anal.*, 2007, **51**, 5867-5875.
16. Fisher NI. *Statistical analysis of circular data*, New York: Cambridge University Press. 1993
17. DeMali KA, Burridge K. Coupling membrane protrusion and cell adhesion. *J. Cell Sci.*, 2003, **116**, 2389-2397.
18. Adams JC. Regulation of protrusive and contractile cell-matrix contacts. *J. Cell Sci.*, 2002, **115**, 257-265.

19. Faix J, Rottner K. The making of filopodia. *Curr. Opin. Cell Biol.*, 2006, **18**, 18-25.

20. McClay DR. The role of thin filopodia in motility and morphogenesis. *Exp. Cell Res.*, 1999, **253**, 296-301.

21. Dalby MJ, Gadegaard N, Riehle MO, Wilkinson CD, Curtis AS. Investigating filopodia sensing using arrays of defined nano-pits down to 35 nm diameter in size. *Int. J. Biochem. Cell Biol.*, 2004, **36**, 2005-2015.

22. Teixeira AI, Abrams GA, Bertics PJ, Murphy CJ, Nealey PF. Epithelial contact guidance on well-defined micro- and nanostructured substrates. *J. Cell Sci.*, 2003, **116**, 1881-1892.

23. Wójciak-Stothard B, Curtis A, Monaghan W, MacDonald K, Wilkinson C. Guidance and activation of murine macrophages by nanometric scale topography. *Exp. Cell Res.*, 1996, **223**, 426-435.

24. Pittenger MF, Mackay AM, Beck SC, Jaiswal RK, Douglas R, Mosca JD, Moorman MA, Simonetti DW, Craig S, Marshak DR. Multilineage potential of adult human mesenchymal stem cells. *Science*, 1999, **284**, 143-147.

25. Park JS, Chu JSF, Cheng C, Chen F, Chen D, Li S. Differential effects of equiaxial and uniaxial strain on mesenchymal stem cells. *Biotechnol. Bioeng.*, 2004, **88**, 359-368.

26. Kurpinski K, Chu J, Hashi C, Li S. Anisotropic mechanosensing by mesenchymal stem cells. *Proc. Natl. Acad. Sci. U. S. A.*, 2006, **103**, 16095-16100.

27. Zhu B, Lu Q, Yin J, Hu J, Wang Z. Alignment of osteoblast-like cells and cell-produced collagen matrix induced by nanogrooves. *Tissue Eng.*, 2005, **11**, 825-834.

28. Dalby MJ, Gadegaard N, Tare R, Andar A, Riehle MO, Herzyk P, Wilkinson CD, Oreffo RO. The control of human mesenchymal cell differentiation using nanoscale symmetry and disorder. *Nat. Mater.*, 2007, **6**, 997-1003.

# SUMMARY

## CHAPTER 1

Human mesenchymal stem cells (MSCs) are promising feeder cells for expanding hematopoietic stem cells (HSCs), but their potential is heterogeneous. The hematopoiesis-supporting activity of human MSC was examined at the clonal level in relation to the osteogenic potential and gene expression. Hematopoiesis-supporting activities of stably immortalized clonal human MSC lines were evaluated by the expansion of $CD34^+CD38^-$ cells after 7-day coculture with human cord blood-derived $CD34^+$ cells. Six of 16 clones expanded the numbers of $CD34^+CD38^-$ cells > 500-fold. These hematopoiesis-supportive clones also showed high gene expression of Jagged1, a Notch ligand, as well as high potential to deposit calcium after osteogenic induction. Thus, osteogenic human MSC clones may provide proper microenvironments for HSCs expansion, ultimately conveying self-renewal signals to HSCs via the Notch pathway. They, however, lost hematopoiesis-supporting activity after osteogenic differentiation. The hematopoiesis-supportive clones are potentially useful for hematopoietic microenvironments studies and as components of a coculture system for expansion of HSCs, free from contamination by xenogeneic pathogens.

## CHAPTER 2

Expansion of HSCs from cord blood is highly desired for treatment and transplantation of adult patients for hematologic diseases. For efficient proliferation of HSCs, $CD34^+$ cells from cord blood were co-cultured with microencapsulated murine stromal cells (HESS-5) or immortalized MSCs in their conditioned media (CM). Bioactive substances for HSC proliferation in CM at the onset of culture are likely consumed by HSCs with time, and co-culturing with microencapsulated feeder cells ensures a continuous supply. The cell number of $CD34^+$ cell progeny efficiently increased under these culture conditions, and progeny were analyzed by flow cytometry, the colony assay and the cobblestone area-forming cell (CAFC) assay. Total nucleated cells and $CD34^+$ cell number increased 194-fold and 7.4-fold, respectively, in the presence of microencapsulated HESS-5 in CM. Colony forming cells and CAFCs were well maintained. The effective expansion of total cells and maintenance of primitive progenitor cells suggest that transfusion of the progeny obtained from $CD34^+$ cell culture with microencapsulated HESS-5 in CM could shorten the time to engraftment by bridging the pancytopenic period and support functional hematopoietic repopulation.

## CHAPTER 3

Conventional assays for hematopoietic progenitor cells (HPCs) require

long-term culture, a labor-intensive procedure, and technique proficiency. To develop a high-throughput method to determine frequency of quiescent primitive HPCs, a combination of the micro-multiwell plate and 5-fluorouracil (5-FU) treatment was performed. The micro-multiwell plate was made of a silicone sheet with 6 × 6 holes (diameter, 1 mm) and a glass substrate. To enrich primitive HPCs in $CD34^+$ population, $CD34^+$ cells and stromal cells were applied to micro-multiwells and cultured in the presence of 5-FU for 2 days. The quiescent primitive HPCs were survived after 5-FU treatment, and then expanded with cytokines in the absence of 5-FU for a further 10 days. After culture, cells were immunostained and the number of primitive HPCs in inoculated $CD34^+$ cells was estimated from fluorescent intensity for each well under a stereoscopic fluorescent microscope. The frequencies of primitive HPCs were well correlated with frequencies of cobblestone area-forming cells for two $CD34^+$ cell lots. This method can realize high-throughput assays for primitive HPC in $CD34^+$ cells.

## CHAPTER 4

Recently, cell responses to micro- and nanoscale structures have attracted much attention. Although interesting phenomena have been observed, there have been some difficulties in elucidating purely topographical effects on cell behaviour. These problems are partially attributable to the introduction of functional groups and the persistence of chemicals during surface processing. In this chapter, supercritical $CO_2$-assisted embossing was introduced, which plasticizes a polycarbonate plate by dissolving supercritical $CO_2$ and thus can emboss wide-scale patterns onto the plate at a

lower temperature than the polycarbonate glass transition temperature. Uniform micro- and nanopatterned surfaces were observed across the whole area of the polycarbonate plate surfaces. Nickel, fluorine, and nitrogen were not detected on the fabricated surfaces, and the surface carbon-to-oxygen ratios were equivalent to the theoretical ratio (C:O = 84.2:15.8) calculated from the polycarbonate molecular structure. Human MSCs were cultured on the fabricated microlens and nanogroove substrata. Cell-adhered areas became smaller on the microlens than on non-treated polycarbonate. Meanwhile, cells aligned along the ridges of nanogrooves with valleys deeper than 90 nm. This supercritical $CO_2$-assisted embossing can produce fine substrates for studying the effects of surface topography of synthetic materials on cell behaviors.

# CHAPTER 5

Cells elongate on a surface with nanogrooved patterns and align along that pattern. Although various models have been proposed for how this occurs, much remains to be clarified. Studies with fixed cells do not lend themselves to answering some of these open questions. In this chapter, the dynamic behaviours of living MSCs on an nanogrooved substrate with a 200-nm groove depth, 870-nm ridge width, and a 670-nm groove width were observed using time-lapse microscopes. It was found that filopodia movements were isotropic: no specific direction was observed for their extension and retraction against the nanogrooved structure. This finding suggests that filopodia probing does not play a major role in cell alignment. On the other hand,

anisotropy of movements of cell protrusions was found, especially in their retraction phase. Cell protrusions perpendicular to the nanogrooved pattern retracted more rapidly than those parallel to the grooves. Cell protrusions isotropically extended, but some of those parallel to the grooves persisted longer than cell protrusions perpendicular to the grooves. These cell protrusion dynamics force a cell to elongate and align along the nanogrooved pattern.

# LIST OF PUBLICATIONS

**CHAPTER 1**

Fujita S, Toguchida J, Morita Y, Iwata H.

Clonal analysis of hematopoiesis-supporting activity of human mesenchymal stem cells in association with Jagged1 expression and osteogenic potential.

*Cell Transplant*., in press

**CHAPTER 2**

Fujimoto N, Fujita S, Tsuji T, Toguchida J, Ida K, Suginami H, Iwata H.

Microencapsulated feeder cells as a source of soluble factors for expansion of CD34(+) hematopoietic stem cells.

*Biomaterials*, 2007, **28**, 4795-4805.

**CHAPTER 3**

Fujita S, Morita Y, Iwata H.

High-throughput evaluation of quiescent hematopoietic progenitor cells using a micro-multiwell plate.

*Anal. Bioanal. Chem*., 2008, **391**, 2753-2758.

**CHAPTER 4**

Fujita S, Ono D, Ohshima M, Iwata H.

Supercritical $CO_2$-assisted embossing for studying cell behaviour on microtextured surfaces.

*Biomaterials*, 2008, **29**, 4494-4500.

**CHAPTER 5**

Fujita S, Ohshima M, Iwata H.

Time-lapse observation of cell alignment on nanogrooved patterns.

*J. R. Soc. Interface*, (Submitted)

**International Conference**

Fujita S, Kitahara N, Tsuji T, Toguchida J, Iwata H.

Hematopoiesis Supporting Ability of Immortalized Mesenchymal Stem Cells.

*The 8th Annual meeting of Tissue Engineering Society International*, 2005 Oct. Shanghai.

**Other Publication**

Fukiage K, Aoyama T, Shibata KR, Otsuka S, Furu M, Kohno Y, Ito K, Jin Y, Fujita S, Fujibayashi S, Neo M, Nakayama T, Nakamura T, Toguchida J.

Expression of vascular cell adhesion molecule-1 indicates the differentiation potential of human bone marrow stromal cells.

*Biochem. Biophys. Res. Commun.*, 2008, **365**, 406-412.

# ACKNOWLEDGEMENTS

The present research was carried out from 2003 to 2008 under the continuous guidance of Dr. Hiroo Iwata (Professor of Institute for Frontier Medical Sciences, Kyoto University). The author would like to express heartfelt gratitude to Professor Iwata for his patient guidance, invaluable discussions, encouragement, and detailed criticism on manuscripts throughout the present work. The accomplishment of the present research would not have been possible without his guidance and support.

The author is also very grateful to Dr. Koichi Kato (Associate Professor of the Institute for Frontier Medical Sciences, Kyoto University) for his enriching suggestions, and intimate advices throughout the present research. The author is also indebted to Dr. Masahiro Ohshima (Professor of Department of Chemical Engineering, Kyoto University) for valuable advices and providing an opportunity to use an embossing machine, to Dr. Junya Toguchida (Professor of Institute for Frontier Medical Sciences, Kyoto University) and Dr. Tomoki Aoyama (Assistant Professor of Institute for Frontier Medical Sciences, Kyoto University) for their pragmatic comments and providing immortalized MSC clones, to Dr. Takashi Tsuji (Associate Professor of Tokyo University of Science) for his significant advices on hematological experiments and providing HESS-5. The author wishes to express his sincere appreciation to Dr. Yutaka Morita (Director of Department of Obstetrics and Gynecology, Itabashi Chuo Medical Center), Dr. Hiroshi Suginami (ex-Vice President of Natinal Hospital Organization Kyoto Medical Center) and Dr. Kenji Ida (Natinal

Hospital Organization Kyoto Medical Center) for providing donated umbilical cord blood.

The author also would like to express his thanks to all the members of Professor Iwata's laboratory for kind helps and candid comments. Especially, Dr. Hideki Sato (Gunze Ltd.) deserves the author's gratitude for worthy discussions, suggestions and encouragements. Ms. Nanae Fujimoto inspired the author with suggestive discussions on hematopoietic potential of MSC. Sharing ideas with Mr. Daizaburo Ono developed into the author's understanding about the topographic effect on cell responses. General acknowledgements are due to Ms. Yoshiko Suzuki.

The author's earnest feelings of reverence are due to Mr. Shuichi Narita (ex-President of Itabashi Medical Laboratory Inc.) and Mr. Jun Fueki (President of Itabashi Medical Laboratory Inc.). Without their hearty supports, the author would not have been able to continue to study in Kyoto University. The author would also like to express sincere regards to Mr. Takahisa Sasahara, Dr. Koichi Saito, Ms. Kyoko Suzuki (Regenerative Medical Center, Itabashi Medical Laboratory Inc.), and Mr. Aritada Yuasa (President of Aywill Inc.) for their continuous supports.

Finally, the author deeply thanks to his parents for their unfaltering supports and immense encouragements. A special acknowledgment and gratitude must be given to the author's wife and their son, who have always provided the author solace through every ordeal.

October, 2008

Kyoto

藤田聡

Satoshi Fujita